CRC Report No. A-120

EMPIRICAL ANALYSIS OF HISTORICAL AIR QUALITY AND EMISSIONS INFORMATION TO DEVELOP OBSERVATIONALLY-BASED MODELS OF OZONE-VOC-NOX RELATIONSHIPS IN SOUTHERN CALIFORNIA

Final Report

September 2021

COORDINATING RESEARCH COUNCIL, INC.
5755 NORTH POINT PARKWAY • SUITE 265 • ALPHARETTA, GA 30022

The Coordinating Research Council, Inc. (CRC) is a non-profit corporation supported by the petroleum and automotive equipment industries. CRC operates through the committees made up of technical experts from industry and government who voluntarily participate. The four main areas of research within CRC are: air pollution (atmospheric and engineering studies); aviation fuels, lubricants, and equipment performance; heavy-duty vehicle fuels, lubricants, and equipment performance (e.g., diesel trucks); and light-duty vehicle fuels, lubricants, and equipment performance (e.g., passenger cars). CRC's function is to provide the mechanism for joint research conducted by the two industries that will help in determining the optimum combination of petroleum products and automotive equipment. CRC's work is limited to research that is mutually beneficial to the two industries involved. The final results of the research conducted by, or under the auspices of, CRC are available to the public.

Empirical Analysis of Historical Air Quality and Emissions Information to Develop Observationally Based Models of Ozone-VOC-NOx Relationships in Southern California

Final Report
To the Coordinating Research Council

From
Yu Qian, Petros Vasilakos, Yongtao Hu, Talat Odman, Jennifer Kaiser, and Armistead Russell

Georgia Institute of Technology
Atlanta, GA 30340

Table of Contents

Executive Summary

In this project, we developed, applied, and evaluated different methods to estimate ozone-emission relationships, with a focus on the South Coast Air Basin (SoCAB) in California. One objective of the work was to investigate the spatial patterns and variation of ozone isopleths by expanding the regression-based empirical method and applying that approach to multiple monitoring sites in different locations in the SoCAB. Another focus was to conduct extensive air quality modeling of the SoCAB for a number of historical and future years to understand how well the current chemical transport models (CTMs) capture ozone dynamics and the response to controls of NOx and VOC. Finally, ozone responses to emissions were directly compared between empirical and chemical transport model-derived sensitivities (including the use of isopleths). Major activities and findings of this project are as follows:

Empirical modeling finds that the ozone-emissions relationships varied across the SoCAB, with downwind peak ozone concentrations being generally higher than those found in the city core or near the coast and the higher levels are more sensitive to emissions of NO_x. Under zero anthropogenic emissions, the ozone design values (ODVs) are almost constant over the air basin, though slightly higher at the coast. Model evaluation suggests that, at least near the observation sites , the models capture how ozone responds to emissions changes.

Development and use of a basin-wide empirical modeling approach finds that ozone exposure decreased from 1980 to 2019 as VOC and NOx emissions decreased. For ozone exposures at higher ozone levels (using the peak station concentrations and all concentrations higher than 60 ppb, 70 ppb), initially controlling NOx emissions led to increases in ozone exposure with decreases in response to NOx controls in more recent years.

CMAQ-HDDM was applied to both past (1985, 2001, 2011, 2016) and future (2028) emission estimates at a 4-km resolution over the SoCAB. For the most part, the five-year set of simulations were consistent with the observed decreases in ozone. However, the 1985 and 2001 results both tended to be biased low (by about 20%) at capturing peak ozone levels, and increasing estimated VOC and NOx emissions by about 40% and 20%, respectively, improved performance. Application to 2028 showed ozone would continue to decrease in the future assuming meteorological trends do not overwhelm expected emissions reductions. For comparison, simulated peak 2028 levels are about 18 ppb less than those in 2016.

We conducted a set of 11 CMAQ-HDDM simulations to develop ozone-NOx-VOC isopleths at locations across the basin. The CMAQ-derived isopleth for Crestline (the monitoring location with the highest modeled ozone for 2016) found that for much of the 1975–2018 period, peak ozone levels have been sensitive to reducing VOCs while, until at least 2005, NOx controls would have led to ozone increases. Recent NOx emissions reductions, however, are pushing the SoCAB to a regime where, on a percentage emissions basis, NOx emissions reductions will lead to greater ozone reductions than VOC emissions controls.

The empirically and CMAQ-derived isopleths were compared and found to be similar for downwind locations. More centrally-located and coastal sites often had much different isopleths. While both methods have weaknesses, the empirically derived relationships are derived from actual observations over multiple decades, and uncertainty analysis found that they can provide accurate estimates of how ozone will respond, both for future small emissions perturbations, as well as along the "emissions trajectory", i.e., along the historical emissions path. Detailed comparison of the ozone-emissions sensitivities using historic (estimated) emission conditions found that CMAQ-derived NOx emissions sensitivities were closer to the observed sensitivities than were the VOC-sensitivities.

Results from both empirical and CMAQ methods revealed similar patterns of the spatial distribution, though CMAQ captures more detail at a finer granularity. Ozone is higher over the northeastern part of the air basin and lower over the southwestern part of the air basin. The coastal areas have a $dO_3/dENO_x$ (sensitivity of ozone concentration to NOx emissions or simply NOx sensitivity) close to zero, and this does not change significantly over time. With time, the area with a negative NOx sensitivity has decreased, and now only the urban LA core area continues to have a negative NOx sensitivity. On the other hand, dO_3/dEVOC (ozone-to-VOC emission sensitivities) are almost always positive, although they have decreased over time. Spatially, the dO_3/dEVOC is higher in inland areas and lower along the coast. This pattern indicates that the role of VOC reductions in ozone control has been beneficial historically.

The two methods used to develop ozone isopleths have their individual strengths and limitations, though there is no simple way to say which method is better than the other. The empirical method is based on actual ozone observations, but also based on estimated emissions, and for that, it's most accurate for conditions with emissions similar to past observations. It is also open to uncertainty analysis with respect to emissions changes. On the other hand, the empirical approach does not have observations for very low emissions, i.e., much lower than historically observed, and cannot capture how climate change may impact ozone in the future. CMAQ-derived isopleths are also subject to emissions uncertainties, as well as uncertainties in input meteorology, though using the same meteorology over time removes some aspects of the latter uncertainties' impact on isopleth development and assessment of emissions sensitivities. Both methods are able to capture the ozone concentration trends along the historical emissions trend, but the HDDM-based isopleths tend to be biased high in recent years (while better capturing a leveling-off and even increases in the ODVs from and after 2012) and biased low in early years because of the biased-low estimation of 1985 ozone levels.

The impact of changing boundary conditions from the default approach to using boundary conditions derived from hemispherical modeling had little effect on the CMAQ modeling results of either the ozone levels or the sensitivities for the 2016 base case. However, using a zero-anthropogenic emissions case, estimated ozone concentrations using the fine-scale (4-km resolution) Southern California domain nest being driven by the hemispheric model-derived boundary conditions were substantially different than found using the default conditions. This difference was found to be driven by a fire at the northern boundary of the 4-km domain, and that the hemispheric modeling used a somewhat different inventory for fires. When the 4 km Southern California domain is nested in to a 12 km Western US domain nested in the hemispherical domain, and the 12 km domain used the same emissions as the default, the differences with the default case are small, suggesting little impact from utilizing different boundary conditions if the emissions are treated consistently.

Overall, the major "take-home" messages are:

- Empirically developing ozone responses to emissions (and, likewise isopleths) is a potentially powerful method to understand how emissions controls have impacted peak ozone levels historically, and, within their limits, how they will respond to future emissions changes
- Empirical modeling can be used to develop isopleths at individual locations or basin-wide
- Use of an empirically-derived, spatial, ozone-emissions model finds that much of the reduction in exposure over the last four decades has come from VOC emissions reductions, and that future exposure reductions can be derived from both VOC and NOx emissions reductions
- CMAQ modeling captured the reductions in ozone due to emissions decreases, but modeled levels were low for the two earliest years, and thus the simulated reductions were low
- The CMAQ-derived isopleth were similar to those derived empirically for inland, higher ozone locations (though were biased low for high emissions levels), with a high correlation
- CMAQ-derived ozone sensitivities to NOx emissions were more highly correlated with those derived empirically than with VOC emissions sensitivities
- CMAQ- and empirically derived isopleths both show that in earlier years (before about 2005) that VOC emissions reductions led to decreases in higher levels of ozone, off-setting potential increases due to NOx emissions reductions. In more recent years, ozone levels have become increasingly sensitive to reductions in NOx emissions, and that anthropogenic VOC emissions reductions will become less effective, though still beneficial, at reducing peak ozone levels downwind of the Los Angeles core area. Using CMAQ-HDDM, it is found that peak ozone levels in an increasingly small area of the core of Los Angeles will continue to be negatively sensitive to NOx emissions reductions.

Chapter 1: Introduction

The South Coast Air Basin (SoCAB) of California has the highest peak ozone levels in the US, despite stringent controls imposed over the last few decades. While significant ozone reductions have been realized, recent trends have found a leveling off in the ozone design value (ODV), and even an increase in the middle of the 2010-2020 decade. These observations have heightened interest in further understanding the response of ozone levels to changes in precursor emissions, mainly volatile organic compounds (VOCs) and nitrogen oxides (NOx). Historically, many methods have been developed to explore this relationship, from smog chambers to box models to chemical transport models (CTMs) (Jin and Demerjian, 1993; Kanaya et al., 2009; Kelly and Gunst, 1990; Menut et al., 2000; Milford et al., 1989; Sierra et al., 2013). Each of these approaches has its limitations, and arguably the least limited of the three, CTMs, have not been able to fully capture the observed trends of ozone in Los Angeles.

Multiple questions arise, including: 1. How will ozone respond to the proposed further emissions changes? 2. What is the most effective approach to reducing peak ozone levels and ozone exposure? 3. How effective have past controls been in relation to the advantages of NOx vs. VOC controls? 4. What is the ultimate background ozone level? and 5. How well do CTMs, which are used to develop control strategies, capture ozone trends and, more importantly, sensitivity to emissions?

To investigate the ozone-emissions relationship, the use of isopleths is particularly attractive, since isopleths have been used widely in analyses of air quality control strategies in the SoCAB (Kinosian, 1982; William and Burke, 2016; Yang et al., 2021), and can be developed using CTMs such as CMAQ and CAMx (Hakami et al., 2004; Milford et al., 1989; Reynolds et al., 2004), box models (Fujita et al., 2003), and more recently, empirically constructed isopleths (Qian et al., 2019). Isopleths allow visual identification of the "ridge line" often used to suggest where NO_x or VOC emissions controls are most effective as well as regions where NOx emission reductions will actually lead to increased ozone. Box model-derived isopleths do not capture meteorological impacts or provide spatial and diel responses. Also, they are typically derived using concentrations, not emissions, as inputs.

Using CTMs to investigate the relationship between ozone and its precursors typically involves the repeated modeling of several levels of emissions to generate the isopleth by applying an integrating or kriging method over wide portions of the emissions space. The computational cost of so many simulations is generally steep and has been studied before, with the goal of producing a reduced form model to construct the isopleth, for example, by using sensitivity analysis techniques (Cohan et al., 2005; Hakami et al., 2004).

In addition to the computational burden involved in CTM-based methods, the uncertainties of CTMs can also bias results. The accuracy of a CTM-generated isopleth depends on the accuracy of the model algorithms, the physical and chemical processes captured by the model, boundary conditions (e.g., background ozone), and the meteorological and emissions inputs. In particular, the emissions, which are the important inputs of models, are uncertain (Dunker et al., 2020; Fujita et al., 1992; Hanna et al., 2005, 2001; McDonald et al., 2018; Parrish, 2006; Qin et al., 2021; Zhang et al., 2015), though the trends are probably better captured than the absolute levels (Qian et al., 2019). Background ozone uncertainties can be particularly important when considering near-zero anthropogenic emissions of either VOC or NOx emissions or both, leading to low simulated ozone. The uncertainties involved in ozone simulations with CTMs have been analyzed in earlier studies (Dunker et al., 2020; Emery et al., 2017, 2012; Hanna, 2007; Qin et al., 2019; Simon et al., 2012; Zhang et al., 2015), which have found typical errors of about 25% (mean fractional error) with only a moderate correlation ($R^2 \sim 0.5$) between the predicted and observed ozone concentrations.

Given the limitations and uncertainties of using model-based isopleths, despite the amount of effort invested in their generation, observation-based empirical methods have also been developed to investigate the response (Baidar et al., 2015; Pusede and Cohen, 2012) and the weekday/weekend effect (Fujita et al., 2003; Kim et al., 2016; Pollack et al., 2012). A major advantage of observation-based (empirical) methods is that they capture how the actual atmosphere responds to actual emissions changes. In Qian et al. 2019 (Qian et al., 2019), we introduced an observationally driven empirical method applied in the SoCAB, based on using historical ODVs and historical estimates of NOx and VOC emissions, to develop non-linear regression models to quantify sensitivities and develop ozone isopleth diagrams. This method generates isopleths with good model performance and limited uncertainty, and provides insights for future ozone reduction strategies. Limitations of the method are that it uses estimated emissions (which are uncertain) and that uncertainties grow as the model is applied to conditions further away from the past observations upon which it was constructed.

In the project described in this report, we address a number of issues raised in our prior work, as well as more generally in the use of both empirical and CTM-based approaches for assessing how air quality in the SoCAB has responded to emissions changes, and how levels will respond in the future.

In our prior study, an isopleth for the SoCAB's ODV was developed, although previous studies indicated that the response of ozone-to-emissions changes can differ significantly for different areas in the same region (Milford et al., 1989), indicating that the same ozone control strategy can have location-dependent effects. One objective of the work conducted as part of this project is to investigate the spatial pattern and variation of isopleths by expanding on the regression-based empirical method applied to monitoring sites in different locations in the SoCAB. As part of this, we introduce a method that integrates spatial information into the model, which can not only be used to generate isopleths for different locations but can also be used to predict the spatial distribution of ODVs under different emissions levels and be used to quantify how ozone exposure responds to emissions changes.

Another focus of this study is to conduct extensive air quality modeling of the SoCAB for a number of historical and future years to understand how well the current CTMs capture ozone dynamics and the response to NOx and VOC controls. While the focus here is on ozone, the analysis provides similar results for particulate matter. Our analysis includes more traditional approaches (e.g., modeling using emissions from one or more historical years) and three approaches that go beyond typical studies: 1) extensive first- and second-order sensitivity analysis (with uncertainty analysis of sensitivities), 2) use of isopleths to provide a more direct, visual analysis tool (that can also be quantitative), and 3) direct comparison of modeled sensitivities with empirically derived sensitivities (including the use of isopleths).

Chapter 2: Spatial Variation of Ozone-Emissions Relationships and Exposure Study in Southern California: An Empirical Analysis of Historical Air Quality and Emissions Information to Develop Observationally Based Models

2.1 Introduction

The South Coast Air Basin (SoCAB) of California has the highest peak ozone levels in the US, despite stringent controls over the past few decades. These observations have heightened interest in further understanding the response of ozone levels to changes in precursor emissions, mainly volatile organic compounds (VOCs) and nitrogen oxides (NOx). For the purpose of investigating the ozone-emissions relationship, the use of isopleths is particularly attractive, since isopleths allow visual identification of the "ridge line," often used to suggest where NO_x or VOC emissions controls are most effective, as well as regions where NOx emission reductions will actually lead to increased ozone. Empirically constructed isopleths (Qian et al., 2019) have been used in analyses of air quality control strategies in the SoCAB. A major advantage of observation-based (empirical) methods is that they capture how the actual atmosphere responds to actual emissions changes. In our prior study, an isopleth for the SoCAB's ozone design value (ODV) was developed, although previous studies have indicated that the response of ozone-to-emissions changes can differ significantly for different areas in the same region (Milford et al., 1989), indicating that the same ozone control strategy can have location-dependent effects. The main objective of the work conducted in this chapter is to investigate the spatial pattern and variation of isopleths by expanding the regression-based empirical method applied to monitoring sites in different locations in the SoCAB. As part of this, we introduce a method that integrates spatial information into the model, which can not only be used to generate isopleths for different locations, but can also be used to predict the spatial distribution of ozone design values under different emissions levels and be used to quantify how ozone exposure responds to emissions changes.

2.2 Method

Empirical analysis of the ozone-emissions response is based on developing a regression model between ODV and NOx and VOC emissions to estimate the response of the ODV to emissions controls over the past few decades. We used site-specific annual ODVs as the response variable, annual estimated NOx and VOC emissions as predictor variables, and spatial information (longitude and latitude) as predictor variables. Least squares regression led to a model relating ODVs to emissions levels and spatial locations. These coefficients can further be used to build ozone-emissions isopleths and ozone spatial distributions under different emission levels.

2.2.1 Study Domain

The South Coast Air Basin is California's largest metropolitan region, which includes parts of Los Angeles, Riverside, and San Bernardino counties, and all of the Orange County. The region covers approximately 17,100 km^2 and includes much of the Greater Los Angeles Area, which is home to approximately 18 million people (2020 census). A detailed description can be found in The California Almanac of Emissions and Air Quality (Cox et al., 2009).

2.2.2 Data

This study used ozone observational data for 24 monitoring sites within the SoCAB and basin-wide estimated emissions data. Specifically, the data included annual ozone design values (ODVs) based on measurement and annual emissions data for NOx and VOC estimated by the California Air Resources Board (CARB) for the time period of 1975 to 2019 (note that the data availability was not the same over all 24 monitoring sites; this study used all available data for the regression modeling).

Ozone design value (ODV) data: Based on the EPA's definition, "design value" is a statistic that can be used to represent the air quality for a certain location, area, or region, especially relative to the National Ambient Air Quality Standards (NAAQS) (US EPA, 2016). Here, we focus on the maximum daily averaged eight-hour ODV, which is the average of the fourth highest annual maximum daily average eight-hour ozone concentrations over three consecutive years. The data were extracted from the CARB iADAM: Air Quality Data Statistics data base (CARB, 2018) for every monitoring site in the SoCAB. In this study, data from 24 monitoring sites (out of 93) were included based on data quality and availability (Figure 2.4). A particular limitation is the length of time for which the data are available. Only sites with more than 20 years of ozone data were included.

Emissions data: NO_x and reactive organic gases (ROG) emission data (tons/day, annual average) of the SoCAB were obtained from the California Almanac of Emissions and Air Quality (Cox et al., 2013, 2009). Here, two editions of the Almanac (2009 and 2013) were used together to calculate the emissions over the whole study period. Data from the 2013 edition only covered years after 2000, and the 2009 edition covered a complete set of estimated emissions throughout the study period. However, the estimated emissions from the 2009 edition for years after 2000 are much higher than the newer 2013 edition estimation, and in comparison with the NEI inventory, we see that the 2013 edition estimation is more consistent for recent years. Therefore, we used the emissions data from Almanac version 2013 for years after 2000 and adjusted the emissions from Almanac version 2009 for years before 2000 by applying an adjustment ratio between 2009 and 2013 estimated 2000 emissions. For years where estimates were not given, we calculated the annual emissions values using a linear interpolation method based on the reported emissions value for each five years. The analysis uses only anthropogenic emissions estimates and does not include biogenic sources or the effect of climate change on biogenic emissions.

Between these two Almanac editions, organic ozone precursors were treated using two different terms. Historically, CARB used ROG to refer to the organic carbon-containing ozone precursors and changed to VOC in the 2013 edition. Based on the CARB's definition (Schwehr and Propper, 2009), ROG is not identical to the US EPA's term "VOC," but the two are similar with few differences in the list of exempted compounds. We conducted a comparison between estimated VOC and ROG emissions, as well as between the Almanac and SCAQMD inventory, and they showed a consistency with a very limited difference (average ROG to VOC ratio is 1.15, R^2 = 0.98).

2.3 Development of Ozone Isopleths Using Non-linear Regression Modeling

Prior studies (Hakami et al., 2004; Qian et al., 2019) suggested that the quadratic function can be used to fit both simulated and observed ozone concentrations with the precursor emissions of NOx and VOC to estimate their relationship, and develop the isopleth to visually illustrate that relationship. The resulting ozone isopleths show similar shapes to isopleths developed by chemical transport models and box models. Thus, this similar form was explored using traditional least squares fitting. This led to a well-performing fit for the observed values, although it also led to predicted ozone values for emissions levels well away from prior levels. In this study, we used the least squares regression method and made some modifications to construct the relationship between ODV and emissions. The idea was to fit a multivariable function between the ODV and the VOC and NOx emissions.

ODV (E_{NOx}, E_{VOC}) or Log_{10}(**ODV** (E_{NOx}, E_{VOC})) = **Xb** + **e** (EQN 2.1)

where

$$\mathbf{ODV} = (\mathrm{ODV}_1, \dots, \mathrm{ODV}_n)' \in \mathbb{R}^n \text{ is the } n \times 1 \text{ response vector}$$

$$\mathbf{X} = [1_n, \mathbf{x}_1, \dots, \mathbf{x}_p] \in \mathbb{R}^{n\times(p+1)} \text{ is the } n \times (p+1) \text{ design matrix}$$

$$\mathbf{b} = (\mathrm{b}_0, b_1 \dots, \mathrm{b}_p)' \in \mathbb{R}^{p+1} \text{ is the } (p+1) \times 1 \text{ vector of coefficients}$$

$$\mathbf{e} = (\mathrm{e}_1, \dots, \mathrm{e}_n)' \in \mathbb{R}^n \text{ is the } n \times 1 \text{ error vector}$$

n is the number of observations.

p is the number of variables.

The ordinary least squares (OLS) solution has the following form:

$$\hat{\mathbf{b}} = (\mathbf{X}'\mathbf{X})^{-1}\mathbf{X}'\mathbf{ODV} \qquad \text{(EQN. 2.2)}$$

The fitted values are calculated as:

$$\widehat{\mathbf{ODV}} = \mathbf{X}\hat{\boldsymbol{b}} = \mathbf{X}(\mathbf{X}'\mathbf{X})^{-1}\mathbf{X}'\mathbf{ODV} \qquad \text{(EQN. 2.3)}$$

In our previous study (Qian et al., 2019), we found that both quadratic and log quadratic relationships could accurately capture the SoCAB's ODV trend with time in response to NOx and VOC changes, i.e.,

$$\mathrm{ODV}\ (E_{NOx},\ E_{VOC}) = \beta + \alpha_{NO_x} * E_{NO_x} + \alpha_{VOC} * E_{VOC} + \alpha_{NO_x-VOC} * (E_{NO_x} * E_{VOC}) + \alpha_{NO_x^2} * E_{NO_x}^2 + \alpha_{VOC^2} * E_{VOC}^2 \qquad \text{(EQN. 2.4)}$$

where ODV is the input ozone design value from observations (e.g., ppb), E_{voc} and E_{NOx} are input annual average estimated VOC and NO_x emission rates (e.g., tons/day) respectively, and the α_is are output regression coefficients calculated by the least squares fitting method.

We also suggested a second fitting function using a logarithmic form:

$$\mathrm{Log}_{10}\,(\mathrm{ODV}\,(E_{NOx}, E_{VOC})) = \beta + \alpha_{NO_x} * E_{NO_x} + \alpha_{VOC} * E_{VOC} + \alpha_{NO_x-VOC} * (E_{NO_x} * E_{VOC})$$

$$+\alpha_{NO_x^2} * E_{NO_x}^2 + \alpha_{VOC^2} * E_{VOC}^2 \qquad \text{(EQN. 2.5)}$$

This form leads to positive ozone levels for all levels of VOC and NOx emissions. Other non-linear forms could also potentially be robust, though the two above lead to results that have a typical form of ozone isopleths and utilize relatively few parameters, limiting overfitting. Higher order terms can bring small changes in the fitted value but could introduce greater uncertainty when extrapolating away from the historical observations.

This regression approach was first applied to each of the individual sites included in this study independently by using the local observed ODV as the response variable and basin-wide emissions as independent variables, and was then extended to develop a single model that included spatial variables to develop a single model that could estimate ozone levels across the SoCAB. In both cases, we used basin-wide emissions trends, recognizing that there have been changes in the spatial distribution of emissions. The regression results for each site can be used to build the ODV emissions isopleth for a specific site.

For the spatially integrated model, instead of applying the model to each single monitoring site independently, we integrated location information (longitude and latitude) into the model as predictor variables, and then used the information of all monitoring sites together to train the model to produce the isopleth for any location. Equation 2.1 shows the general formation of this model, with 35 variables in total (Table 2.1). We introduced two new basic variables into the model: the longitude (y) and latitude (x) of the monitoring sites. Considering that the quadratic form has been proven effective, we also form the model with all the quadratic combinations of location and emissions variables (Table 2.1). ODV effectively equals the linear combination of all 35 variables.

Table 2.1 Variables included in the spatially integrated model (35 in total). y is latitude and x is longitude (unit in degree) for each monitoring site. NOx and VOC are the emissions (units in tons/day) for the SoCAB total annual average emissions for each year. Variables marked in red are those removed from the full model to obtain the reduced model with fewer variables.

y	**y*NOx**	**xy*NOx**	**x^2*NOx**
x	**y*VOC**	**xy*VOC**	**x^2*VOC**
xy	**y*NOX*VOC**	**xy*NOX*VOC**	**x^2*NOX*VOC**
y^2	**y*NOx^2**	**xy*NOx^2**	**x^2*NOx^2**
x^2	**y*VOC^2**	**xy*VOC^2**	**x^2*VOC^2**
NOx	**x*NOx**	**y^2*NOx**	
VOC	**x*VOC**	**y^2*VOC**	
NOx*VOC	**x*NOX*VOC**	**y^2*NOX*VOC**	
NOx^2	**x*NOx^2**	**y^2*NOx^2**	
VOC^2	**x*VOC^2**	**y^2*VOC^2**	

In addition to the full model, we also used the partial Akaike Information Criterion (AIC) method to conduct the model selection to generate reduced models based on statistical significance of variables and the overall performance of the model. The reduced model has 30 variables with 5 variables removed from the full model (marked red in Table 2.1). The results of both the full model and the reduced model were compared to evaluate the different methods.

Empirical methods, although they have several advantages, still involve uncertainty and need to be evaluated. The uncertainty involved in empirical methods comes from several sources. 1) The emissions inventory has inherent uncertainty since it is estimated. This implies that the absolute amounts of estimated emissions may not be accurate, which has been investigated by several studies (e.g., Dunker et al., 2020; Hanna et al., 2005, 2001; McDonald et al., 2018). On the other hand, emissions trends are probably better captured; that is, some observations have found that the long-term decreasing rate can be better captured (Hassler et al., 2016; Henneman et al., 2017a; Kim et al., 2016; Pollack et al., 2013; Warneke et al., 2012).

In a previous study (Qian et al., 2019) we conducted a comprehensive analysis to evaluate the uncertainty of the CARB inventory used in this study and the impact of inventory uncertainty on empirical model performance, and demonstrated that it was robust to use the CARB inventory for similar empirical analysis. Statistically there are uncertainties involved in the calculated coefficients themselves, and the relationship(s) are likely not exactly those predefined in the model fit, as is evident by the differences in the models developed here. There are different methods for calculating and identifying the uncertainty related to the regression process. One approach is to compare the estimated ozone levels for a certain location developed using different models (base model, log model, single-site model, and spatially integrated model), plotting the model difference.

Another analysis was conducted based on the statistical analysis of the regression models described by Helwig (2017) and further developed and applied by Qian et al. (2019).

2.4 Ozone Exposure Modeling

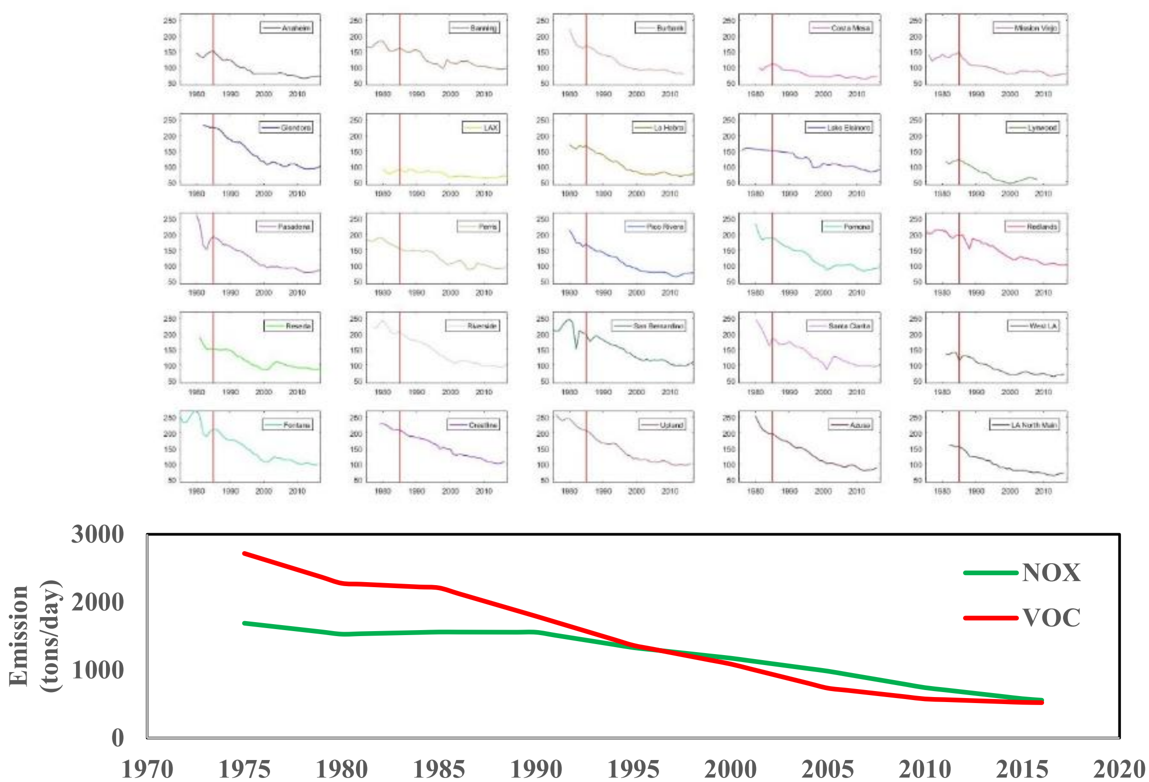

Figure 2.1 Top: The ODV trends for different monitoring sites in the South Coast Air Basin from 1975 to 2016 (if available); Bottom: The NOx and VOC emissions trends for the South Coast Air Basin from 1975 to 2016.

For the spatially integrated model, the ODVs from 1980 to 2019 at 24 sites and the longitude and latitude data were used to build the model. Here, we expanded the application of this approach to further develop an exposure model to investigate the empirical model-based exposure isopleth for the SoCAB. Ozone is considered an air pollutant that causes respiratory and other health effects in humans. Ozone exposure is a critical metric for evaluating ozone effects in health and is conducted to inform policies and health-related research. Based on potentially different interests, we filtered the ozone concentration data by five metrics so we could not only use ODV as the response variable but also train the model and build the exposure for different ozone metrics. Those metrics include: the maximum ozone value of each year, the annual mean of the eight-hour maximum ozone for each day, and the annual mean of the maximum ozone for the days when the maximum ozone was higher than 40 ppb (the background ozone concentration), 60 ppb (potential future ozone standard), and 70 ppb (equivalent to the current ozone standard). Since the historical data have little information for scenarios involving high VOC but almost zero NOx emissions, high NOx but almost zero VOC emissions, and almost zero VOC and NOx emissions, previous research on background ozone and CMAQ simulation was utilized to provide background ozone data points.

Estimating potential population exposure involves weighting the location-specific ozone metric by the population in that location. For a given location, the population weight is calculated based on the population data for the location, and the ozone concentration is provided using the spatial regression model. Typically, ozone exposure has a positive relationship with ozone level and population, and can be estimated using EQN. 2.6:

$$\text{Ozone Exposure} = [O_3] \times Population \text{ (EQN. 2.6)}$$

The ozone exposure in SoCAB is the sum of ozone exposure for each place in SoCAB. The exposure model can be described as EQN.17, where ozone values are evaluated by the reduced model in both base quadratic form and log quadratic form.

$$Ozone\ Exposure = \sum_{x,y} Ozone\ Exposure_{x,y} = \sum_{x,y} O_3(E_{NO_x}, E_{VOC}, x, y) \times \frac{Population_{x,y}}{\sum_{i,j} Population_{i,j}}$$

(EQN. 2.7)

2.5 Results and Discussion

2.5.1 ODV and Emissions of NOx and VOC Analysis

Figure 2.1 shows the trend of the monitoring site ODVs and basin-wide emissions estimates of NOx and VOC from 1975 to 2016 in the SoCAB, California. Estimated NOx emissions were reduced by 67%, and VOC emissions were reduced by 81%. In response, ODVs declined for almost all monitoring sites, but the degree of reduction varied over the air basin. Meteorological variations led to non-steady reductions in ozone levels. We note that recent (2019) levels of ODV had much less spatial variation; the highest was 108 ppb in Crestline and the lowest was 69 ppb in Costa Mesa. In 1985, the highest ODV was 273 ppb at Fontana, and the lowest was 92 at LAX. This indicates that for a certain monitoring site, the lower the ODV levels in earlier years, the lower the observed reduction. For example, the reduction of the ODV in LAX was only 28%, but the reduction in Azusa's ODV was 65%.

We also observed that the sites close to the coast tended to have a lower ODV and a slower reduction rate. This has been studied extensively and is the result of the combined effect of an eastward surface sea breeze and the mountain barrier on the west (Lu and Turco, 1996a; Yarwood et al., 2008). It also shows that the location of the highest ozone levels has changed over time. The relationship between ODV and NOx, as well as VOC emissions, is expected to differ spatially, even though the investigation between ODV and emissions for most of the sites showed a good fit with high R^2, which is consistent with the theory that ozone concentration is closely controlled by NOx and VOC concentration. We generally observed a positive relationship between ODV and NOx or VOC emissions; however, when ODV was higher, it tended to be more often related to VOC emissions than NOx emissions. This indicates that, in the SoCAB, when ozone concentration was high, its decline was mainly a result of VOC controls. The more detailed response of ODV to emissions reductions, especially in later years, will be further investigated later in this report.

2.5.2 Single Site Regression Model Result

Multivariate regression was used to construct a quadratic (second-order in emissions of NOx and VOCs) function of ODV values at each location using both a model based on the ODV and log(ODV). For all 24 monitoring sites in this study, both methods (base quadratic model and log quadratic model) led to similar functional forms, and the average resulting R^2 was 0.96. This performance suggests that, at least near the observational values, the models capture how ozone responds to emissions changes. In order to further test the predictive ability of this model, we conducted a 10-fold cross validation leading to stable results with a high R^2 (> 0.9) and low RMSE. This analysis indicates that the decline of ODV in SoCAB over the past several decades is mainly (> 90%) caused by emissions reductions. Meteorology may have played a role, but not as significant, at least for the long-term trends. Regression coefficients are listed in Table 2. The results for three representative monitoring sites were selected based on the distance from the coast (LA N. Main < Pasadena < Azusa).

Los Angeles North Main Street

$ODV(E_{NOx}, E_{VOC}) = 41.9 + 0.06*E_{NOx} - 0.02*E_{VOC} + 4*10^{-5}*(E_{NOx}*E_{VOC}) - 5*10^{-5}*(E_{NOx}^2) + 8*10^{-6}*(E_{VOC}^2)$

(EQN 2.8)

$Log_{10}(ODV(E_{NOx}, E_{VOC})) = 1.71 + 2*10^{-4}*E_{NOx} - 2*10^{-5}*E_{VOC} + 2*10^{-7}*(E_{NOx}*E_{VOC})$

$- 3*10^{-7}*(E_{NOx}^2) - 8*10^{-9}*(E_{VOC}^2)$ (EQN. 2.9)

Pasadena

$ODV(E_{NOx}, E_{VOC}) = 34.1 + 0.2*E_{NOx} - 0.06*E_{VOC} + 6*10^{-5}*(E_{NOx}*E_{VOC}) - 1*10^{-4}*(E_{NOx}^2) + 3*10^{-5}*(E_{VOC}^2)$

(EQN. 2.10)

$Log_{10}(ODV(E_{NOx}, E_{VOC})) = 1.73 + 3*10^{-4}*E_{NOx} + 4*10^{-5}*E_{VOC} + 3*10^{-7}*(E_{NOx}*E_{VOC})$

$- 3*10^{-7}*(E_{NOx}^2) - 4*10^{-8}*(E_{VOC}^2)$ (EQN. 2.11)

Azusa

$ODV (E_{NOx}, E_{VOC}) = 9.1 + 0.1*E_{NOx} + 0.05*E_{VOC} + 8*10^{-5} *(E_{NOx}*E_{VOC}) - 1*10^{-4} *(E_{NOx}^2) - 2*10^{-5} *(E_{VOC}^2)$

(EQN. 2.12)

$$Log_{10} (ODV (E_{NOx}, E_{VOC})) = 1.68 + 3*10^{-4} *E_{NOx} + 2*10^{-4} *E_{VOC} + 3*10^{-7} *(E_{NOx}*E_{VOC}) - 3*10^{-7} *(E_{NOx}^2) - 1*10^{-7} *(E_{VOC}^2) \quad \text{(EQN. 2.13)}$$

In our previous work (Qian et al., 2019), based on ozone chemistry, the sign of those regression coefficients should follow a certain pattern to correctly reflect the relationship between ozone and its precursors. The first-order sensitivities of ODV to both NOx and VOC emissions should be positive, meaning that increasing both emissions from a zero-emissions base leads to increasing ODV levels. On the other hand, the second-order sensitivities to both emissions should be negative, meaning that as one emission type increases, the sensitivity of ozone to that emission decreases, i.e., if there is a large abundance of one species, further ozone formation becomes insensitive, or even negatively sensitive, to those emissions. For example, for very high NOx emissions, ozone levels decrease.

As found here, the second-order sensitivities to VOCs are smaller than those to NOx, implying that further increasing VOC emissions may not lead to a negative sensitivity. However, the sensitivity to NOx can be negative at higher ODV levels, under which circumstances the further increase of NOx will lower the ODV levels. The coefficient of the interaction term should be positive, meaning that as both emissions of VOC and NOx increase, ozone tends to increase. By applying the regression coefficients to an emission space defined by various levels of NOx and VOC emissions, we were able to construct the ODV emissions isopleth to reflect the response of ODVs to emissions changes at different emissions levels (historical and future; Figure 2.2).

By examining the regression coefficients and isopleths for different sites (Table 2), we arrived at several findings. First, looking at the coefficient signs for the various locations, we noticed that the single-site regular model had a number of sites (19 out of 24) that contained at least two variables with coefficients of opposite signs to what was expected (19 out of 24). The log model had only 12 out of 24 sites. This is observed in the isopleths (Figure 2.2). For LA North Main and

Pasadena, the isopleths developed by the regular model show an unrealistic relationship between ODV and VOC when NOx emissions are low, which fails to reflect the NOx control effect. Another issue with the regular model is that when VOC emissions are low, extensively increasing NOx emissions leads to a negative ODV, which is not possible. Even though there is no statistically significant difference between the performance of those two models, the above observations indicate that the log model reflects the ODV emissions response more accurately, especially when NOx emissions are low. The log model can also prevent any negative ODV being predicted. The base quadratic model overestimated the role of VOC to ODV regardless of emissions levels; this is, in fact, not true (Qian et al., 2019).

The model estimated the signs of some coefficients incorrectly because most of the sites with atypical isopleths were near the coast. These sites have lower ODVs and less reduction over time. When the ODV response to emissions reductions is small, and meteorologically induced fluctuations are apparent, it is more difficult to capture the relationship. For all except one case in the log model, an abnormal sign of the linear emissions coefficient was found for the response to VOC emissions, and in those cases, the quadratic term is also of the opposite sign, offsetting the impact. This is tied to the lack of variation in the ODV over time to fully capture the non-linear response to VOC emissions.

Table 2.2 Regression coefficients for 24 monitoring sites in SoCAB. Result shown here are for the log model. The numbers marked in different colors indicate that the sign of this coefficient is abnormal.

	Intercept	αNOx	αVOC	αNOx*VO	αNOx^2	αVOC^2	R^2
Azusa	1.76	2E-04	2E-04	3E-07	-3E-07	-9E-08	0.95
Glendora	1.78	3E-04	2E-04	3E-07	-4E-07	-1E-07	0.95
West LA	1.69	3E-04	-8E-05	2E-07	-3E-07	6E-08	0.93
LA North Main	1.72	1E-04	1E-04	2E-07	-2E-07	-5E-08	0.97
Reseda	1.80	5E-04	-1E-04	2E-07	-3E-07	4E-08	0.86
Burbank	1.68	5E-04	2E-05	2E-07	-4E-07	-4E-09	0.96
Pico Rivera	1.73	2E-04	9E-05	2E-07	-2E-07	-5E-08	0.95
Pomona	1.79	3E-04	3E-05	3E-07	-3E-07	-2E-08	0.93
Pasadena	1.74	3E-04	1E-04	3E-07	-4E-07	-4E-08	0.96
Long Beach	1.66	3E-04	-2E-05	1E-07	-2E-07	5E-08	0.96
LAX	1.67	-3E-05	4E-04	3E-07	-2E-07	-2E-07	0.93
Santa Clarita	1.80	5E-04	-1E-04	2E-07	-4E-07	4E-08	0.90
Anaheim	1.72	3E-04	-1E-04	1E-07	-3E-07	7E-08	0.95
Mission Viejo	1.72	5E-04	-4E-05	2E-07	-3E-07	2E-09	0.91
La Habra	1.76	2E-04	-6E-05	2E-07	-2E-07	3E-08	0.93
Banning	1.77	6E-04	-6E-05	2E-07	-4E-07	6E-09	0.88
Perris	1.77	4E-04	1E-05	2E-07	-3E-07	-3E-08	0.90
Riverside	1.77	5E-04	4E-05	3E-07	-4E-07	-4E-08	0.95
Lake Elsinore	1.73	5E-04	2E-05	2E-07	-3E-07	-3E-08	0.93
Crestline	1.79	5E-04	1E-04	3E-07	-4E-07	-9E-08	0.97
Upland	1.80	4E-04	1E-04	3E-07	-4E-07	-7E-08	0.96
Fontana	1.77	4E-04	1E-04	3E-07	-4E-07	-8E-08	0.95
Redlands	1.78	4E-04	2E-04	3E-07	-4E-07	-1E-07	0.94
San Bernardino	1.79	4E-04	1E-04	3E-07	-4E-07	-7E-08	0.93
Average	1.75	4E-04	5E-05	2E-07	-3E-07	-3E-08	0.94

Another finding from the results is that the ODV's response to emissions was different in different locations, which has also been investigated in previous studies (e.g., Milford et al., 1989). By comparing the isopleths of LA North Main and Azusa, it is obvious that locations near the coast (upwind) have relatively lower ODV levels, and ODVs are less sensitive to emissions reductions than inland locations (typically downwind during high ozone periods). This is mainly caused by the meteorology and geographic features of the LA region and is related to the combined effects of surface sea breeze and mountain barriers. Sea breeze causes the transport of precursor pollutants from the coast inland, while mountain barriers lead to the accumulation of pollutants.

Based on these models, the average ODV values over all the sites corresponding to zero emissions (both NOx and VOC) were 57 ppb from the base quadratic model and 61 ppb from the log quadratic model. This is comparable to other studies (Huang et al., 2015; Lu and Turco, 1996b; Parrish et al., 2017), but should not be used as an estimate of background ozone for several reasons (Qian et al., 2019).

First, it involves extrapolation beyond the data on which the model is based, significantly increasing the uncertainty (here, it is ± 15 ppb when looking between sites; a more formal uncertainty analysis of the model for the basin-wide ODV led to an uncertainty of approximately 30 ppb). Further, the zero-emission ODV will likely occur at a different location and time than the current one (e.g., Crestline during the summer: studies suggest that the highest background values occur in the spring).

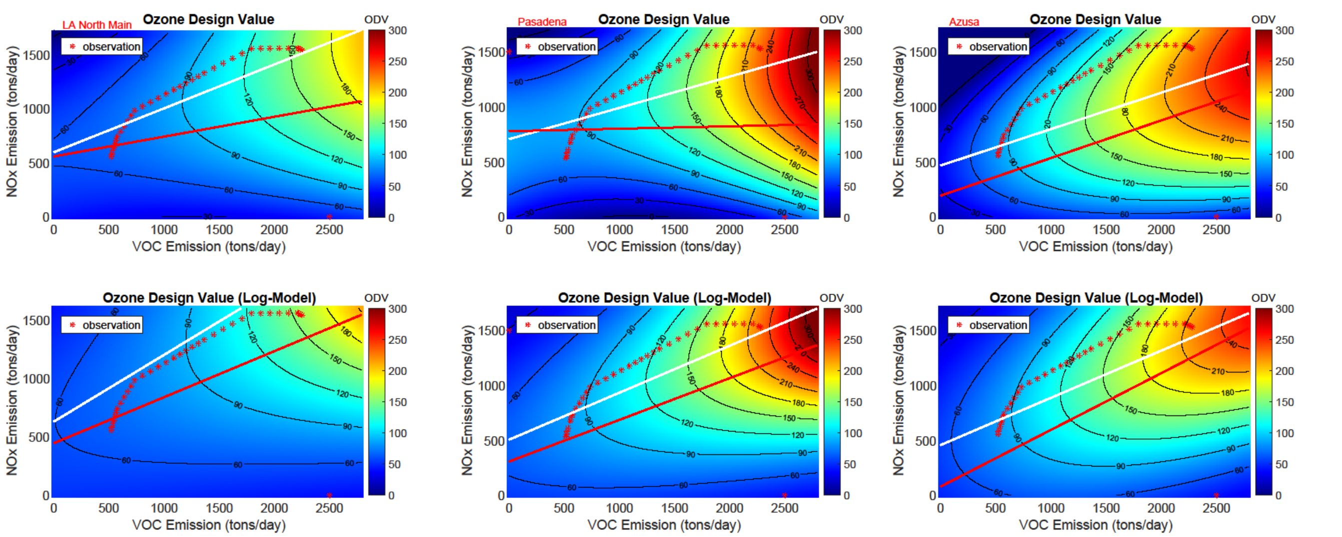

Figure 2.2 ODV-emissions isopleths constructed by single site multivariate regression model. The NOx-VOC emissions space is defined with various levels of estimated NOx and VOC emissions. ODVs calculated by the models are indicated with color. Historical emissions levels are marked as red spots. White lines indicate the zero-NOx sensitivity ridge lines (above the line means negative ODV to NOx sensitivity). Red lines indicate the equal NOx-VOC sensitivity ridge lines (below the line means more NOx control condition). From left to right are the result for three monitoring sites: LA North Main, Pasadena, and Azusa. The first row is the developed isopleths based on regular models. The second row is the developed isopleths based on regular models.

Qian et al. (2019) proposed that one insightful application of the equations developed was to estimate both sensitivity analysis and source apportionment. It is relatively straightforward to calculate the sensitivities to both NOx and VOC emissions using the derivatives of the regression models with respect to NOx and VOC emissions. We can calculate the first-order derivatives as follows:

$$\frac{\partial \mathrm{ODV}}{\partial E_{\mathrm{NOx}}} = 2\alpha_{\mathrm{NO_x^2}} \mathrm{E_{NOx}} + \alpha_{\mathrm{NOx-VOC}} \mathrm{E_{VOC}} + \alpha_{\mathrm{NOx}} \qquad \text{(EQN. 2.14)}$$

$$\frac{\partial \mathrm{ODV}}{\partial E_{VOC}} = 2\alpha_{VOC^2} \mathrm{E_{VOC}} + \alpha_{\mathrm{NOx-VOC}} \mathrm{E_{NOx}} + \alpha_{\mathrm{VOC}} \qquad \text{(EQN. 2.15)}$$

For NOx, if the sensitivity is set to zero, this becomes:

$$E_{NOx} = -\frac{\alpha_{NOx}}{2\alpha_{\mathrm{NO_x^2}}} - \frac{\alpha_{\mathrm{NOx-VOC}}}{2\alpha_{\mathrm{NO_x^2}}} \mathrm{E_{VOC}} \qquad \text{(EQN. 2.16)}$$

This can be understood as the line that separates the regions where increased NOx emissions increase ozone (below the line) or decrease ozone (above the line, i.e., NOx-saturated conditions).

Another interesting feature of the ozone isopleth is the location of equal sensitivities to NOx and VOC emissions, and the equal NOx-VOC sensitivity is given as:

$$E_{NOx} = \frac{\alpha_2 - \alpha_1}{2\alpha_4 - \alpha_3} + \frac{2\alpha_5 - \alpha_3}{2\alpha_4 - \alpha_3} \mathrm{E_{VOC}} \qquad \text{(EQN. 2.17)}$$

This was done for both models for each site, and plots of the resulting sensitivities show that the VOC sensitivities tended to stay positive, but there is a line where the sensitivities to NOx emissions change sign in the isopleth plots (Figure 2.2). Since the models we developed are in quadratic form, both the equal NOx-VOC sensitivities and the zero-NOx-sensitivity are shown as lines (linear relationship). This potentially simplified the calculation of sensitivity compared to other methods (e.g., CTMs) using a more complex algorithm. Thus, in order to derive this relationship using CTMs, a heavy load of computation is required. Other methods involving a reduced form of CTMs can generate similar linear forms as well.

These results are particularly important in providing information on the variation of sensitivities of ODV to emissions, both temporally and spatially. This provides insightful input for policy making regarding future emissions at different locations. Since the ODV emissions response is spatially different, we also observed different patterns of those two ridgelines (Figure 2.2). Under the same emissions trends over the whole air basin (assumed), the relationship between the emissions trajectory and those ridgelines vary spatially. In the early years (for about 20–30 years), Pasadena and Azusa were in the more VOC-controlled region. Thus, the reduction of NOx could potentially elevate the ozone level. For LA, the base model and log model yielded opposite results. When examining more recent years, we noticed that all sites had crossed the zero-NOx-sensitivity lines, which means that further reductions in NOx emissions would be much more beneficial for ozone control. This observation is consistent with previous studies based on observations or empirical methods (Baidar et al., 2015; Henneman et al., 2017b; Pusede and Cohen, 2012; Qian et al., 2019). This finding is consistent with previous studies related to the weekday/weekend effect (Chow, 2003; Fujita et al., 2003).

We also noted that, while Azusa just crossed the zero-NOx-sensitivity line, LA crossed the equal NOx-VOC sensitivity line, which means it has been in the NOx-limited region, and further reductions of NOx will be more effective compared to other sites. This suggests that the optimum control strategy may vary by location, and the coastal area seems to benefit more from NOx reductions, at least in recent and future years.

2.5.3 Spatially Integrated Multivariate Regression Model

Another method used to develop ODV-emission relationships across multiple sites is the spatially integrated regression model. In this case, a single model was developed for all sites in the basin by including spatial variables along with emissions. Similarly, both a regular model and a log model were developed. After training the model with information from all the monitoring sites, we can obtain a relationship similar to EQNs 2.4 and 2.5, but including latitude and longitude. These equations can be used to develop an isopleth at any location (e.g., Azusa (Figure 2.3)). Isopleths for each site are found in Appendix A.

The model performance of the spatially integrated model is similar to that of the single-site models. For all 24 monitoring sites in this study, both methods (base quadratic model and log quadratic model) led to similar functional forms, and the average resulting R^2 was 0.92. This performance suggests that, at least near the observational values, the models are able to effectively capture how ozone responds to emissions changes, and also capture the spatial variations in the site-specific ODVs. By comparing the regression coefficient between the two methods, we noted that for the monitoring sites, the spatial model also caused about half (14 out of 29) of the sites to have incorrect signs. This observation supports the hypothetical reason mentioned earlier: Other factors may dominate the ODV variation when the ODV levels are low. More detailed comparison between those two methods is in the uncertainty analysis section.

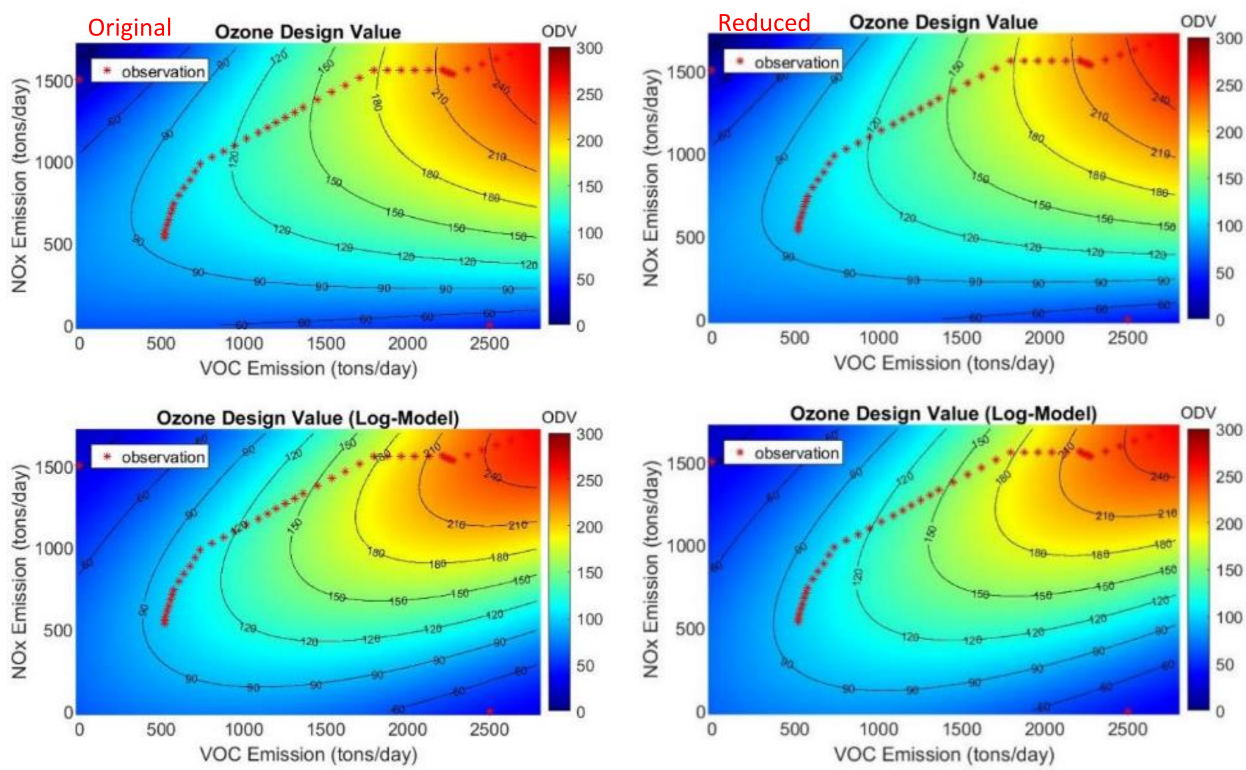

Figure 2.3 ODV-emissions isopleths constructed by spatially integrated multivariate regression model. Monitoring site is Azusa. The NOx-VOC emissions space is defined with various levels of estimated NOx and VOC emissions. ODVs calculated by the models are indicated by color. Historical emissions levels are marked as red spots. Left is the original model (full model), right is the reduced model. The first row is the developed isopleths based on regular models. The second row is the developed isopleths based on regular models.

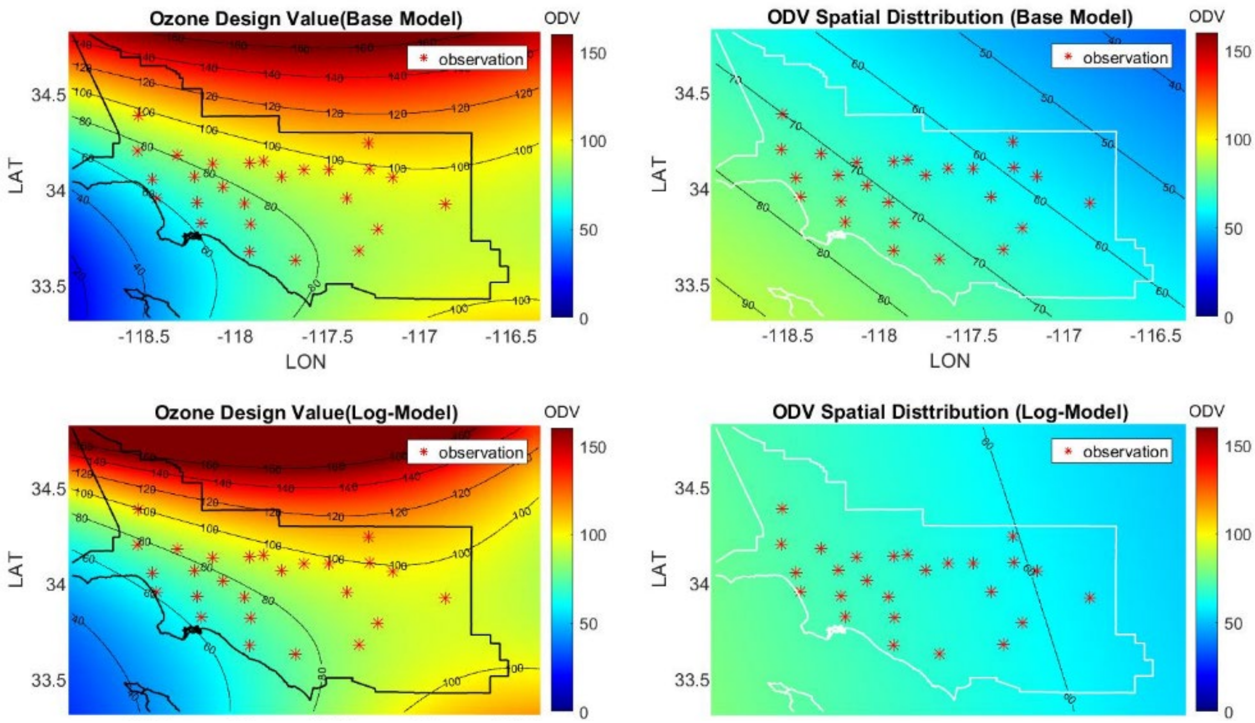

Figure 2.4 ODV spatial distribution over SoCAB estimated by spatially integrated multivariate regression model. ODVs calculated by the models are indicated by color. Monitoring sites are marked as red spots. Left is under current emissions level, right is under zero anthropogenic emissions. The first row is based on regular models. The second row is based on log models.

In addition to these full models, we also developed reduced models with fewer variables (by removing x, y, xy, x^2, and y^2) to trim the model to elevate performance and prevent overfitting. We also developed isopleths based on the reduced form for each site (e.g., LA North Main (Figure 2.3). Compared to the full model, the two isopleths are very similar (Figure 2.3).

The spatially integrated model has some advantages over the collection of models developed for each site, particularly given that the performance is similar. First, the spatial model can estimate the isopleth for locations without any monitoring site. Another application is to use the model to generate the ODV spatial distribution at varying emission levels (e.g., recent (Figure 2.4 left), and zero (Figure 2.4 right)). We see that, at recent emissions levels, the ODVs are lower along with the coast and increase when moving inland. Under zero anthropogenic emissions, the log model indicated that the ODVs would be almost constant over the air basin, though slightly higher at the coast. The base (non-log) model shows a higher level at the coast, with a stronger negative gradient going inland. The reduced variable model has a constant zero-emission level across the basin of X (base) and Y (log model).

Limitations of this method exist. To generate the proper ODV emissions equation requires the training set (monitoring sites) to cover the study domain. The estimation of an isopleth for a remote area may be significantly biased. Also, the estimation accuracy for one monitoring site can be compromised by other sites with low data quality.

2.5.4 Ozone Exposure Model Results

Comparing the base quadratic model and the log quadratic model, ozone exposure isopleths have similar patterns, while estimations of ozone exposure under high NOx and VOC emissions from the log quadratic model are higher than those from the quadratic model.

From the ozone exposure isopleths, ozone exposure decreased from 1980 to 2019 as VOC and NOx emissions decreased. For ozone exposure under high ozone levels (ODV, peak, higher than 60 ppb, 70 ppb), emissions were transferred from above the zero-NOx-sensitivity line to below the zero-NOx-sensitivity line. This means that controlling NOx emissions led to ozone exposure, which increased slightly in the earlier years while decreasing in recent years. Also, emissions in recent years have been below the equal NOx-VOC sensitivity ridgeline, which suggests that controlling NOx is beneficial for decreasing high-level ozone exposure. For exposures higher than 40 ppb ozone, emissions for most previous years were above the zero-NOx-sensitivity line, while emissions were below the zero-NOx-sensitivity line and near the equal NOx-VOC sensitivity line in recent years. That indicates controlling VOC was more effective in previous years, while either controlling VOC or NOx decreased exposure in recent years. For mean ozone exposure, emissions were above the zero-NOx-sensitivity line in recent years, which suggests that decreasing VOC emissions diminishes exposure from the mean ozone.

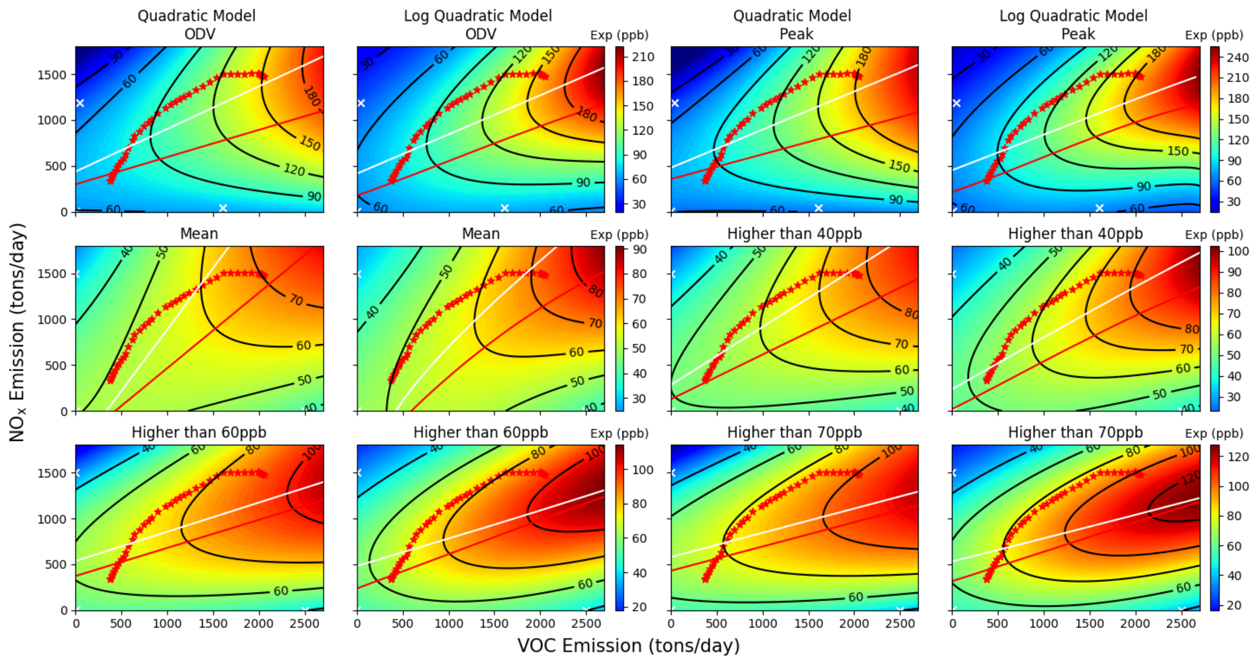

Figure 2.5 Ozone exposure isopleths developed by a reduced spatially integrated multivariate regression model and ozone values under different selection criteria. Ozone exposure values calculated by the model are indicated by color. Historical emission levels are marked as red spots. Included emissions for background ozone are marked as white crosses. White lines indicate zero-NOx-sensitivity ridgelines. Red lines indicate equal NOx-VOC sensitivity ridgelines.

2.5.5 Uncertainty Analysis

We conducted further uncertainty analysis to evaluate the model by comparing ODVs predicted by different methods (full spatially integrated model, reduced spatially integrated model, and single-site regression model). Figure 2.5 illustrates the model differences. For the predicted ODVs for historical emissions, we noted that the difference between the models was very small (Figure 2.6), and all the methods were highly consistent with each other, predicting ODVs significantly close to observation levels. This makes sense, since all the methods had a high R^2 individually.

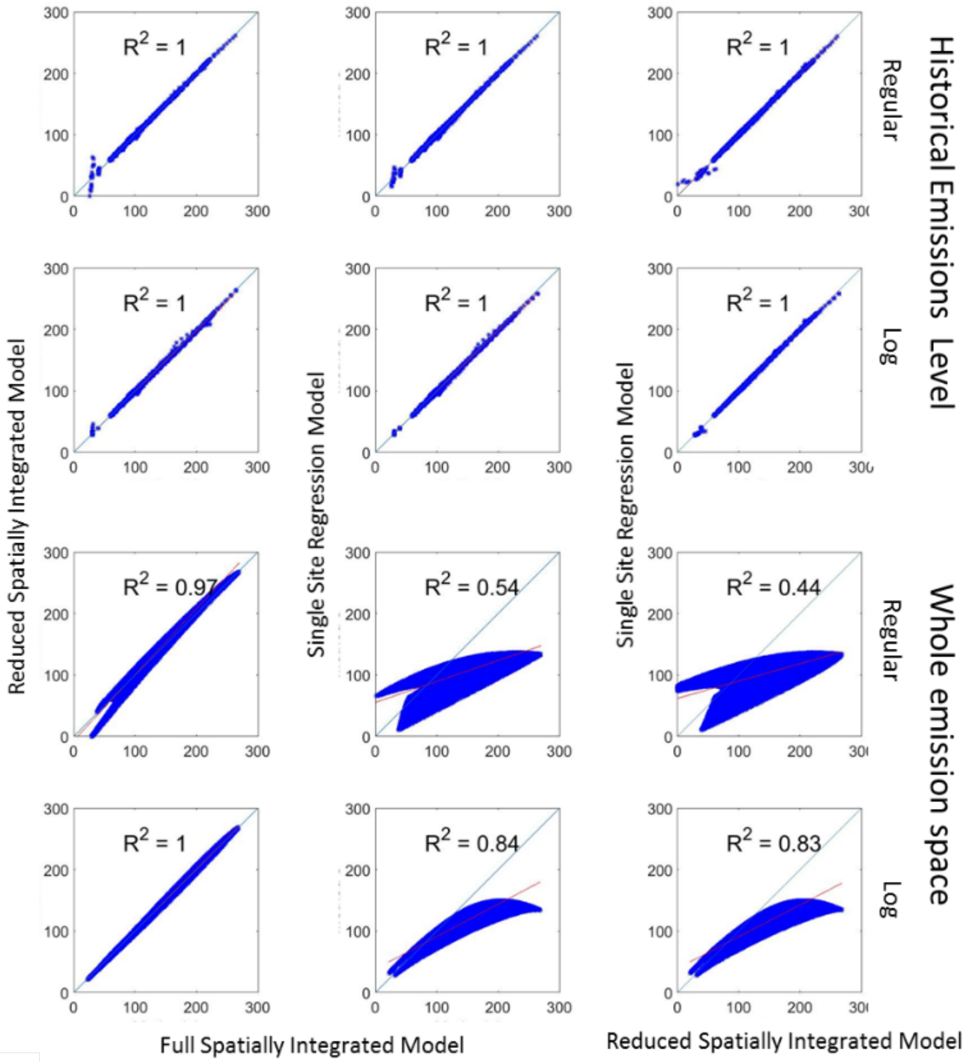

Figure 2.6 Comparison between predicted ODVs by different models for all of the monitoring sites. The first two rows are the comparison results for predicted ODVs under historical emissions levels. The last two rows are the comparison results for predicted ODVs over the whole emission space (comparison of isopleth generated by different models). The first and third rows show the result for the regular model and the second and fourth rows show the results for the log model.

When looking at the comparison between predicted ODVs under a wider range of emissions levels, which is actually a comparison between the isopleths generated by different methods, more deviations were observed. The difference between full and reduced spatially integrated models is still very small, which makes sense, since those two methods are very similar. On the other hand, predicted ODV isopleths show relatively larger deviations between the single-site model and the spatially integrated model, especially for the regular models. This indicates that, when the emissions levels get away from the observations, the uncertainty of these methods becomes greater. Similar to our previous findings between the regular and log models, the log model is able to significantly reduce the uncertainty. On the other hand, we noted that when ODV levels are relatively low, those methods agree well, indicating that for future prediction purposes, we expect these methods would have limited uncertainties.

For the high-order multivariate regression model, it is hard to use typical statistical methods to evaluate the uncertainty, since the design matrix can easily be ill-conditioned when the order is high. For this reason, we conducted a Monte Carlo analysis to evaluate the uncertainty of the ozone exposure models' results. Since the uncertainty of NOx and VOC emissions estimates are the main sources of ozone exposure model's uncertainty, and since previous work (Hassler et al., 2016; Henneman et al., 2017a; Kim et al., 2016; Pollack et al., 2013; Warneke et al., 2012) show that the emission trends are captured better than the values, it is reasonable to maintain the emission trends (decrease or increase between two years next to each other) while perturbing the change rate for each Monte Carlo experiment. We chose 1980 as the starting point and perturbed the change rate using a Gaussian distribution ~ $N(0, 0.2^2)$, and we also included the background ozone data as mentioned before in each experiment. After 1,000 experiments, a standard deviation was calculated to estimate the uncertainty of ozone exposure results. Figure 2.7 shows the uncertainty that corresponds to the ozone exposure results in Figure 2.5.

The uncertainty of the base and log quadratic models is relatively low along the observations from the least squares method. Also, the uncertainty near the emissions of background ozone data is low, since we include the same background ozone data for each experiment. By comparing the uncertainty with ozone exposure models, the relative uncertainties were lower than 5%. By comparing the two models, the log quadratic model has relatively higher uncertainty than the base quadratic model in high ozone level areas. This may be because the log quadratic form has a higher increase rate than the base quadratic form at high ozone level areas, which can be reflected by the derivatives of the forms of these two different models' formulas. The log quadratic model has relatively low uncertainty in regions with high NOx emissions and low VOC emissions. Also, the log quadratic model has comparable uncertainty when the emission levels are lower than the maximum of historical emissions. Since both the log quadratic model and the base quadratic model have lower uncertainty for low emissions levels, which are the current and expected future status of emissions, both models are acceptable for evaluating ozone exposure.

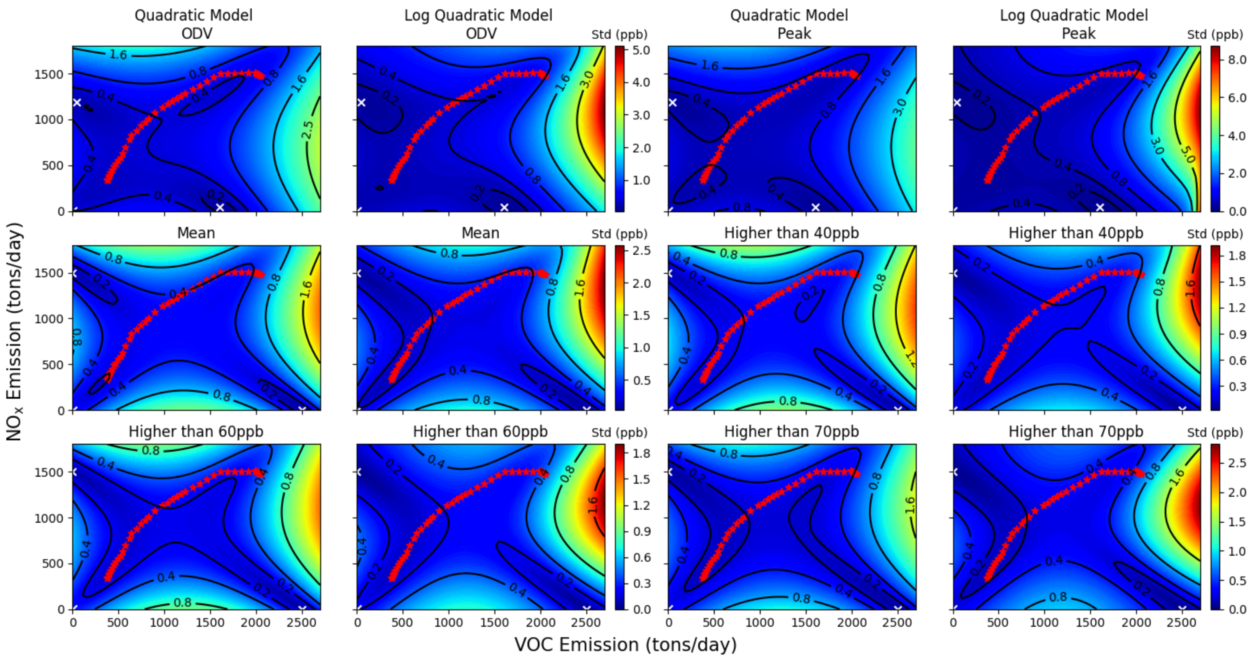

Figure 2.7 Ozone exposure uncertainty values estimated using the Monte Carlo method. Ozone exposure uncertainty calculated by the method is indicated by color. Historical emission levels are marked as red spots. Included emissions for background ozone are marked as white crosses.

2.6 Summary

In this section, we described the work we have done for the development and evaluation of the empirical methods to investigate the spatial variation of the response of ODV to NOx and VOC emissions changes. This study focuses on 24 single monitoring sites within the SoCAB. Two different methods were developed and applied: 1) a multivariant regression model with ODV of each monitoring site as the response variable and annual average estimated NOx and VOC emissions as the predictor variable in a quadratic formulation to be applied to each single monitoring site; and 2) a multivariant regression model, in addition to the single-site model, which further integrated the longitude and latitude data of monitoring sites as spatial information into the multivariant regression model to build a single regression model with the information from all sites being used to train the model. By applying the regression coefficients to an emission space defined by various levels of NOx and VOC emissions, we were able to construct the ODV emissions isopleth to reflect the response of ODV to emissions changes at different emissions levels.

One major finding from the results is that ODVs respond to emissions changes differently in different locations, which has also been investigated in previous studies (e.g., Milford et al., 1989). By comparing the isopleths of LA North Main and Azusa, it is obvious that the location near the coast (upwind) has relatively lower ODV levels, and the ODVs are less sensitive to emissions reductions compared to inland locations (typically downwind during high ozone periods). This is mainly caused by the meteorology and geographic features of the LA region and is related to the combined effects of surface sea breeze and mountain barriers. Sea breezes cause the transport of precursor pollutants from the coast inland, while mountain barriers lead to the accumulation of pollutants.

When examining the coefficient signs for the various locations, we noticed that the single-site log model had 12 out of 24 sites that contained at least two variables with coefficients of opposite signs than expected. Most of the sites with atypical isopleths are near the coast. These sites have lower ODVs and less reduction over time. When the ODV response to emissions reductions is small, and meteorology-induced fluctuations are apparent, it is more difficult to capture the relationship. For all except one case in the log model, an abnormal sign of the linear emission coefficient was found for the response to VOC emissions, and in that case, the quadratic term was also the opposite sign, offsetting the impact. This is tied to the lack of variation in the ODV over time to fully capture the non-linear response to VOC emissions. When moving on to recent years, we noticed that all the sites had crossed the zero-NOx-sensitivity lines, which means that further reduction of NOx emissions would be much more beneficial for ozone control.

For both methods, the average resulting R^2 is higher than 0.9. This suggests that, at least near the observational values, the models capture how ozone responds to emissions changes. In order to further test the predictive ability of this model, we also conducted 10-fold cross validation leading to stable results with a high R^2 (> 0.9) and low RMSE. This analysis indicates that the declines in the ODV in SoCAB over the past several decades were mainly (> 90%) caused by emissions reductions.

The spatially integrated model has some advantages over the collection of models developed for each site, particularly given that the estimated isopleth and observed performance are similar. Firstly, the spatial model can estimate the isopleth for locations without any monitoring site. Another insightful application is to use the model to generate ODV spatial distribution at varying emission levels. We see that at current emissions levels, the ODVs are lower along the coast and increase when moving inland. Under zero anthropogenic emissions, the log model indicated that ODVs would be almost constant over the air basin, although slightly higher at the coast. The base (non-log) model shows a higher level at the coast, with a stronger negative gradient going inland. The reduced variable model has a constant zero-emissions level across the basin of 55.6 ppb.

Overall, these results are particularly important in providing information on the variation of sensitivities of ODV to emissions, both temporally and spatially. This is an important input for policy making related to future emissions at different locations.

Chapter 3: Development of the Ozone-NOx-VOC Emissions Isopleth using CMAQ-HDDM and Inverse Distance-Weighted Method for Southern California

3.1 Introduction

California's South Coast Air Basin (SoCAB), which includes all of Orange County and parts of Riverside, Los Angeles, and San Bernardino counties, experiences the highest peak ozone levels in the US despite stringent controls. While significant ozone reductions have been realized, recent trends have found a leveling off in the ozone design value (ODV), with increases in some years. Multiple questions arise, including: 1. How will ozone respond to the proposed further emissions changes? 2. What is the most effective approach to reducing peak ozone levels and ozone exposure? 3. How effective have past controls been in relation to the advantages of NOx vs. VOC controls? 4. What is the ultimate background ozone level? and 5. How well do chemical transport models, which are used to develop control strategies, capture ozone trends and, more importantly, sensitivities to emissions?

Historically, many methods have been developed to explore this relationship, from smog chambers to box models to chemical transport models (CTMs; Jin and Demerjian, 1993; Kanaya et al., 2009; Kelly and Gunst, 1990; Menut et al., 2000; Milford et al., 1989; Sierra et al., 2013). Each of these approaches has its limitations, and arguably the least limited of the three, CTMs, has not been able to fully capture the observed ozone trends in Los Angeles.

The particular focus of this study is to conduct extensive air quality modeling of the SoCAB for a number of historical and future years to understand how well current CTMs capture ozone dynamics and the response to the controls of NOx and VOC. Our analysis includes more traditional approaches (e.g., modeling multiple years) and two approaches going beyond typical studies: 1) extensive first- and second-order sensitivity analysis (with uncertainty analysis of sensitivities), and 2) use of isopleths to provide a more direct, visual analysis tool (that can also be quantitative).

The use of isopleths is particularly attractive since they have been used widely in analyses of air quality control strategies in the SoCAB (Kinosian, 1982; William and Burke, 2016; Yang et al., 2021), and can be developed using CTMs such as CMAQ and CAMx (Hakami et al., 2004; Milford et al., 1989; Reynolds et al., 2004), box models (Fujita et al., 2003), and more recently, empirically constructed isopleths (Qian et al., 2019). Isopleths allow visual identification of the “ridge line” often used to suggest where NO_x or VOC emissions controls are most effective as well as regions where NOx emission reductions will actually lead to increased ozone.

3.2 Methods

CMAQ was applied to the SoCAB to elucidate the dynamics of ozone and its spatial and temporal responses to emissions using two meteorological periods and emission inventories for five different years. The simulated ozone levels and sensitivities were used to construct CTM-based ozone-emission isopleths, and identify potential biases.

3.2.1 Modeling Domain and Period

Chemical transport modeling, using CMAQ (version 5.0.2) and the CB6 mechanism (Yarwood et al., 2010) was conducted, first, for two 2016 episodes during which the SoCAB experienced high ozone: from June 2 to June 4 and from July 20 to July 29. The year 2016 was chosen as it is the focus year for a number of groups nationally, and is the base year for scientific and regulatory modeling using the 2016 NEI. A nested grid modeling domain was used. The outer domain covers the continental US using a 12 km horizontal resolution (Appendix Figure B.1), and the inner domain has a 156 × 165 4 km × 4 km horizontal grid covering the SoCAB region. The model height is approximately 11 km, with 13 vertical layers. The simulations span the period from June 1, 2016 to July 31, 2016. This two-month period generally covers a large fraction of the high ozone days during a typical year in most regions across SoCAB, including two of the highest ozone periods in 2016.

After model application and evaluation for the 2016 episodes, those meteorological fields were used along with emissions inventories for 1985, 2001, 2011, 2016 and 2028. The years 2001 and 2011 were chosen because they have been used extensively in prior modeling, 2028 was chosen as an EPA emissions platform year, 1985 was chosen as a historic year with high ozone, and aligns with the empirical analyses used to develop ozone isopleths for the SoCAB. Estimated 1985, 2001, and 2028 emissions were applied using the 2016 meteorology to separate meteorological influences from emissions changes, again focusing on the high ozone meteorologies. Past studies have shown that long-term meteorological changes are typically small compared to the impact of emissions, except at more extreme ozone levels, which is important for ozone control policies (Henneman et al., 2011; Russell et al., 2018).

3.2.2 Meteorological Modeling

The 2016 meteorological fields were generated using the Weather Research and Forecasting (WRF) model version 3.9.1.1, with inputs from NAM analysis and ADP observational datasets. The National Land Cover Database 2011 (NLCD2011) was used for land use in WRF simulations. Details on the WRF configuration options used can be found in Appendix Table B.1. The METSTAT program was used to evaluate the performance of the meteorological fields against TDL North American surface weather station observations. Model performance (Appendix Table B.2) was well within the guidelines.

3.2.3 Emissions

Emissions inputs for the years 2001, 2011, 2016, and 2028 were developed using the EPA's emissions modeling platforms ("www.epa.gov/air-emissions-modeling/2014-2016-version-7-air-emissions-modeling-platforms"). Emissions for 2011 were developed using the 2011v6.3 Platform with the 2011en_11g inventory, while emissions for 2016 used the 2016v7.2 (beta and Regional Haze) Platform with the 2016ff_16j inventory, and emissions for 2028 used the 2016v1 Platform with the 2028fh_16j inventory. Emissions for 2001 were developed using the 2011v6.1 Platform with the 2002ef_11g inventory used by the EPA to support the Chesapeake Bay Study, and were combined with CEM emissions for 2001 and fire emissions from 2001 v2 inventory (US EPA, 2001).

When utilizing these recent EPA emissions modeling platforms, the four years' model-ready emissions were internally consistent with each other. BEIS was used to produce biogenic emissions off-line to help ensure consistency. These emissions modeling platforms all use SMOKE programs to generate hourly, gridded, model species emissions fields that CMAQ requires as inputs. However, due to the development of national emissions inventories over the years, newer versions of the SMOKE program are used for the later years. Emissions inventories from CARB for the same years were used as reference for comparison to the NEI inventories. The 2016 inventory is the product of extensive analysis by the US EPA and other federal, state, local, tribal, and industrial stakeholders. This was chosen as the primary inventory given the extensive, and recent, analyses that went into its development. All NEI emissions inventory totals for different pollutants were compared with the CARB inventory for the same year to make sure the total levels and trends were consistent (see Appendix Table C.2).

There was no spatially and temporally detailed inventory available for 1985, so one was constructed based on back-casting the 2016 inventory, accounting for changes in sources (e.g., industrial, transportation, and population-linked activities) and population distributions. The spatial redistribution of emissions was done using census data (Manson et al., 2020) and annual emissions (CEPAM, 2009), and source- and county-specific estimates from CARB (the historical CARB emission estimates for 1985 are given by county for California but are not spatially more refined.) County-specific, spatially detailed, population data were obtained for each county in the 4 km inner modeling domain (in and outside of the SoCAB). Census data for 1980, 1990, and 2016 were available, and 4 km, gridded (using the same grid as used for CMAQ modeling) population fields for 1985 (the average of 1980 and 1990) and 2016 were constructed. County-level population was then used to calculate the population in each 4 km x 4 km grid (Appendix Figure C.1).

County-level, source-specific emissions data for 1985 and 2016 were collected from CARB's standard emissions tool, including criteria pollutants in the form of detailed emissions categories, which were then regrouped into source sectors. The ratio of emissions between 1985 and 2016 was found for each county and combined with population fields to evaluate how much emissions changed in each grid cell, for each pollutant, and for each source sector (Appendix Figure C.2). The 1985 VOC speciation was modified using historical data (Harley et al., 1992). Further details of the calculation can be found in Appendix C.

The generated 1985 emissions were compared with CARB's 1985 emissions inventory (Appendix Table C.1) and were found to be consistent, although not the same, because the 2016 CARB inventory is not the same as the 2016 NEI. Also, for those counties not entirely within the 4 km modeling domain (Fresno, Inyo, Monterey, and San Benito), the calculated total emissions used in the modeling are lower than the county total emissions. The extreme case is San Benito, since only a very small part of it is in the 4 km domain. Another major difference is that some of the counties outside of the SoCAB had high fire-related emissions, and these are not included here because those same fires likely would not have occurred in prior or future years, and the focus here is on anthropogenic emissions impacts.

3.3 Chemical Transport Modeling

CMAQ with the high-order decoupled direct method (HDDM; Cohan et al., 2005; Dunker, 1981; Dunker, 1984; Dunker et al., 2002; Hakami et al., 2003; Hakami et al., 2004; Yang et al., 1997) was used to simulate pollutant concentrations and calculate both first- and second-order pollutant sensitivities for the June 2 to June 3 and July 20 to July 29 periods that had the highest ozone levels within the June–July period.

CMAQ-HDDM was used to calculate the semi-normalized first- and second-order sensitivities of ozone concentration to anthropogenic NOx and VOC emissions. The sensitivity coefficients are expressed in the same units as ozone concentration as follows:

$$S_V = \frac{\partial C_{O_3}}{\partial \varepsilon_V} \qquad \text{(EQN 3.1)}$$

$$S_N = \frac{\partial C_{O_3}}{\partial \varepsilon_N} \qquad \text{(EQN 3.2)}$$

$$S_{VV} = \frac{\partial^2 C_{O_3}}{\partial \varepsilon_V^2} \qquad \text{(EQN 3.3)}$$

$$S_{NN} = \frac{\partial^2 C_{O_3}}{\partial \varepsilon_N^2} \qquad \text{(EQN 3.4)}$$

$$S_{VN} = \frac{\partial^2 C_{O_3}}{\partial \varepsilon_V \partial \varepsilon_N} \qquad \text{(EQN 3.5)}$$

The model was evaluated using observations taken throughout the basin, including ozone, NO_2, and CO. We used 24 monitoring sites because they had more continuous and comprehensive monitoring data throughout the study period. There was limited monitoring of VOC speciation, which was used to assess how well the modeling captured VOC trends.

3.4 Developing CMAQ-HDDM-based Isopleths

In this study, we conducted a set of 15 CMAQ-HDDM simulations with different emission levels (Fig. 3.1; Table 3.1). Eleven of the cases were used to develop ozone isopleth diagrams. Those scenarios include emissions for the five years discussed above (1985, 2001, 2011, 2016, and 2028). Also, starting with the 2016 as base emissions, five adjusted emissions levels were developed and used for the CMAQ-HDDM simulations, including those with 1% of the 2016 NOx and VOC emissions, 10% of the 2016 NOx emissions with 100% and 400% VOC emissions levels, and 10% of the 2016 VOC emissions with 100%, 200%, and 300% of the NOx emissions levels. These adjusted emissions scenarios were used to help cover the low emissions region over the emissions space and reduce uncertainties in those regions. In addition to the 11 emissions cases used directly for developing the ozone-emissions isopleth, four other cases with adjusting the NOx and/or VOC emissions by ± 10% around the 2016 base case were conducted to evaluate the accuracy of the first- and second-order sensitivities calculated using CMAQ-HDDM. This will be discussed in detail later in a section regarding uncertainty analysis.

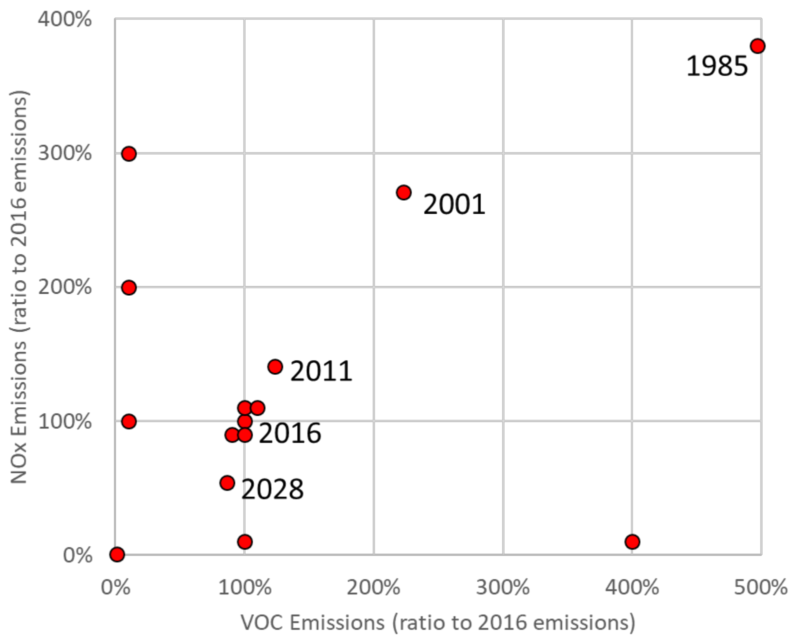

Figure 3.1 Emissions Levels of CMAQ-HDDM simulations in the emissions space

*Table 3.1 List of 15 emissions levels used for CMAQ-HDDM simulations, including the absolute levels of emissions for NOx and VOC in tons/day, and the ratios to 2016 emissions. *: indicates the cases used for developing ozone-emissions isopleth*

Cases	NOx Emissions		VOC Emissions	
	(tons/day)	*ratio to 2016*	*(Tons/day)*	*ratio to 2016*
***base(2016)**	396	100%	401	100%
***1985**	1506	380%	1993	497%
***2001**	1073	271%	894	223%
***2011**	557	141%	494	123%
***2028**	215	54%	346	86%
***1%**	4	1%	4	1%
***n10v100**	40	10%	401	100%
***n10v400**	40	10%	1604	400%
***n100v10**	396	100%	40	10%
***n200v10**	792	200%	40	10%
***n300v10**	1188	300%	40	10%
n90v90	356	90%	361	90%
n90v100	356	90%	401	100%
n110v100	436	110%	401	100%
n110v110	436	110%	441	110%

In constructing isopleths used both first- and second-order sensitivities, two separate approaches were used to develop isopleths. In one case, isopleths were generated for each of 11 cases (Table 3.1, marked with *), individually based on the simulated ozone levels and the first- and second-order sensitivities with Taylor series expansion (as described by Hakami et al., (2004)). In essence, the sensitivities act as terms in a quadratic Taylor series that are then multiplied by the emissions. It was expected that the individual isopleths would be most accurate near the emissions levels used. The 11 isopleths were then blended using distance-based (in emissions space) square root inverse distance weighting (SRIDW). The different cases had markedly different shapes, reflecting the relationship under certain emissions levels, and the blended case led to an isopleth similar to that observed using the empirical approach to reflect the overall response between ozone and emissions.

The 11 CMAQ-HDDM simulations model ozone concentration and sensitivities on 11 different NOx and VOC emission levels (i.e., 1%, 100% of NO_x, 2001, 2011, 1985, 2028, and several corner values) corresponded to 11 “reference points” on ozone concentration isopleth diagrams derived for monitoring sites. In the ozone concentration isopleth diagrams, the x-axis denotes the percentage of the total anthropogenic VOC emission, the y-axis denotes the percentage of the total anthropogenic NOx emission, and the isopleths themselves represent ozone concentration. The 11 simulations provide ozone levels and their first- and second-order sensitivities at the 11 reference points. The partial derivatives at the 11 reference points were then normalized to the unit of 100% 2016 emissions as follows:

$$\frac{\partial C_{O_3}}{\partial x} = S_V(x, y) \times \frac{1}{x} \qquad \text{(EQN 3.6)}$$

$$\frac{\partial C_{O_3}}{\partial y} = S_N(x, y) \times \frac{1}{y} \qquad \text{(EQN 3.7)}$$

$$\frac{\partial^2 C_{O_3}}{\partial x^2} = S_{VV}(x, y) \times \frac{1}{x^2} \qquad \text{(EQN 3.8)}$$

$$\frac{\partial^2 C_{O_3}}{\partial y^2} = S_{NN}(x, y) \times \frac{1}{y^2} \qquad \text{(EQN 3.9)}$$

$$\frac{\partial^2 C_{O_3}}{\partial x \partial y} = S_{VN}(x, y) \times \frac{1}{x} \times \frac{1}{y} \qquad \text{(EQN 3.10)}$$

where x and y are emissions of the 11 reference points and represent the percentages of VOC and NOx emissions to the 2016 emissions, respectively. For example, the emissions of 1%, 1% represents 1% of 2016 VOC emissions and 1% of 2016 NOx emissions. SV(x, y), SN(x, y), SVV(x, y), SNN(x, y), and SVN(x, y) are modeled sensitivities at the emissions level (x, y). Using SRIDW, we generated the isopleths in the $\sqrt{x}$-$\sqrt{y}$ plane (with the coordinates of square root-transformed x and y). Based on our tests, ozone isopleths generated in this plane were better shaped in terms of the overall pattern and smoothness than those generated in the original x-y plane.

A major challenge in constructing isopleths generated by different emissions scenarios was that the isopleths for a few of the sites were not smooth. As such, we also developed a quadratic fitting method. Qian et al. (2019) developed empirical ozone isopleths using quadratic and log quadratic forms to capture the relationship between ODV, emissions of NOx, and VOC. To develop ozone isopleths utilizing ozone concentrations and sensitivities derived from CMAQ-DDM, we developed quadratic and log quadratic forms using least squares fitting. Similar to the empirical method, a quadratic model was introduced to build the isopleth, which assumed that the ozone concentration $[O_3]$ or the $\log_{10}([O_3])$ had a quadratic relationship with NO_x and VOC emissions:

$$\begin{aligned}&\mathrm{O_3(NO_x, VOC)\ or\ \log_{10}(O_3(NO_x, VOC))}\\&\quad = \mathrm{a_0 + a_1NO_x + a_2VOC + a_3NO_xVOC + a_4NO_x^2 + a_5VOC^2}\end{aligned}$$

EQN 3.11

To find the parameters in Equation 3.11, we used least squares to fit the following system of equations to the simulated ozone level and its sensitivities (where the response variable was either the ozone concentration or log ($[O_3]$):

$$
\begin{cases}
O_3\left(\mathrm{E_{NO_x}}, \mathrm{E_{VOC}}\right)_{\mathrm{sim_i}} = \beta + \alpha_{\mathrm{NO_x}}\mathrm{E_{NO_x}} + \alpha_{\mathrm{VOC}}\mathrm{E_{VOC}} + \alpha_{\mathrm{NO_x-VOC}}\mathrm{E_{NO_x}}\mathrm{E_{VOC}} + \alpha_{\mathrm{NO_x}^2}\mathrm{E_{NO_x}}^2 + \alpha_{\mathrm{VOC}^2}\mathrm{E_{VOC}}^2 \\
\left(\frac{\partial O_3}{\partial \mathrm{E_{NO_x}}}\right)_{\mathrm{sim_i}} = \alpha_{\mathrm{NO_x}} + \alpha_{\mathrm{NO_x-VOC}}\mathrm{E_{VOC}} + 2\alpha_{\mathrm{NO_x}^2}\mathrm{E_{NO_x}} \\
\left(\frac{\partial O_3}{\partial \mathrm{E_{VOC}}}\right)_{\mathrm{sim_i}} = \alpha_{\mathrm{VOC}} + \alpha_{\mathrm{NO_x-VOC}}\mathrm{E_{NO_x}} + 2\alpha_{\mathrm{VOC}^2}\mathrm{E_{VOC}} \\
\left(\frac{\partial^2 O_3}{\partial \mathrm{E_{NO_x}}\,\partial \mathrm{E_{VOC}}}\right)_{\mathrm{sim_i}} = \alpha_{\mathrm{NO_x-VOC}} \\
\left(\frac{\partial^2 O_3}{\partial \mathrm{E_{NO_x}}^2}\right)_{\mathrm{sim_i}} = 2\alpha_{\mathrm{NO_x}^2} \\
\left(\frac{\partial O_3}{\partial \mathrm{E_{VOC}}^2}\right)_{\mathrm{sim_i}} = 2\alpha_{\mathrm{VOC}^2}
\end{cases}
$$

(EQN 3.12)

The left-hand sides of the equations were derived from CMAQ-simulated results. The sensitivities were derived from the CMAQ-DDM-3D model (Napelenok et al., 2006). This was done using 15 emissions levels, leading to a system of 90 equations to find the 6 parameters. For the log quadratic model, the left-hand sides were derived by the chain rule of derivatives based on the simulation results (see Appendix D).

3.5 Results and Discussion

3.5.1 Model Performance Evaluation

CMAQ simulation results were evaluated by comparing the simulated species concentrations with the observed species concentrations (sensitivities are not directly observed, so they cannot be evaluated directly). Here, model performance is evaluated using maximum daily averaged eight-hour ozone, daily averaged CO, and daily averaged NO_2. Because the 2016 meteorology is used throughout, first, the direct model evaluation was done for 2016 using observations matched in time and space. Given that the simulations for the other years also used the 2016 meteorology for consistency of results, an indirect evaluation was developed that uses rank ordering of pollutant concentrations and comparisons of NO_2 and CO observations.

3.5.2 Model Performance Evaluation for 2016

A traditional model performance evaluation was conducted for the 2016 simulation period for the SoCAB (Figure 3.2 and Table 3.2). As seen, ozone performance was generally within the guidelines suggested by previous studies (Emery et al., 2017; Simon et al., 2012). CO and NO_2 levels were also captured.

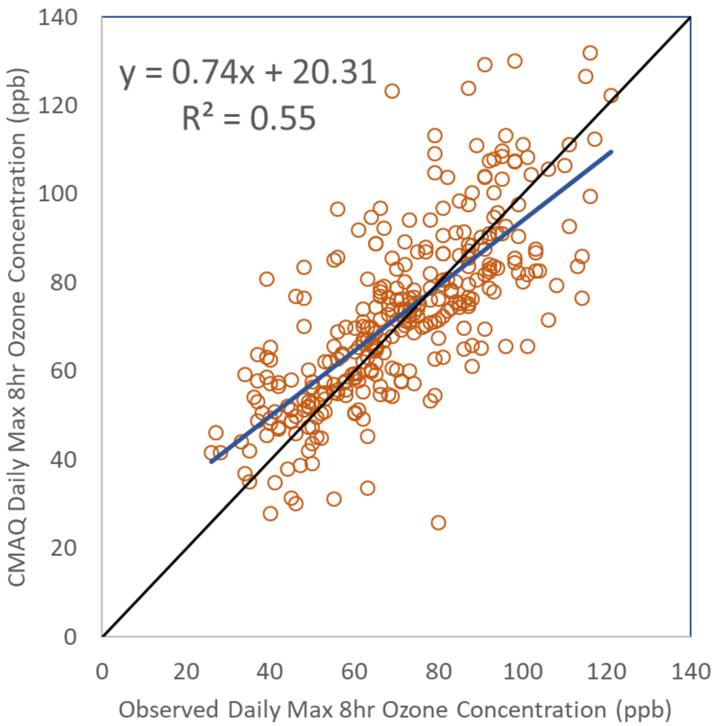

Figure 3.1 Comparison between CMAQ-simulated and observed MDA8 ozone concentrations for all 24 monitoring sites over the 13-day period

Table 3.2 Comparison statistics between CMAQ-simulated and observed MDA8 ozone concentrations for all 24 monitoring sites over the 13-day period

N	312
Mean Model (ppb)	72.6
Mean Obs (ppb)	70.8
MB (ppb)	1.75
ME (ppb)	10.71
NMB (%)	2.5%
NME (%)	15.1%

3.5.3 Model Performance Evaluation for 1985, 2001 and 2011, and Implications

Given that the meteorologies being used were for 2016, not for 1985, 2001, or 2011, a rank-ordered method was used to assess how well the model captured high ozone levels experienced in years other than 2016. Specifically, we picked the peak ozone periods of each individual year with the same length of 13 days, ranked the observed concentrations of all available sites for that period from high to low, and did the same thing for the simulated concentrations. Both the 2011 and 2016 comparisons show high consistency between the simulated and observed MDA8 ozone concentrations (Figure 3.3). These results indicate that the CMAQ simulations captured peak ozone values over our simulated periods.

However, the 1985 and 2001 peak ozone results were biased low by about 20% compared to the observations. There are multiple potential reasons that could have led to this bias, including a bias on the estimated emissions, the mismatch of the meteorology, a bias in the CMAQ chemistry, and other modeling errors. Based on the 2011 and 2016 results, we can see that the model is able to capture peak ozone levels, so we investigated factors other than the model that may have caused the bias between the simulations and observations.

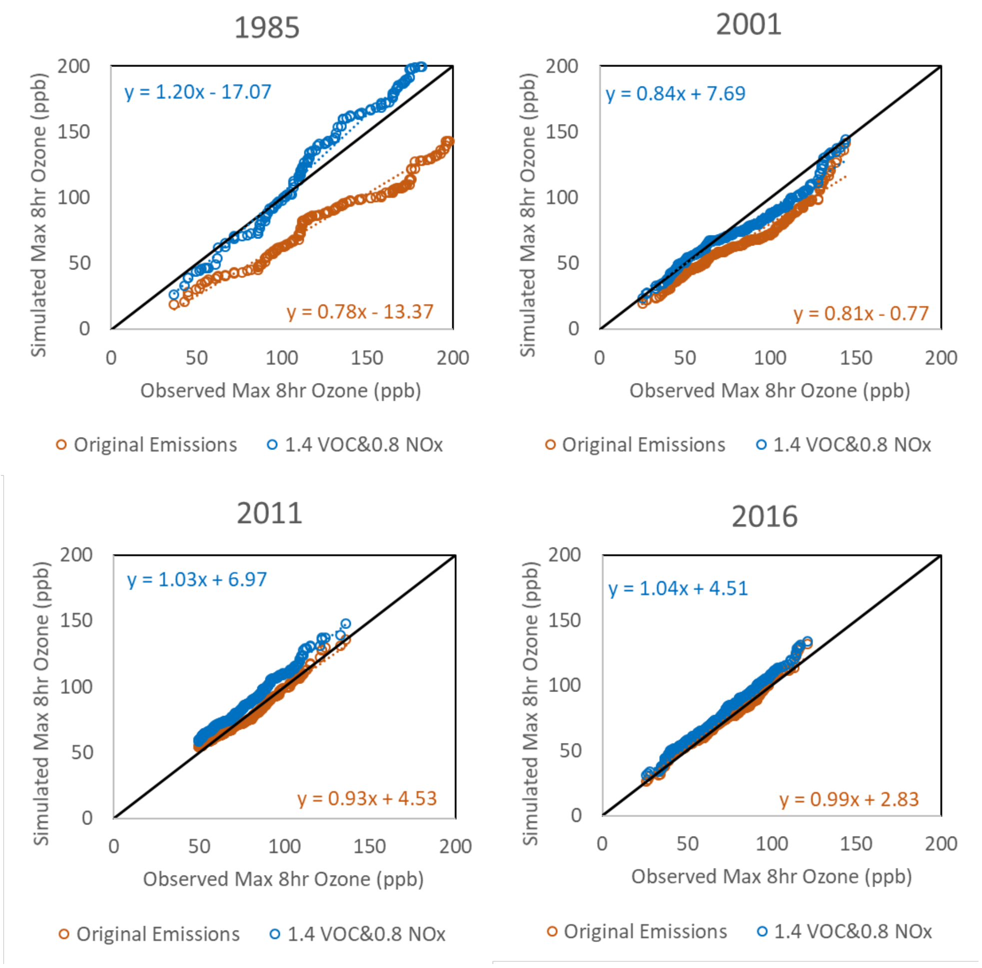

Figure 3.3 Comparison between simulated and observed ozone concentrations (ppb) in a rank-ordered base for 1985, 2001, and 2016. The orange dots indicate the simulation based on original inventory-based emissions, and the blue dots indicate the adjusted emissions with 40% increased VOC and 20% decreased NOx.

3.5.3.1 Potential emissions inventory biases

We adjusted the emissions levels and performed comparisons with the original simulations to identify the impact of differences in emissions on the simulated ozone levels. Based on the DDM-simulated sensitivities and ozone levels for 1985, we tested the projected ozone levels with adjusted emissions. We then conducted another simulation with the 1985 VOC emissions increased by 40% and NOx emissions increased by 20%. After that adjustment, the simulated ozone increased by about 20% compared to the original simulation result (Figure 3.3). Based on the rank-ordered comparison between simulated and observed MDA8 ozone before the adjustment, the simulated ozone was systematically more than 20% lower, and after the adjustment, the comparison was closer, though slightly biased high.

The analysis above implies that the major cause of the underestimation of peak ozone levels relates to the estimated emissions for certain years (e.g., 1985 and 2001). Though the simulated ozone levels for 2011 and 2016 were more consistent with the observed ozone levels, this does not necessarily mean that the emissions for those years were less biased compared to other years, since the ozone-emissions response was different for different years. The effect of emissions bias can differ based on emissions levels. For this reason, we conducted similar analyses for 2011 and 2016 to estimate the projected ozone levels based on the same emissions adjustment. The results show that with the same 40% increase in VOC emissions, simulated ozone levels would not change significantly, since under the emissions levels of those two years, the ozone levels were much less sensitive to VOC emissions compared to 1985 and 2001 emissions levels. Thus, it is possible that the bias on the estimated emissions exists all the time, rather than only for certain years.

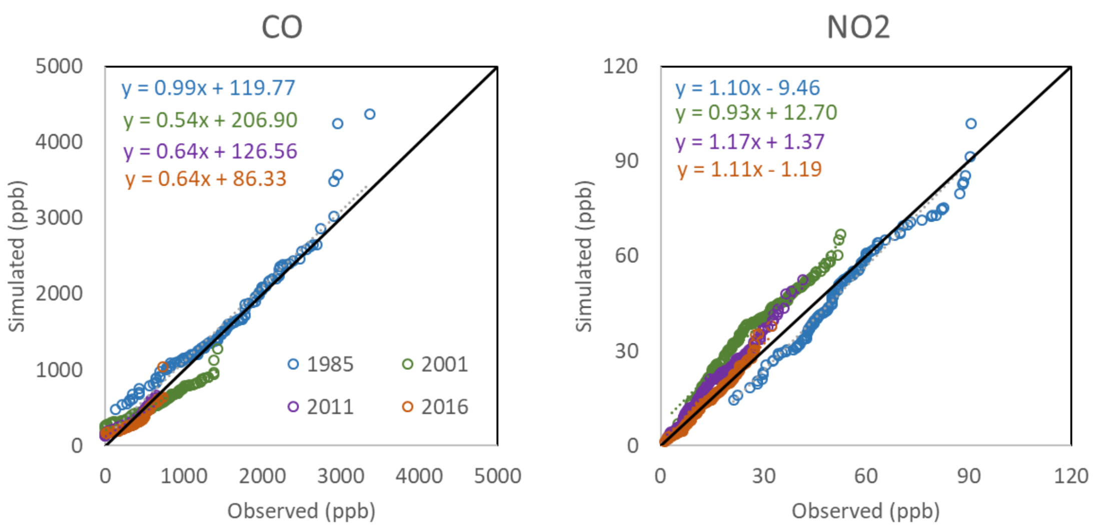

Figure 3.4 Comparison between simulated and observed daily average CO and NO_2 concentrations for all sites together over the simulation period. Different colors indicate different years.

To further understand the details related to this issue, the simulated CO and NO_2 concentrations were compared with the observations (Figure 3.4) based on the rank-ordering method. We evaluated the accuracy of the estimated VOC emissions by comparing the simulated and observed VOC levels. However, VOC, as both a primary and secondary pollutant, is a mixture of more than 50 species. The process between emissions and species concentrations is complicated and may not be directly comparable. Additionally, the VOC observation data were not comprehensive and consistent enough to allow us to conduct the comparison. These factors created difficulties in directly evaluating the estimated VOC emissions.

CO and VOC emissions are always highly correlated, because they are mostly emitted from the same sources (Pollack et al., 2013). Considering the long lifetime and limited production pathway of CO, the ambient concentration is highly controlled by its primary emissions and highly correlated with the CO emissions. Thus, the comparison between simulated and observed CO concentrations can be used to partially evaluate the CO emissions and, further, as an indirect evaluation of the VOC emissions. Though not the case for each year, there is a tendency for the simulated CO levels to be lower than the observed levels for relatively high CO levels (Figure 3.4). This finding implies that the estimated CO emissions based on the inventory are potentially lower than the real emissions, which would be similar for VOC emissions.

A similar analysis can also be applied to evaluate the estimated NO_2 concentrations since NO_2 concentration is also highly controlled by the emissions levels. The results show that, besides 1985, the simulated NO_2 levels tended to be higher than the observed NO_2 levels, especially when NO_2 concentrations were high (Figure 3.4). Since both NOx emissions and NO_2 concentrations have a significant diurnal variation, to further understand the difference between simulated and observed NO_2 levels, we investigated the day/night agreement separately and compared the diurnal variation of simulated NO_2 concentrations, observed NO_2 concentrations, and NOx emissions between different years. The results showed that for 2001, the night time NO_2 concentrations tended to be higher by about 20% compared to the observations, though the daytime NO_2 concentrations agreed relatively well with the observations (Figure 3.5). However, we did not see the same pattern for 2016 (Figure 3.5).

Hence, we hypothesized that the larger bias overnight for 2001 and 2011 was more related to emissions than meteorology because we used the same 2016 meteorology input for all four years. When we look at the diurnal trend of both NO_2 concentrations and NO_x emissions, it is clear that the patterns of both concentrations and emissions differed between 2001 and 2016 (Figure 3.5). Basically, the 2001 NOx emissions peaked at around 15:00, which was about three hours later than the 2016 peak. This finding implies that the emissions inventory allocated excessive NO_x emissions in the later afternoon. When the photochemistry shuts off, the mixing height goes low, and considerable NOx emissions are still introduced, NO_2 can accumulate during the night because of the lack of consumption pathway. Though the difference in diurnal variation patterns of NOx emissions between 2001 and 2016 is possible, the inconsistency between simulated and observed NO_2 concentrations over day and night for 2001 implies that the temporal distribution of 2001 NOx emissions may be problematic.

This finding may partially explain why the 2001 simulated ozone levels were lower than the observed ozone levels. We also looked at the NO_2 to CO ratio based on both the simulated and observed concentrations for each reference year, and found that the simulated NO_2 to CO ratios had the trend of first increasing and then decreasing, which agrees well with the observed ratios trend (Figure 3.6). This trend is consistent with the relative trend of the reduction rate between NOx and CO or VOC (Fujita et al., 1992; Pollack et al., 2013). This finding also indicates that the difference between simulated and observed NO_2 to CO ratios is consistent over the years; the simulated NO_2 to CO ratio is consistently about 1.5 to 2 times of the observation ratio. This difference provides further evidence of bias in the emissions inventory and is consistent with our previous finding that the estimated VOC emissions should be about 40% higher and the estimated NOx emissions should be about 20% lower.

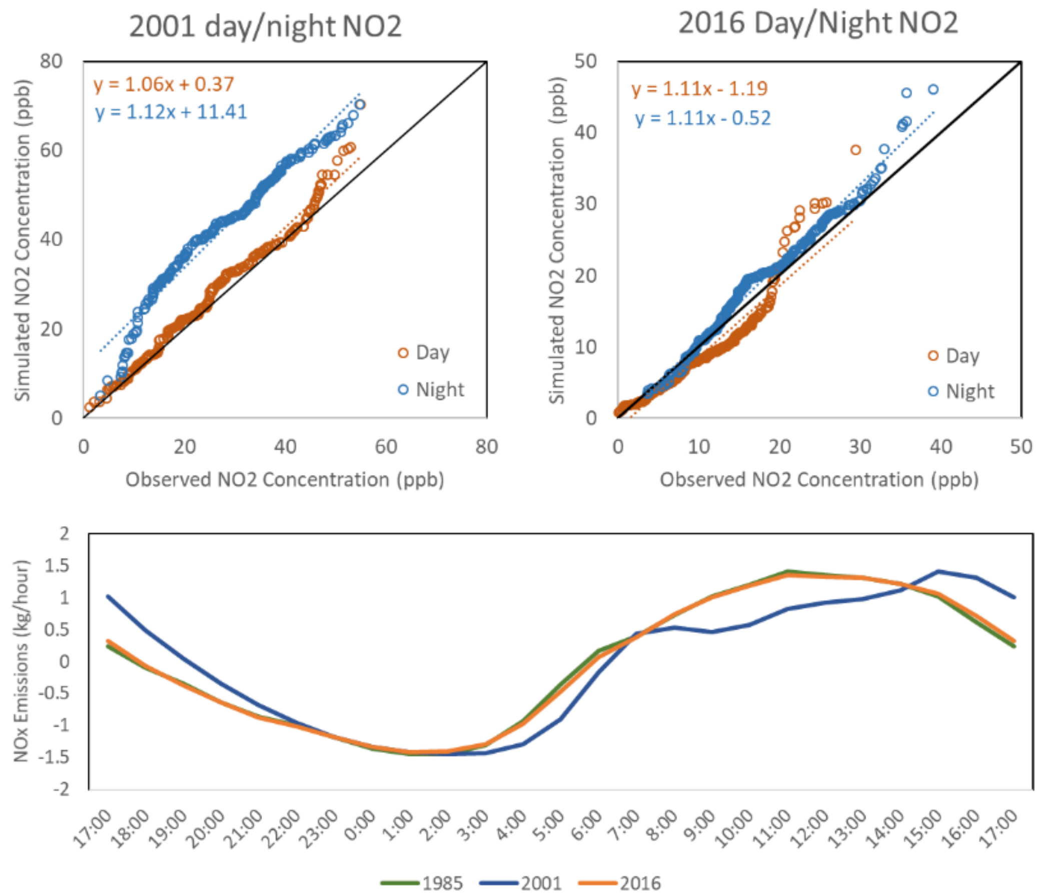

Figure 3.5 Upper row: The comparison between simulated and observed day and night NO_2 concentrations (ppb) in a rank-ordered base for 2001 and 2016. The orange dots indicate the day time NO_2 concentrations and the blue dots indicate the night time NO_2 concentrations. Lower row: Normalized NOx emissions diurnal cycle comparison between 1985, 2001, and 2016.

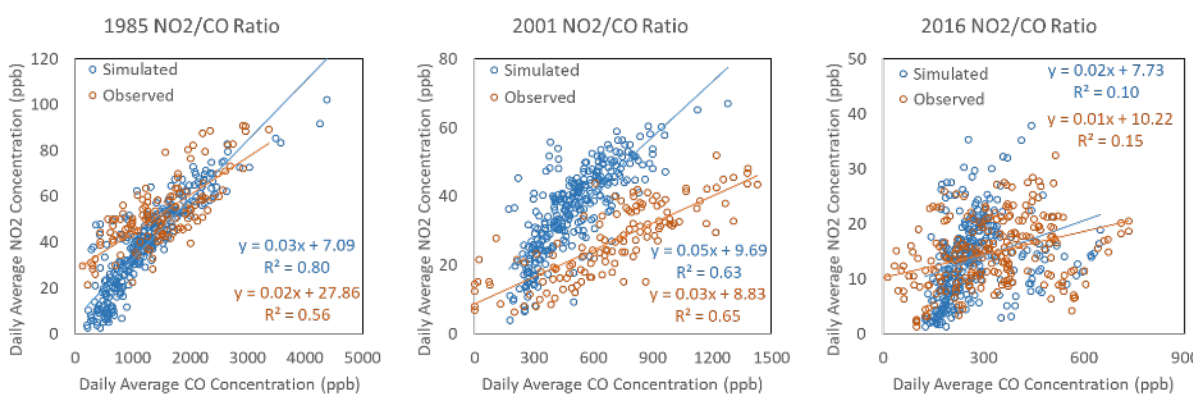

Figure 3.6 Comparison between rank-ordered, simulated, and observed NO_2 and CO concentrations (ppb) for 1985, 2001, and 2016. The orange dots indicate the observed concentrations, and the blue dots indicate the simulated concentrations. Also shown are the linear fits of the NO_2 to CO relationships for both the observed and simulated concentrations. The differences in the slopes of the simulated vs. observed NO_2:CO relationships suggest a potential bias in the mobile source inventory.

With this evidence that the estimated emissions are potentially biased, which leads to a bias in the simulated ozone levels, we further investigated the adjusted emissions trend based on the comparison between isopleth-estimated and observed peak ozone trajectories over the past four decades. By applying a quadratic fit between these two trajectories, we obtained the adjustment coefficients for both VOC and NOx emissions to fit the observed historical trends. This will be discussed in more detail in the following section.

3.5.3.2 Assessing potential biases in the 1985 simulations based on emissions inventory construction

As discussed above, since the rank-ordered ozone in 1985 was biased low by about 20–25% (Figure 3.3), it was necessary to reconstruct a 1985 inventory. We based it on the 2016 NEI inventory that was used for the base case modeling for consistency but used both the spatial distribution and VOC speciation based on available data. We tested the impact of both procedures on our results to assess whether they led to any of the model biases.

3.5.3.2.1 Impact of re-speciating VOC emissions

We investigated VOC emissions composition around 1985 (Harley et al., 1992), mainly for mobile sources and solvents. Using the adjusted VOC emissions, we conducted another simulation and compared it with the original results. We conducted a simulation using the original source-specific VOC speciation used in the 2016 base case. The two sets of results were very similar (Appendix Figure C.3), suggesting that the change in VOC composition between the 2016 and 1985 emissions inventory did not change the simulated ozone significantly.

3.5.3.3 Effect of simulation period

Another potential issue causing bias in the estimated ozone levels is the mismatch of the high ozone period. For the CMAQ-DDM simulation, we picked the high ozone period based on 2016 observations and applied this same period to 1985 simulation. The basic assumption here is that the high ozone periods, while not on the same days, would have similar photochemical activity, although we recognize that this is not always the case. In order to evaluate this in more detail, we conducted another set of simulations for a three-month period from May to July, 2001, which is typically the high ozone season for most years. We still used the rank-ordered method used to compare the simulated and observed ozone concentrations for the three-month period. Similar to the 13-day period, the simulated ozone levels of 1985 for the three-month period were still systematically lower than the observed ozone by about 30%, but the simulated 2016 ozone levels agreed well with the observations (Appendix Figure C.4). Further discussion and results are found in Appendix C. These analysis suggest, but do not fully rule out, that using the 2016 meteorology for all of the analyses, and in particular for 2001, have limited impact on the model bias over time.

3.5.4 CMAQ-HDDM-based Isopleths

Ozone isopleths for the 24 sites were developed using the SRIDW method (Appendix E). On the isopleths, we added the $S_N = S_V$ and SN = 0 lines (Figure 3.7). The SN = SV line divides the diagram into two major regimes: above this line is the VOC-limited regime, where VOC reduction is more effective for reducing ozone concentration, and below this line is the NOx-limited regime, where NOx reduction is more effective. Above the SN = 0 line outlines the NOx-saturated regime—a part of the VOC-limited regime, where NOx reduction increases ozone concentration (Figure 3.7). The sensitivities of ozone concentration to NOx and VOC emissions show an overall VOC-limited regime in SoCAB (SN = 2.4 ppbV, SV = 5.3 ppbV, SN/SV = 0.45), suggesting that VOC reduction is more effective for ozone concentration mitigation, although both NOx and VOC reductions are beneficial. The second-order sensitivities of SNN, SVV, and SNV were -11.0, -3.1, and 5.0 ppbV, respectively. Negative SNN and SVV reflect an increase in SN and SV as the emissions decline. The higher absolute value of SNN compared to SVV (SNN = 11.0, SVV = 3.1) suggests a faster increase in SN as the NOx emission decreases than in SV as the VOC emission decreases by the same percentage. Therefore, although VOC reduction is previously more effective for ozone concentration mitigation, NOx reduction could become more effective as emissions continuously decrease and have a larger potential for ozone concentration mitigation than VOC reduction.

This tendency is confirmed by the ozone concentration isopleths (Figure 3.7), which show a reduction of 4.3 ppbV in ozone concentration due to a 50% reduction in NOx, 28% larger than the ozone concentration reduction achieved by a 50% reduction in VOCs (3.3 ppbV). The corresponding SN (11.3 ppbV) at 100%, 50% is 135% larger than the SV (6.9 ppbV) at 50%, 100%. Unlike the SNN and SVV, the cross-sensitivity SNV (5.0 ppbV) is positive, indicating that reducing either NOx or VOCs would cause the other one to be less effective for ozone concentration abatement (due to a decrease in the first-order sensitivity). For example, the SV decreases from 5.3 to 2.2 ppbV when NOx emissions are reduced by 50%, and similarly, the SN decreases from 2.4 to 0.2 ppbV when VOC emissions are reduced by 50%. As a result, although simultaneously reducing both NOx and VOC emissions would achieve a larger ozone concentration reduction (5.9 ppbV) than solely reducing either NOx (4.3 ppbV) or VOCs (3.3 ppbV), the ozone concentration reduction of the former would be 23% smaller than the sum of the latter two.

Studies revealed that the total anthropogenic NOx emissions in SoCAB continuously decreased by about 67% between 1985 and 2016, and that VOC emissions kept decreasing during the same period, although they flattened out gradually after around 2016 (Figure 2.1). Relying on the reported emission trajectories, the observed ozone concentration values show a generally upward trend between 2012 and 2019 (Figure 2.1). The continued increase in ozone concentration after 2019 despite the recent decline in NOx emissions is due to the negative S_N,which led to an increase in ozone concentration between 2012 and 2019 in response to the reported 25% reduction in NOx emissions. On the other hand, ozone concentration values derived from the isopleths peaked in 2016, followed by a decrease between 2016 and 2017 due to NOx emission reduction. Along the emission trajectory, the ozone concentration varies to a larger extent but remains in the NOx-sensitive regime throughout the period 1985–2014 (Figure 3.7).

Site-specific ozone concentration isopleths are also different and, in some sites, can differ to a larger extent than basin averages. Figure 3.7 illustrates the ozone concentration isopleths for two representative locations in the SoCAB: LA North Main and Crestline. We found that not only could the site-specific ozone concentration values be significantly different from each other, but their sensitivities to NOx and VOC emissions and their positions on the ozone concentration isopleth diagrams were remarkably different (Figure 3.7). For LA North Main, as a coastal site, ozone concentration (S_N = -2.0, S_V = 5.8, S_{NN} = -19.2, S_{VV} = -2.1, S_{NV} = 4.7, unit: ppbV) was located below the zero-S_N line (Figure 3.7), which indicates that further reducing NOx would be beneficial for ozone concentration mitigation; for Crestline, as an inland site, ozone concentration (S_N = 7.8, S_V = 3.0, S_{NN} = -14.9, S_{VV} = -1.8, S_{NV} = 4.1, unit: ppbV) was located in the NOx-sensitive regime (Figure 3.7), well below both the zero-S_N line and the S_N=S_V line, which suggests that NOx reduction is more effective than VOC reduction in reducing ozone concentration.

To show how future ozone concentration trends would differ under different emission reduction strategies, we designed three emission scenarios in which NOx emissions were reduced to 50% of the current level, while VOC emissions either remained constant, decreased by 50%, or equated the 2028 estimated emissions levels. Under the constant-VOC scenario, ozone would change little with the first 10% NOx reduction, and then gradually decrease to 73.5 ppb as NOx emissions were further reduced; under the decreasing VOC scenario, the ozone concentration would decrease to 70.1 ppb. The distinct ozone concentration values at the end of the two scenarios demonstrate the role of VOC reduction in ozone concentration mitigation, but not a significant one. In addition, for the 2028 emissions level (NOx = 60% and VOC = 80%), the average estimated ozone concentration was 88 ppb for SoCAB. All three scenarios show relatively small differences, which indicates that changes in VOCs do not have much impact on ozone concentrations. Despite the differences, when zeroing out the NOx and VOC emissions, the isopleths imply an average background ozone concentration of around 50 ppb.

In addition to the SRIDW method, the quadratic fitting method was also applied to develop the ozone-emission isopleth to help make it smoother and reduce the effect of extreme values from the simulation due to daily variation. For the basic quadratic and log quadratic models, the values of the parameters can capture the relationship between ODV and emissions of NOx and VOC. The intercepts of both models are positive, which reflects the background ozone level. α_{NO_x} and most of α_{VOC} are positive, which means increasing NOx or VOC emissions will elevate ODV levels. Negative values of α_{VOC} in some places close to the coast (Figure 3.8) can be explained somewhat by surface sea breeze and the mountain barrier's influences on the ODV. The relatively low ODV and insignificant changes in these areas may be hard to capture by least squares fitting. Positive $\alpha_{NO_x{}^2}$ shows that the sensitivity of ozone to NOx decreases as NOx increases. Positive α_{NO_x-VOC}

indicates that ozone increases when both NOx and VOC increase. α_{VOC^2} are relatively small and the p-values are higher than 0.5 under the zero value hypothesis, which means that the second-order sensitivity of VOC does not have a significant difference from zero. The results indicate that we can develop a reduced ozone isopleth without the second-order sensitivity of VOC. The ODV estimated by basic quadratic model or log quadratic model are relatively close when emissions of NO_x and VOC are low, but they differ significantly at high ODV regions. This result is due to the lack of simulation results in that area. Comparing the basic quadratic model, and log quadratic model with their reduced models respectively, reduced models have similar patterns as original models. Therefore, reduced models can be used when the second-order sensitivity of VOC is lacking.

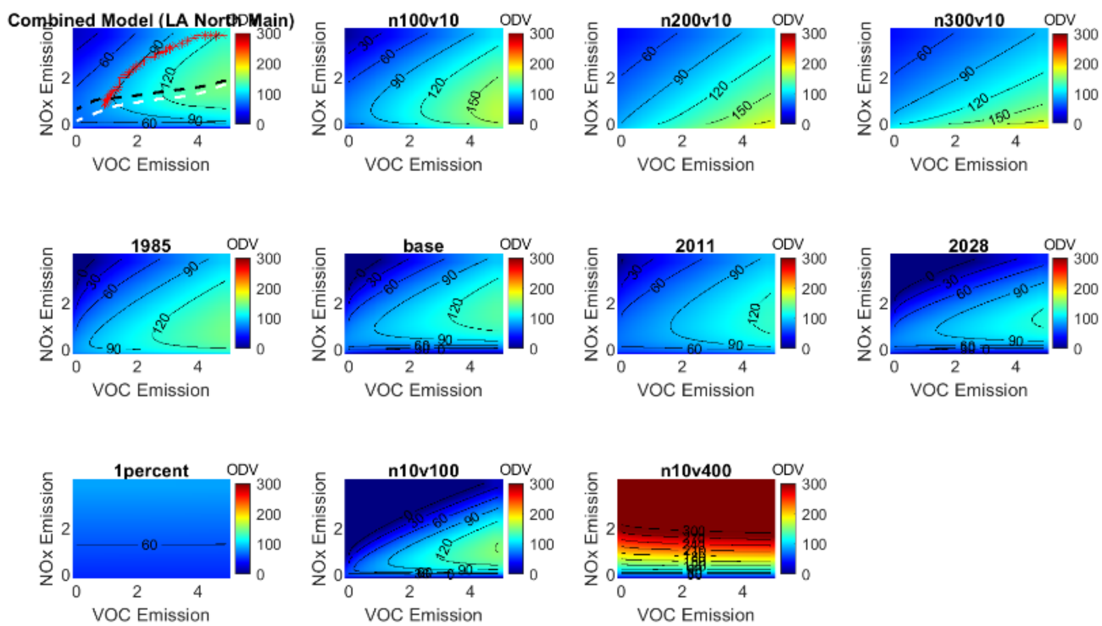

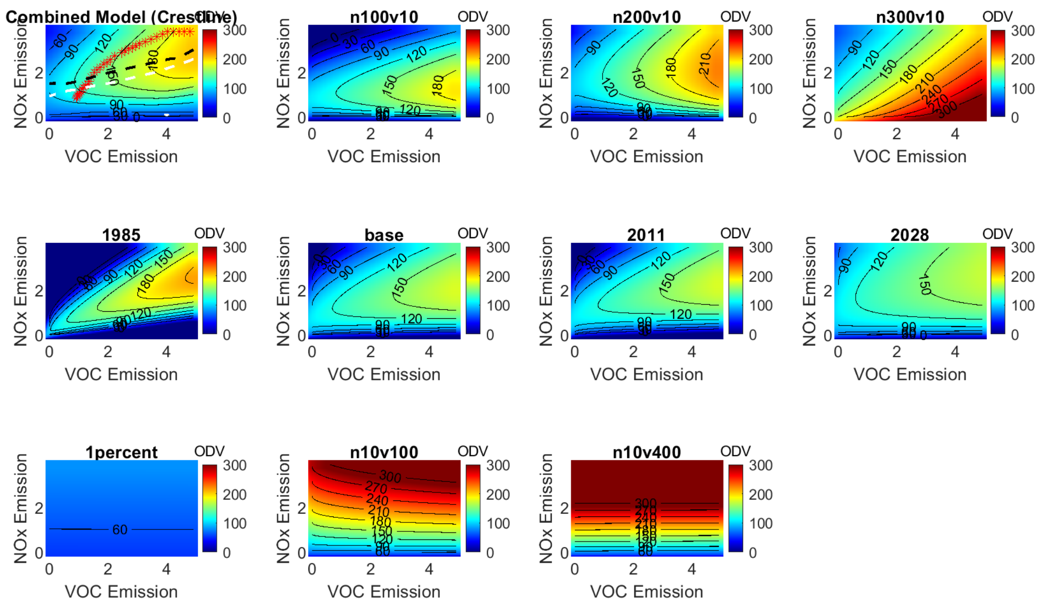

Figure 3.7 The CMAQ-HDDM-based ozone-emissions isopleths for LA North Main and Crestline, including the combined isopleth and all 10 individual isopleths under different emissions scenarios used to build the combined isopleth. In the combined isopleth, the black dashed line indicates the zero ozone-to-NOx emissions sensitivity line. White dashed line indicates the equal ozone-to-NOx and VOC emissions sensitivity line. Red asterisks indicate historical NOx and VOC emissions trajectories.

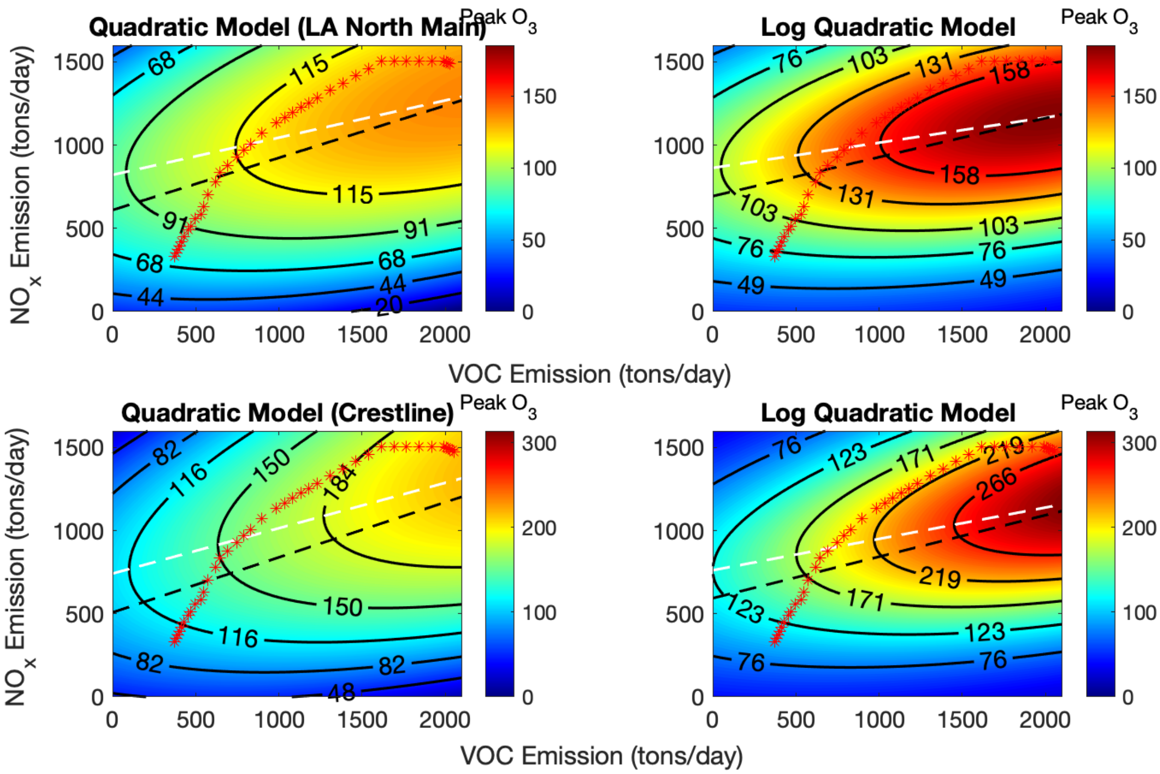

Figure 3.8 Ozone isopleth developed by basic quadratic and log quadratic models for LA North Main and Crestline. The first column is the basic quadratic model and the second column is the log quadratic model. Black dashed lines are the equal NOx-VOC sensitivity ridgelines, and white dashed lines are the zero-NOx sensitivity ridgelines. The red dots represent the historical trajectory of the annual estimated emissions.

3.5.5 Model and Isopleth Uncertainty Analysis

A focus of this section is to conduct extensive uncertainty analysis of simulated ozone and isopleths in the SoCAB, and to better understand how the examined uncertainties may have affected prior modeled trends, future trends, and the construction of isopleths in that region. This has been done by focusing on how simulated ozone and sensitivities impact trend analyses and the construction of isopleths.

We evaluated the DDM results by various means. One analysis we did was to compare the estimated ozone and sensitivities between CMAQ direct simulation results and HDDM sensitivity-based estimation results. Specifically, we used the simulated ozone and sensitivities for each single case to estimate the ozone and sensitivities of all other cases and to compare those two. The results showed that the two compared well and were consistent with each other.

We also evaluated the uncertainty of the developed isopleths using data withholding. We used the model that was trained by all data points as the reference and compared the difference between the models that withheld one data point and the combined model results. The mean and standard deviation of the differences were calculated to evaluate the model's uncertainty (Figure 3.9 and Figure 3.10).

The main purpose of this data withholding was to evaluate the influence of each data point on the ozone isopleth and the stability of the method used to develop the isopleths. Mean bias increased as emissions increased for both the basic quadratic model and log quadratic model due to a lack of data in high ozone level areas. Bias was relatively low in the log quadratic model when VOC and NO_x emissions were low ($E_{VOC} < 2000$ tons/day) compared to the quadratic model, but the log quadratic model had a higher increase rate on the mean of bias in high emissions areas. The standard deviation was lower in the quadratic model than in the log quadratic model, while both had relatively low standard deviations at the low ozone level regions, especially the regions with more CMAQ simulations.

We found that HDDM information at one reference point could explain ozone concentration responses to large changes in NOx and VOC emissions. For example, in Crestline, the isopleths generated by the reference point of 100%, 100% resembled the isopleths generated by 11 reference points (mostly with a difference of <5%) when the changes in NOx and VOC emissions were within -60%–40% (Figure 3.7). Relatively large differences (>10%) were not found until the NOx emissions were reduced by more than 70%. Therefore, the local non-linear responses of ozone concentration to emission changes can be properly captured by running the model just once, indicating that CMAQ-HDDM is an efficient tool for sensitivity analysis. Nevertheless, to cover a wide range of emission changes (down to zero anthropogenic emissions), we used information from all 11 reference points to generate isopleths and conduct subsequent assessments.

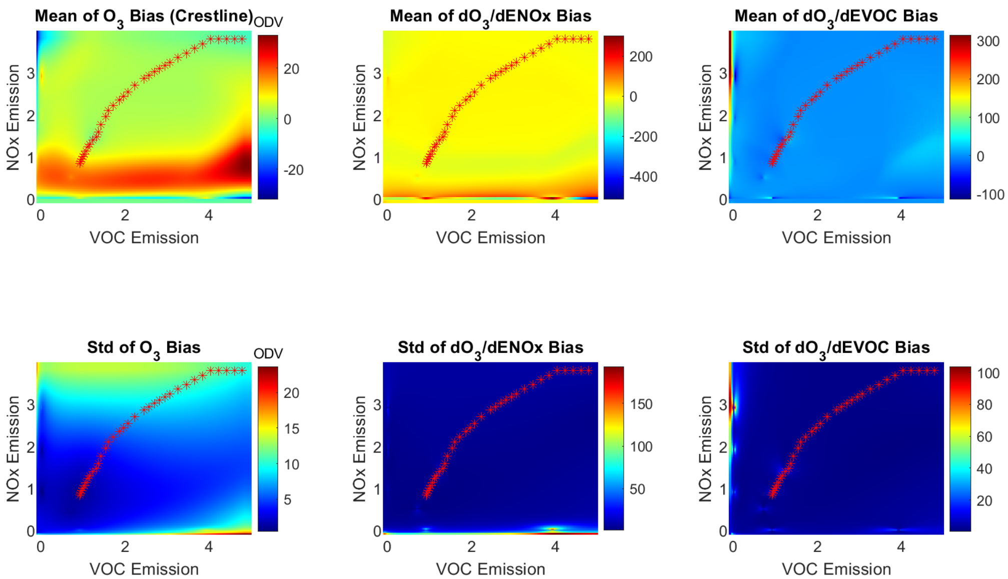

Figure 3.9 Data withholding results of the HDDM SRIDW-based isopleth. The upper row is the average of bias between the isopleth built by 11 reference points and the 11 individual isopleths built by 10 reference points, with one simulation excluded. The lower row is the standard deviation of bias between the isopleth built by 11 reference points and the 11 individual isopleths built by 10 reference points, with one simulation excluded. The site is Crestline.

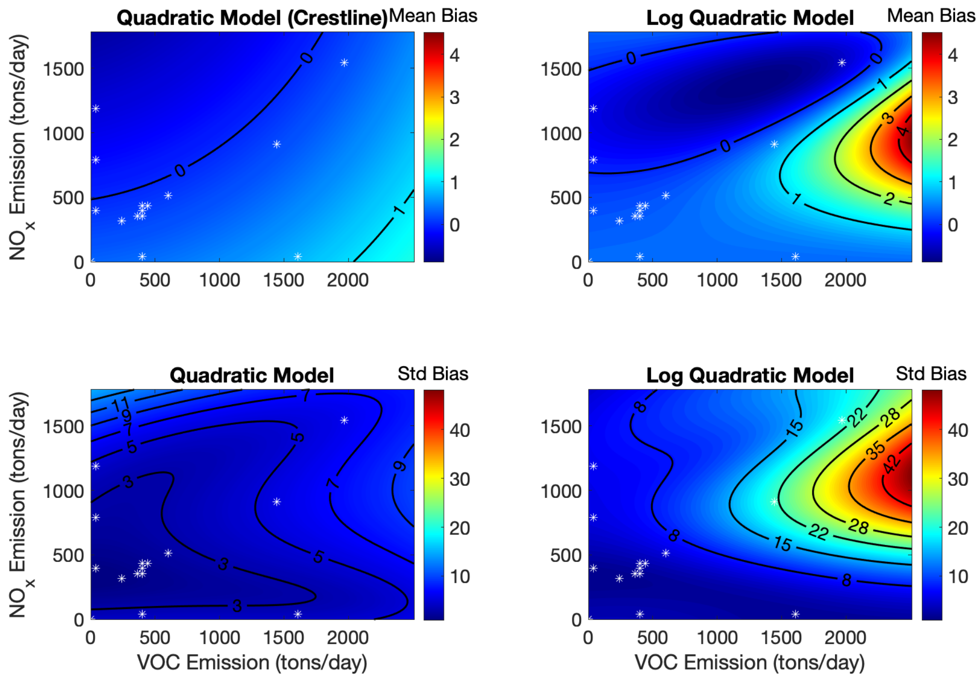

Figure 3.10 Data withholding results of the HDDM quadratic fitting-based isopleth. The upper row is the average of bias between the isopleth built by 11 reference points and the 11 individual isopleths built by 10 reference points, with one simulation excluded. The lower row is the standard deviation of bias between the isopleth built by 11 reference points and the 11 individual isopleths built by 10 reference points, with one simulation excluded. The site is Crestline.

Another analysis to evaluate the isopleth uncertainty is to compare the isopleth-calculated ozone concentration and sensitivities at the reference point against the CMAQ-modeled ozone concentration and sensitivities by site, where R^2 is provided (Appendices H and I). The ozone concentrations calculated by both SRIDW and the quadratic fitting method were all significantly correlated with the CMAQ-modeled ones. Among these methods, SRIDW had R^2 values close to 1, but the R^2 of the quadratic fitting method was much smaller than that of SRIDW (Figure 3.11), suggesting better performance for SRIDW than the quadratic fitting. That is because the quadratic fitting method needs to fit not only ozone concentrations, but also first- and second-order sensitivities. Both of those methods captured HDDM simulated $dO_3/dNOx$ sensitivities well, except for capturing higher $dO_3/dNOx$, which is typically at the three reference points associated with low NOx, i.e., (1%, 1%), (10%, 100%), and (10%, 400%), suggesting that $dO_3/dNOx$ sensitivities tend be biased by these methods as NOx emissions get close to zero.

Similarly, both of those methods captured HDDM simulated $dO_3/dVOC$ sensitivities, but with more bias when estimating $dO_3/dVOC$ at the reference points associated with low NOx. Those biases were mainly caused by the interpolation between different simulations. When NOx emissions are low, both $dO_3/dNOx$ and $dO_3/dVOC$ tends to be extreme, but the isopleths have been smoothed rather than capturing extreme values, which are mostly used to define boundaries. Due to the limitations of these two methods, even though ozone concentration could be estimated well, sensitivities at reference points with low NOx emissions could not be extrapolated well. Overall, the SRIDW method performed well in capturing CMAQ-HDDM simulated concentrations and sensitivities and did a better job than the quadratic fitting method.

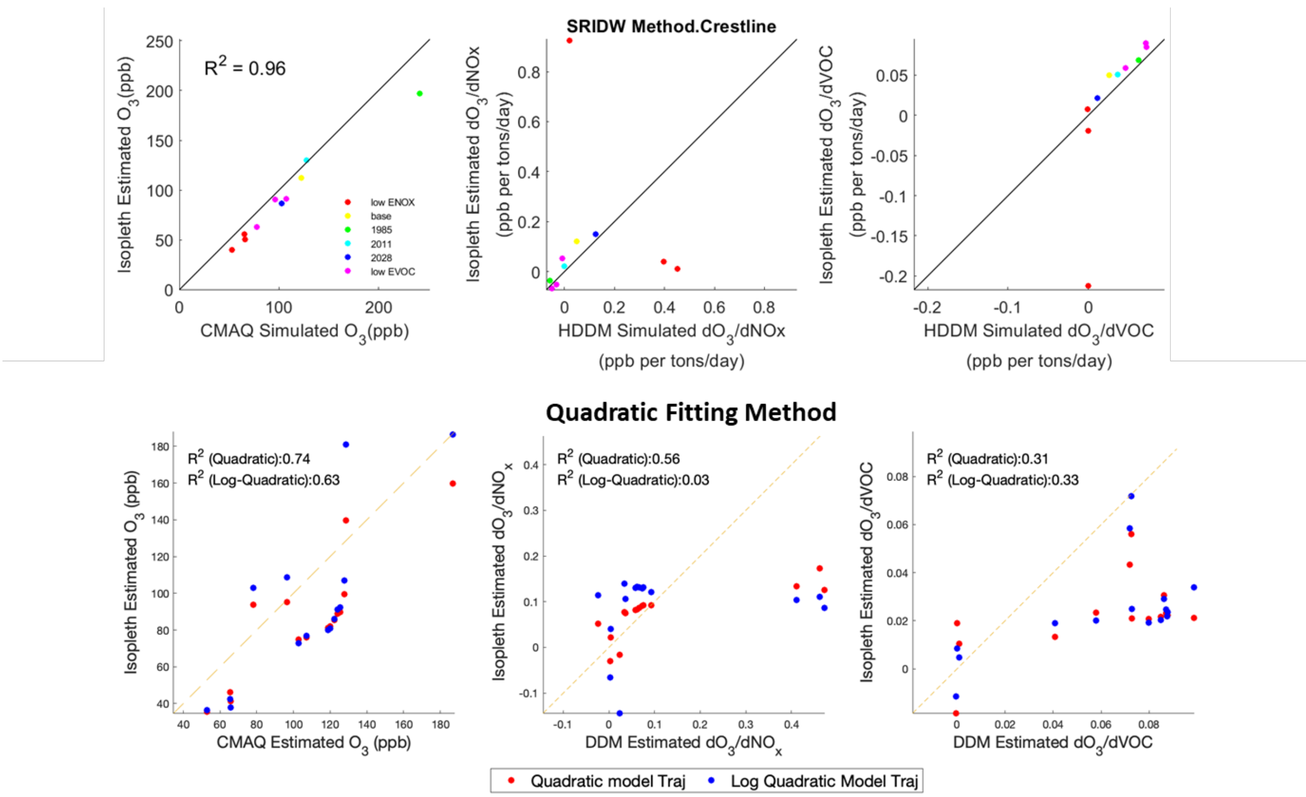

Figure 3.11 Comparison of ozone concentration and sensitivities between isopleth estimation and CMAQ-HDDM simulation for both SRIDW and quadratic fitting methods.

3.6 Emissions Inventory Trends Bias Estimation

Based on the results of the comparison analysis between model estimated and observed concentrations for ozone, CO, and NO_2, we postulated that the emissions inventories had potential bias for both VOC and NOx. In order to further investigate and identify potential bias, we used the observed ozone concentrations based on the isopleths we developed. We assumed that the "true" emissions trend would be a function of the original emissions trend and time (Equation 3.14 and Equation 3.15).

$E_{NOx\_adjusted}(t) = E_{NOx\_original}(t) * (b_{N0} + b_{N1}*t)$ (EQN 3.14)

$E_{VOC\_adjusted}(t) = E_{VOC\_original}(t) * (b_{V0} + b_{V1}*t)$ (EQN 3.15)

where t = year - 1975 (i.e., the number of years since 1975).

Combining equations 3.11, 3.14, and 3.15 allowed for the construction of ozone as a function of the original NOx and VOC emissions, time, and adjustment coefficients. By fitting the isopleth-estimated ozone concentrations to minimize the difference between the estimated and observed ozone concentrations (Figure 3.12), we were able to find the best solution for those adjustment coefficients. We can see that the ozone concentrations estimated by the adjusted emissions trends are highly consistent with the observed ozone concentrations over all sites and years.

By applying the adjustment coefficient to the original emissions trends, we were able to reconstruct the adjusted emissions trends for both NOx and VOC (Figure 3.12). The NOx emissions had a more significant bias for earlier years, and the bias was much smaller for recent years. For VOC, the original estimated emissions tended to be significantly biased low for earlier years, but it switched to high bias for recent years. The calculated adjustment coefficients are as follows: b_{N0} = 0.81, b_{N1}= 0.006, b_{V0}= 1.43, and b_{V1} = -0.047. These results suggest that in order to better estimate the historical peak ozone levels, NOx emissions need to be about 19% lower on average, and the annual reduction rate needs to be about 0.3% slower per year. For VOC, the results indicate that the emissions need to be about 43% higher on average and the annual reduction rate needs to be about 4.7% faster per year. These ratios for the emissions bias are consistent with the results of the sensitivity tests based on CMAQ-HDDM, which was discussed earlier, and the difference between observed and model estimated NO_2 and CO concentrations.

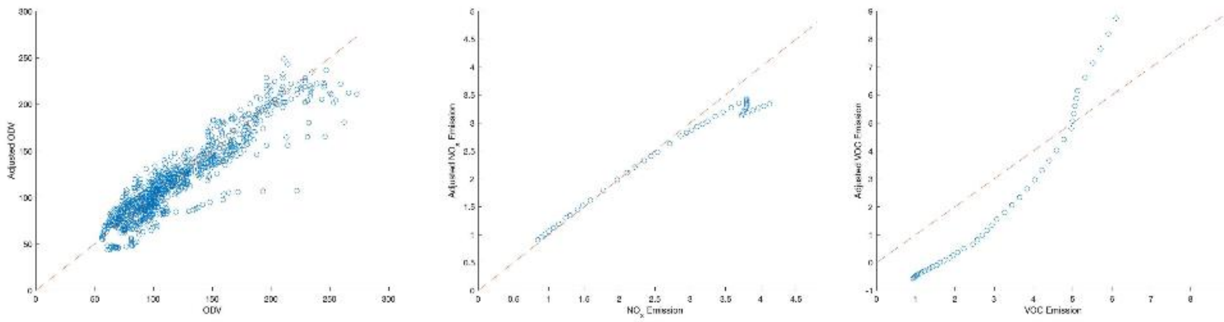

Figure 3.12 The adjustment of emissions inventory trends based on the fit between observed and model estimated annual peak ozone concentrations. (a) Comparison of the annual peak ozone concentrations between the adjusted and observed. (b) Comparison between the adjusted and original estimated NOx emissions trend. (c) Comparison between the adjusted and original estimated VOC emission trends.

3.7 Further Discussion

The sensitivities that determine ozone concentration regimes can be affected by various factors, and the most direct factors are precursor emissions. High local NOx emissions, for example, tend to induce a VOC-limited regime, but this tendency can be prevented by high VOCs (Figure 3.7). Meteorological and climate conditions and topographic characteristics also play important roles in shaping ozone concentration regimes. High temperature increases biogenic VOC emissions and the rates of photochemical reactions driving ozone concentration formation toward a NOx-limited regime. Wind speed and precipitation are associated with the pollutants' accumulation and removal; places at high altitudes are more likely to be affected by background ozone concentration from regional transport; and land surfaces with a high coverage of vegetation release more biogenic VOCs. All of these factors affect ozone concentration formation.

From demographic and socioeconomic perspectives, factors such as population density, urbanization rate, and economic development may also be associated with ozone formation because of their associations with energy consumption and precursor emissions. To quantitatively elucidate the factors affecting ozone sensitivities and regimes, there are potential ways to conduct correlation and regression analyses for the ozone concentration sensitivities using site-level variables, but these will not be explored in this report.

3.8 Summary

For the work covered in this section, we simulated and analyzed ozone concentrations and sensitivities to NOx and VOC emissions derived by state-of-the-science air quality modeling using CMAQ-DDM over the SoCAB. Those results, including the sensitivities, were used to construct the ozone-emission isopleths by using a modified inverse distance-weighted method.

Chemical transport modeling was conducted for both past (1985, 2001, 2011, 2016) and future (2028) periods at a 4 km resolution over the SoCAB using the CMAQ air quality model (version 5.0.2) and the CB6 mechanism. The study domain covers southern California with 156 × 165 horizontal grid cells resolved at 4 km spatial resolution and 13 vertical layers extending to ~11 km above ground. Simulations span the period from June 1, 2016 to July 31, 2016, and the same meteorology (based on high ozone days in 2016) was used. Emissions inventories for five years (1985, 2001, 2011, 2016, and 2028) were developed based on the NEI inventories. CMAQ's HDDM was used to calculate both first- and second-order sensitivities.

We conducted a set of 15 CMAQ-HDDM simulations with different emissions levels, and 11 of the cases were used to develop ozone-NOx-VOC isopleth diagrams. Individual isopleths for each emissions scenario were generated using the first- and second-order sensitivities as terms in a quadratic Taylor series. A SRIDW method was developed primarily to integrate the individual isopleth and produce the combined isopleth. Another method was used to develop ozone isopleth by conducting basic quadratic and log quadratic forms and least squares fitting. The CMAQ simulation results were evaluated by comparing the simulated species concentrations with the observed species concentrations.

Both the 2011 and 2016 comparisons showed high consistency between the simulated and observed MDA8 ozone concentrations. These results indicate that the CMAQ simulation can effectively capture peak ozone values over our simulated period, even though we used the 2016 meteorology for the 2011 simulation. However, the 1985 and 2001 results showed a different pattern, and the simulation tended to underestimate peak ozone levels by about 20% compared to the observations. We investigated multiple potential reasons that could lead to this bias, and the final results suggest that the most probable reason could be the bias in estimated emissions, indicating that the estimated VOC emissions should be about 40% higher and the estimated NOx emissions should be about 20% lower than what the inventory estimated.

By investigating several potential algorithms to build the ozone isopleth with CMAQ-HDDM-estimated ozone concentrations and sensitivities, we developed a modified inverse distance-weighted method under a square root emissions scale and used the peak ozone day of each simulation. This method allowed the ozone-emission isopleth to be built, which has a similar shape to isopleths developed by other studies and through empirically derived approaches. By looking at the SN = SV and SN = 0 lines, the key observation is that although VOC reduction was previously more effective for ozone concentration mitigation, NOx reduction is becoming more and more effective as emissions continuously decrease, and had a larger potential for ozone concentration mitigation than VOC reduction.

Site-specific ozone concentration isopleths are different and, in some sites, can differ to a larger extent than basin averages. We found that not only were the site-specific ozone concentration values not close to each other, but their sensitivities to NOx and VOC emissions and their positions on the ozone concentration isopleth diagrams were remarkably different. The coastal ozone concentration was located below the zero-S_N line, which indicates that further reducing NOx would be beneficial for ozone concentration mitigation. The inland ozone concentration was located in the NOx-sensitive regime, well below the zero-S_N line and the $S_N = S_V$ line, which suggests that NOx reduction is more effective than VOC reduction in reducing ozone concentration.

Despite the difference in first-order sensitivities, especially in S_N which differ in sign, the second-order sensitivities between inland and coastal areas were similar. We evaluated the DDM results themselves by various means, including comparing the DDM and brute force results and evaluating the uncertainty of the developed isopleth by using data withholding. The ozone concentrations calculated by the isopleths are all significantly correlated with the CMAQ-modeled results, with R^2 values very close to 1. In order to further investigate and identify the potential bias related to emissions trends, we conducted analyses to find the adjusted emissions trends to better fit the model estimated and observed ozone concentrations based on the isopleth we developed. The results suggest that in order to better estimate the historical peak ozone levels, NOx emissions need to be about 19% lower on average, and the annual reduction rate needs to be about 0.3% slower per year. For VOC, the results indicate that the emissions need to be about 43% higher on average and the annual reduction rate needs to be about 4.7% faster per year.

Chapter 4: Comparison of Ozone Responses to NOx and VOC Emissions using Empirical and Chemical Transport Modeling.

4.1 Introduction

Another aim of this study was to conduct an extensive comparison of isopleths constructed by different methods to understand how well the current chemical transport models (CTMs) captured ozone dynamics and the response to the controls of NOx and VOC. Historically, many methods have been developed to explore this relationship, from smog chambers to box models to CTMs (Jin and Demerjian, 1993; Kanaya et al., 2009; Kelly and Gunst, 1990; Menut et al., 2000; Milford et al., 1989; Sierra et al., 2013). Each of these approaches has its limitations, and arguably the least limited of the three, CTMs, has not been able to fully capture the observed ozone trends in Los Angeles.

It should be noted that the CTM-based sensitivities and the empirically derived sensitivities are not directly comparable, and that the uncertainties are different in different regions of the isopleth domains. For example, the empirical approach has increased uncertainties away from historical observations (Qian et al., 2019), and the integration of different CMAQ-HDDM simulations under different emissions levels would introduce further uncertainty between those emissions levels. Further, the absolute levels of emissions are uncertain, although the trends are probably better captured. CTM results are subjected primarily to uncertainties in the boundary conditions (including background ozone) and emissions, although other uncertainties may be of importance. Background ozone uncertainties are particularly important when considering lower ozone levels near-zero anthropogenic emissions of either VOC or NOx emissions, or both.

Therefore, it is important to investigate the advantages and disadvantages of various methods. Our analysis included more traditional approaches (e.g., modeling using emissions from one or more historical years) and newly developed empirically based methods to construct the isopleth. Based on the results from Chapters 2 and 3, we have seen that both methods can capture ozone levels well and construct isopleths that are similar to previous studies but still have their own limitations. Thus, the comparison of modeled with empirically derived ozone concentrations, sensitivities, and isopleths can provide more insights into the ozone-emissions response.

4.2 Method

Ozone responses to emissions changes and ozone-emission isopleths in the SoCAB are derived using an empirical modeling approach (Qian et al., 2019; Chapter 2) and chemical transport modeling using CMAQ-HDDM (Chapter 3).

4.2.1 Empirical Modeling

Ozone responses to emissions reductions in the SoCAB were derived by developing ozone isopleths for 24 locations in the SoCAB using the methods described in Qian et al. (2019) and Chapter 2. Briefly, ozone data starting in 1975 for monitoring locations in the basin were used to construct empirical equations capturing how ozone responded to emissions reductions. The equations derived are the linear and quadratic terms of the Taylor series linking ozone (or log[O_3]) to emissions:

$$\mathrm{ODV}\ (E_{NOx},\ E_{VOC})\ \text{or}\ \mathrm{Log}_{10}\ (\mathrm{ODV}\ (E_{NOx},\ E_{VOC})) = \beta + \alpha_{NO_x} * E_{NO_x} + \alpha_{VOC} * E_{VOC} + \alpha_{NO_x-VOC} * (E_{NO_x} * E_{VOC}) + \alpha_{NO_x^2} * E_{NO_x}^2 + \alpha_{VOC^2} * E_{VOC}^2 \qquad \text{(EQN 4.1)}$$

While originally developed based on using a single site's ozone trends, a second approach can include spatial terms to map out the response over an area (Chapter 2). The spatial model can be used to develop ozone isopleths for any location in the SoCAB.

Based on the EPA's definition, the "design value" is a statistic that can be used to represent the air quality for a certain location, area, or region, especially relative to the National Ambient Air Quality Standards (NAAQS; US EPA, 2016). Here, we focus on the maximum daily averaged eight-hour ozone design value (ODV), which is the average of the fourth highest annual maximum daily average eight-hour ozone concentration over three consecutive years. The data were extracted from the California Air Resources Board's iADAM: Air Quality Data Statistics data base (CARB, 2018) for every monitoring site in SoCAB. In this study, data from 24 monitoring sites (out of 93 sites) were included based on data quality and availability (e.g., from locations near the coast and inland).

We used historical ODVs, individual monitor ozone values, and historical estimates of NOx and VOC emissions to develop non-linear regression models that can be used to quantify sensitivities and develop ozone isopleth diagrams. In Chapter 2, we described in detail the development and results of the empirical method to investigate the ozone-emissions relationship.

4.2.2 Chemical Transport Modeling

Ozone responses to emissions controls can also be directly calculated using chemical transport modeling. Here, CMAQ-HDDM (Hakami et al., 2004) was used to calculate ozone sensitivities to emissions controls. After being evaluated for a two-month (June–July) period in 2016 with multiple high ozone episodes, the model was applied to historical (1985, 2001, 2011, and 2016) and future (2018) estimated emissions, along with additional scenarios to capture more extreme emissions reductions (see Chapter 3) to derive ozone isopleths for the grids containing the 24 monitoring locations used for empirical modeling. The ozone isopleths being developed here are for the maximum daily averaged eight-hour concentrations for a more direct comparison to the empirical method.

A nested grid modeling domain was used, with the outer domain covering the continental US using a 12 km horizontal resolution (Appendix Figure B.1), and the inner domain having a 156 × 165 4 km x 4 km horizontal grid covering the SoCAB region. The model height is approximately 11 km, with 13 vertical layers.

Emissions inputs for the years 2001, 2011, 2016, and 2028 were developed using the EPA's emissions modeling platforms ("www.epa.gov/air-emissions-modeling/2014-2016-version-7-air-emissions-modeling-platforms"). By utilizing these recent EPA emissions modeling platforms, the four years' model-ready emissions are internally consistent with each other. BEIS was used to produce biogenic emissions off-line to help ensure consistency. These emissions modeling platforms all use SMOKE programs to generate hourly, gridded model species emissions fields that CMAQ requires as inputs. Emissions for 1985 were constructed based on back-casting the 2016 inventory, accounting for changes in sources (e.g., industrial, transportation, and population-linked activities) and population distributions.

Further details of the model application and performance evaluation are found in Chapter 3 and Appendices B and C.

4.3 Comparison of the Ozone and Sensitivity Isopleth Between HDDM-Based and Empirically Based Methods

Developing ozone isopleths provides a direct method for comparing sensitivities between the empirical and CTM-based models. Qualitative approaches for comparing the two include visual inspection of ozone isopleths generated by the two methods (Figures 4.1 & 4.2; Appendices H & I), and similarly comparing sensitivity isopleths (Figure 4.1; Appendix H). Given that the empirical method was developed using historical observations, the model has the least uncertainty along the "emissions trajectory" (Qian et al., 2019), i.e., the annual levels of emissions estimates starting in 1975 (shown as the series of "*" in the figures). This trajectory is also of specific interest for assessing the model, given that past modeling applications included emissions associated with previous years. Further, those points align with past conditions in the SoCAB. As such, the maximum eight-hour CTM-derived sensitivities to NOx and VOC emissions are compared to the empirically derived ODVs (which are also based on maximum daily eight-hour ozone levels) along the emissions trajectory (Figures 4.3 & 4.4).

4.3.1 Ozone Isopleth Comparisons

HDDM-based isopleths and empirically based isopleths have different patterns under different emissions levels (Appendix H). When both emissions are high (ENOx > 1000 tons/day and EVOC > 1500 tons/day), which is the level during and before the 1990s, the HDDM-based method tends to estimate ozone concentrations lower than the empirically based estimation. This is likely driven by the biased low estimation of ozone concentrations from the 1985 CMAQ-HDDM simulations, which may be related to the biased emissions inventory in the early years, as described in Chapter 3. In the middle range of both NOx emissions (from 100 to 1000 tons/day) and VOC emissions (from 0 to 1500 tons/day), which are the levels from the year 2000 to potential future years, the HDDM-based method tends to estimate ozone concentrations higher than the empirically based estimation for most of the sites. The high bias of the HDDM-based method in estimating ozone levels is likely reflected in the estimated ozone sensitivities. Also, the empirical model uses the ODV, which is the average of three consecutive year's fourth highest ozone concentrations, whereas the HDDM-based isopleths just use peak MDA8 ozone concentrations. Another major difference appeared when NOx emissions were much lower and close to zero, where the empirically estimated ozone levels tended to be higher than those from CMAQ (about 55 ppb vs. 40). This is because the empirically derived isopleths are driven by observations that do not go to zero-NOx emissions, while the CMAQ isopleths explicitly include cases with very low NOx and VOC emissions (1% to 10% of the baseline 2016 emissions). The CMAQ-based isopleths likely better capture the responses under low emissions, which is of potential importance to estimate more accurately the future emission controls needed to obtain the NAAQS.

These are the general patterns of the comparison for most of the sites within the SoCAB, but the spatial variation of the difference is also significant (Figure 4.1). The HDDM-based isopleths vary more spatially than the empirical model (Figure 4.1; Appendix H), although this is not surprising given that the empirical model only includes linear and quadratic spatial terms, while the sensitivities found using CMAQ-HDDM have a significant texture (Fig. 4.1). This is driven by the spatial variations in both emissions and meteorology, which are critical inputs to CMAQ but are not explicitly included in the empirical modeling.

For the LA North Main site, located in a highly urbanized, core portion of the SoCAB, we see that the ozone and ozone sensitivity isopleths, and the estimated ozone-emissions responses along the emissions trajectory differed somewhat between the two methods (Fig 4.1). For Crestline, which is the location that most often has the highest ODV basin-wide in recent years, the differences between methods were relatively small compared to the LA North Main site (Figure 4.1), although the difference had a similar distribution over the emissions space compared to the Crestline site. This spatial difference can arise from the choice of episodes: the episodes simulated using CMAQ were chosen to capture the highest observed ozone levels in the SoCAB, which happened downwind (e.g., at Crestline), while the highest ozone levels in the core downtown areas could occur on different days. Also, the core areas were negatively sensitive to NOx, and so were very sensitive to local NOx emissions.

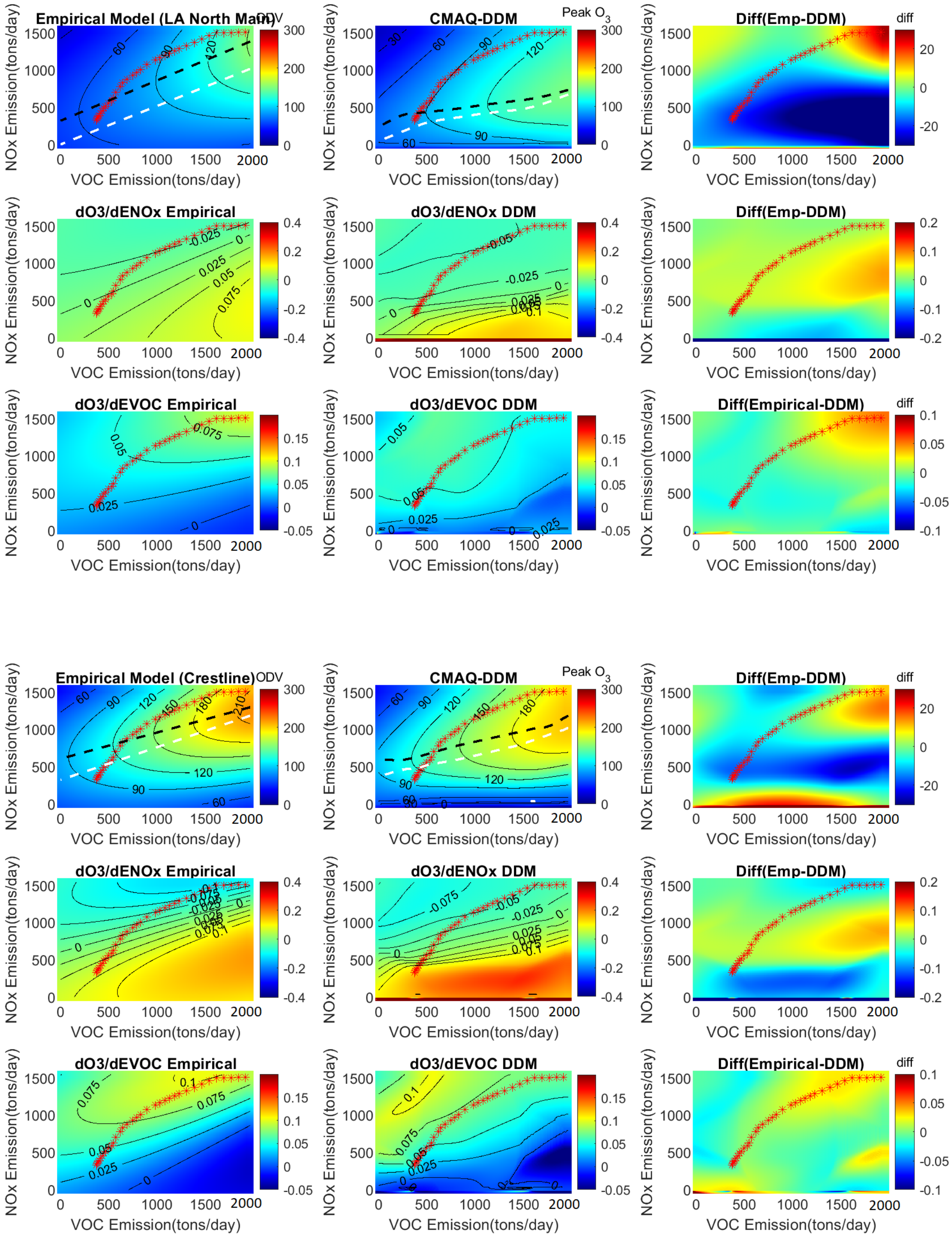

Figure 4.1 CMAQ-HDDM-based ozone-emissions concentrations and sensitivity isopleths (based on the SRIDW method) and the comparison with empirically derived isopleths for LA North Main and Crestline. The first column shows the empirically derived isopleths. The second column are the CMAQ-HDDM based isopleths. The third column shows the difference between those two. The first row is the ozone concentration isopleths; the second row is the ozone-to-NOx emissions sensitivity isopleths; and the third row is the ozone-to-VOC emissions sensitivity isopleths. The black dash line indicates the zero-NOx-sensitivity line, and the white dash line indicates the equal-NOx-VOC sensitivity line.

We also compared the CMAQ-based quadratic fitting method with the empirical model. The patterns of the difference under different emissions levels appeared similar to the difference between the SRIDW method and the empirical model. However, we observed that the HDDM quadratic-fitted isopleth was more similar to the empirically developed isopleth (Figure 4.2). This was expected, since both of those two methods assumed the ozone isopleth should follow a quadratic formation of VOC and NOx emissions, and used ordinary least squares to calculate the coefficient. The similarities held even though the training sets were totally different: the empirical model used historical observations as the training set, while the HDDM quadratic fitting used HDDM simulated ozone concentrations and first- and second-order sensitivities as the training set.

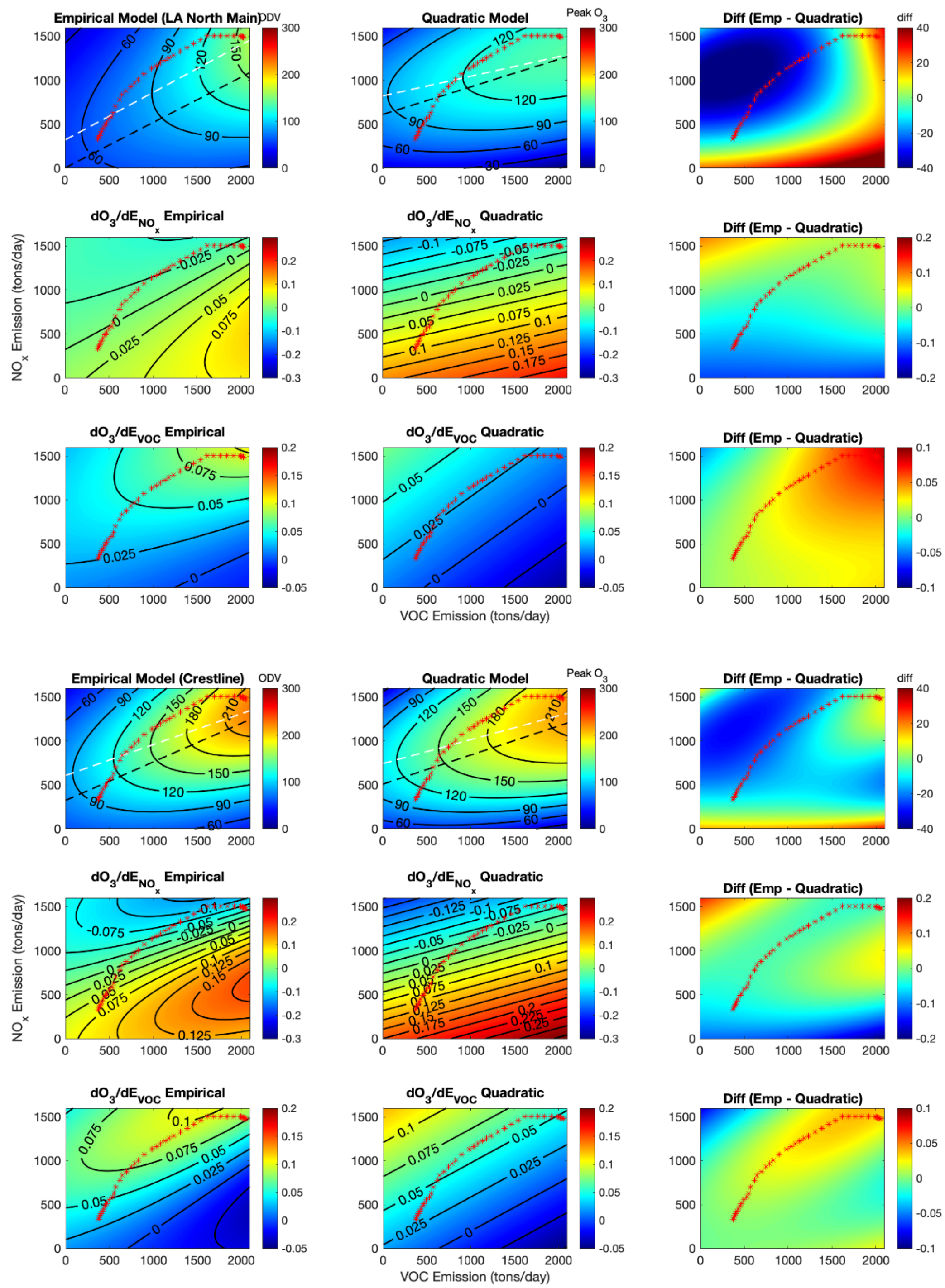

Figure 4.2 CMAQ-HDDM-based ozone-emissions concentrations and sensitivity isopleth (based on quadratic fitting method) and the comparison with empirically derived isopleths for LA North Main and Crestline. The first column shows the empirically derived isopleths. The second column are the CMAQ-HDDM based isopleths. The third column shows the difference between those two. The first row is the ozone concentration isopleths; the second row is the ozone-to-NOx emissions sensitivity isopleths; and the third row is the ozone-to-VOC emissions sensitivity isopleths. The black dash line indicates the zero-NOx-sensitivity line, and the white dash line indicates the equal-NOx-VOC sensitivity line.

4.4 Comparison between Empirical and CMAQ-HDDM Estimations of Ozone Concentration and Sensitivities along the Historical Emissions Trajectory

A further evaluation of the differences between CMAQ-derived isopleths and the empirically derived isopleths can be made by comparing the estimated historical trends (along emissions trajectories) of ozone concentrations and ozone-to-emissions sensitivities. Using the isopleth, we were able to produce the trajectory for both ozone concentrations and sensitivities (Figure 4.3), which can be a good representation of how well the CTM captures the historical trends of the ozone response to emissions changes. Table 4.1 lists a summary of R^2 for the comparison between CMAQ-based and empirically based results along the trajectory for ozone concentration, ozone-to-NOx emissions first-order sensitivity (SN), and ozone-to-VOC emissions first-order sensitivity (SV).

Similar to the isopleth comparison, we found that the observed ozone trends were well captured based on the CMAQ-derived isopleth for most of the sites (average R^2 = 0.82), although for more than half of the sites, the CMAQ-estimated ozone levels tended to be a bit lower for earlier years (during and before 1990s) and higher after the year 2000 (Figure 4.3). This finding indicates that the CTM was able to capture historical ozone concentration trends quite well in different locations by applying a robust integration method (SRIDW here) to produce the isopleth. We also observed that both the CMAQ-based and empirically based methods had a similar trend in estimating the SN and agreed well with each other (Table 4.1). SN decreased during the 1980s for the first few years and started increasing continuously after 1990. The estimated increasing rates were similar from 1990 to 2010, based on both methods.

After 2010, we see that the CMAQ-estimated SN started growing much faster than the empirically estimated SN. This fact has also been observed and discussed when comparing the ozone isopleth based on the two different methods, where we have seen that the empirically derived isopleths are driven by observations that do not go to zero-NOx emissions, while the CMAQ isopleths explicitly include cases with very low NOx and VOC emissions (1% to 10% of the baseline 2016 emissions). The CMAQ-based isopleths likely better capture responses under low emissions, which is of potential importance in more accurately estimating the efficiency of future emission controls.

Although we see that this general pattern of SN comparison is similar for different sites, it still varies spatially in the absolute levels of the estimated SN. For the LA North Main site, although the CMAQ-estimated and empirically estimated SN are well correlated (R^2 = 0.81), the CMAQ-estimated SN is constantly lower than the empirically estimated SN until 2010. This fact is important since the estimated time of when this site changed from NOx non-beneficial to NOx beneficial (from SN < 0 to SN > 0) would be different. Based on the empirical estimation, LA North Main started being NOx beneficial after 2010, while that did not occur until 2015 based on the CMAQ-based estimation. In contrast, the estimated times for Crestline to cross the SN = 0 ridges were more similar around the year 2000. This spatial variation may indicate that the driving forces of SN variation are spatially different.

Given that the sensitivities using CMAQ-HDDM have significant texture, using both emissions and meteorologies as input, while the empirical model only includes linear and quadratic emissions and spatial terms, the difference in the estimated SN would be more significant at a site like LA North Main, which is located in a highly urbanized area where the driving force of SN variation is more complicated than emissions alone. For Crestline, which is the location that most frequently has the highest ODV basin-wide, the SN variation is mainly driven by precursor emissions. Thus, the differences between methods are relatively small compared to the LA North Main site (Figure 4.3). This spatial difference can also arise from the choice of episodes (the episodes simulated using CMAQ were chosen to capture the highest observed ozone levels in the SoCAB, which happened downwind (e.g., at Crestline), while the highest ozone levels in the core downtown areas could occur on different days. Also, the urban areas are negatively sensitive to NOx, and are very sensitive to local NOx emissions.

For ozone-to-VOC emissions sensitivity (SV), the correlations between CMAQ and empirically estimated results are relatively low for most of the sites, and the spatial variation of the correlation is more significant. For sites like Crestline, CMAQ-estimated SV tends to be constant with little variation before 2000, while the empirically estimated SV decreased continually from the 1980s onwards. For sites such as LA North Main, while the empirically estimated SV keeps decreasing from the 1980s, the CMAQ-estimated SV has an increasing trend from the 1980s to about 2000. After 2000, for most sites, the two estimations tended to agree much better in both trend and absolute levels. These observations, again, are likely driven by the biased-low estimation of ozone concentrations from the 1985 CMAQ-HDDM simulations, which underestimated the second-order sensitivity of ozone-to-VOC sensitivities.

Overall, by comparing the two methods used to develop the HDDM-based ozone-emissions isopleth, there is no simple answer as to which one is better than the other. Each has its own advantages in specific applications. Both methods are able to effectively capture the ozone concentration trend along the historical emissions trend, but the HDDM-based isopleth tends to be biased high for recent years (while it can better capture a leveling off and even increases in the ODV from 2012) and biased low for early years because of the biased-low estimation of 1985 ozone levels. The CMAQ-based method has a significant advantage in better capturing the spatial variations of sensitivities, which is especially important for urban sites that are sensitive to local emissions and meteorologies. However, for the coastal and urban core sites, there is a larger discrepancy between the observed and model-derived ozone-emission sensitivities.

While a number of reasons have been identified for such differences, it suggests that CTMs, when applied to episodes chosen to capture high levels in the downwind locations, may not capture how the higher ozone levels will respond in the locations further west, which includes much of the more highly populated regions. CMAQ-based methods also can better capture the rapid increase of SN when NOx emissions are much lower, while the empirical methods cannot since there are no observation points with extremely low NOx emissions to train the model.

While lacking the significant texture of sensitivities that the CMAQ-HDDM method has, the empirical method is still a good tool to capture the overall trend of ozone concentrations and sensitivities for inland sites like Crestline in a more computationally effective way.

Table 4.1 Summary of the R^2 between empirical and CMAQ-HDDM estimated ozone concentration, $dO^3/dENOx$ (SN), and $dO^3/dEVOC$ (SV) respectively along the historical emissions trajectory

R^2	O3	SN	SV
Azusa	0.92	0.69	0.13
Glendora	0.95	0.58	0.22
West LA	0.86	0.76	0.78
LA North Main	0.95	0.81	0.02
Reseda	0.69	0.73	0.17
Burbank	0.79	0.94	0.44
Pico Rivera	0.85	0.76	0.00
Pomona	0.78	0.72	0.49
Pasadena	0.92	0.69	0.00
Long Beach	0.82	0.64	0.07
LAX	0.60	0.24	0.51
Santa Clarita	0.79	0.73	0.16
Anaheim	0.81	0.84	0.00
Mission Viejo	0.75	0.77	0.20
La Habra	0.75	0.87	0.00
Banning	0.67	0.76	0.07
Perris	0.79	0.78	0.07
Riverside	0.86	0.82	0.34
Lake Elsinore	0.88	0.76	0.20
Crestline	0.91	0.76	0.87
Upland	0.86	0.73	0.48
Fontana	0.87	0.73	0.49
Redlands	0.87	0.79	0.62
San Bernardino	0.83	0.80	0.47
Overall	**0.82**	**0.74**	**0.28**

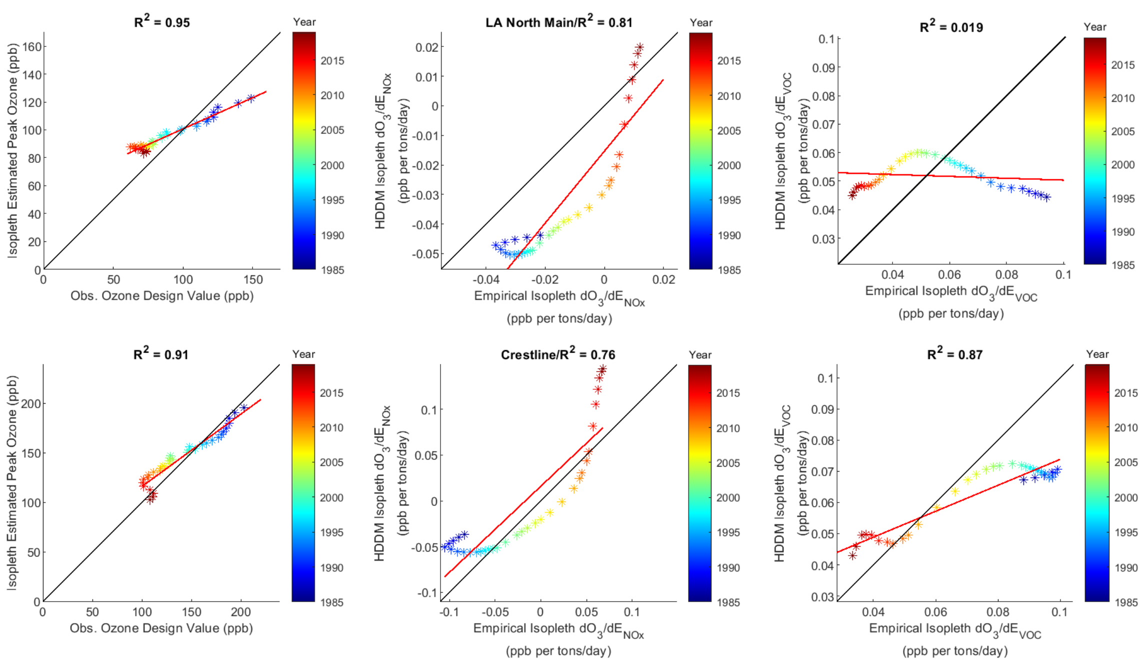

Figure 4.3 The comparison between HDDM-derived (SRIDW method) and empirically derived ozone and sensitivities trend trajectory from 1985 to 2019. (a) The comparison between HDDM and empirically derived ozone trends; (b) the comparison between HDDM and empirically derived ozone-to-NOx emissions first-order sensitivity trend; (c) the comparison between HDDM and empirically derived ozone-to-VOC emissions first-order sensitivity trend. The color indicates the year of the spot, the upper row shows the LA North Main site, and the lower row shows the Crestline site.

For the quadratic fitting method, a comparison between simulated and observed ozone over the historical years' trajectory was conducted (Figure 4.4). Both the basic quadratic model and the log quadratic model had an R^2 higher than 0.7 (except for LAX), and most were even higher than 0.9. It can be inferred that the ODV values estimated by the developed ozone isopleths have a high correlation with the observed ODVs. Nonetheless, the isopleths for LAX and other sites close to the coast had relatively low R^2 due to meteorology and topography, as previously mentioned. The basic quadratic model overestimated ODVs at low ozone levels and underestimated ODVs at high ozone levels at most sites, while the log quadratic model overestimated ODVs at most sites.

First-order sensitivities of the developed isopleths were also compared with the observed sensitivities, which were estimated by the empirical model. Both the basic quadratic model and the log quadratic model had a high R^2, which means that the developed isopleths captured the trend of sensitivities during the time period. While at most sites, the basic quadratic model had a higher R^2 for the first-order sensitivity of NOx, the log quadratic model had a higher R^2 for the first-order sensitivity of VOC. Notwithstanding these differences, the isopleths developed by those two methods were highly consistent with each other, which indicates that the HDDM simulation could effectively capture historical ozone trends in general compared to the relevant observations. In addition to the full quadratic fitting model, we tested a number of alternative forms of reduced models to remove statistically insignificant variables (e.g., the second-order derivative of VOC). The isopleths based on the reduced models were highly similar to the original models.

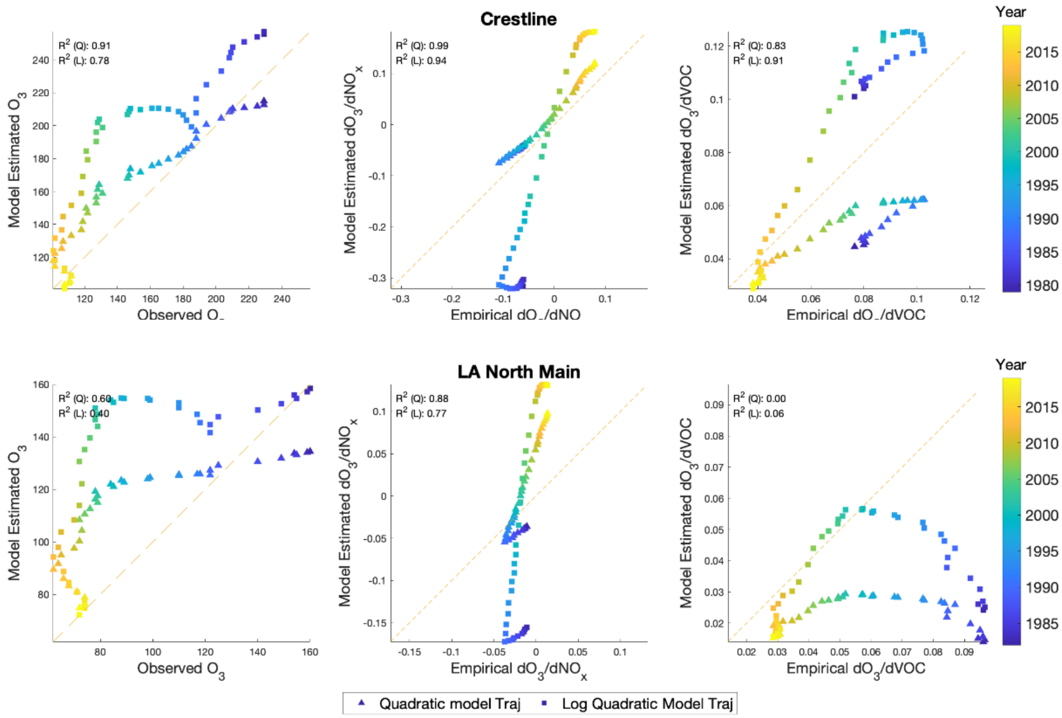

Figure 4.4 The comparison between HDDM-derived (quadratic fitting method) and empirically derived ozone and sensitivities trend trajectory from 1980 to 2016. (a) The comparison between HDDM and empirically derived ozone trends; (b) the comparison between HDDM and empirically derived ozone-to-NOx emissions first-order sensitivity trend; (c) the comparison between HDDM and empirically derived ozone-to-VOC emissions first-order sensitivity trend. The color indicates the year of the spot, the upper row shows the LA North Main site, and the lower row shows the Crestline site.

4.5 Comparison Between Empirical and CMAQ-HDDM Estimated Spatial Distributions of Ozone Concentration and Sensitivities

In addition to the temporal emissions trajectory analysis, both the empirical and CMAQ-HDDM methods can be used to investigate the spatial distribution of ozone concentration and ozone-to-emissions sensitivities. For the spatially integrated regression method, since ODV is a function of both location and emissions variables, ODV can be a function of location variables when we set the emissions to certain values (e.g., emissions levels of historical years). Therefore, we can calculate the spatial distribution of both ozone concentrations and ozone-to-emission sensitivities analytically for certain historical years (e.g., 1985, 2001, 2011, 2016, 2028, and zero emissions scenario). At the same time, CMAQ-HDDM is a natural tool to conduct spatial analysis. It should be noted that, as discussed in the previous section, the daily variations of the concentration and sensitivities estimated by the CMAQ-HDDM method are significant because of the significant variation in meteorology. In order to reflect the spatial distribution of high ozone meteorology, we mainly investigated the peak ozone day during the 13-day simulation period.

The results from both methods revealed some similar patterns in spatial distribution (Figures 4.5 and 4.6). Firstly, the ozone concentrations were higher over the northeastern part of the air basin and lower over the southwestern part. This pattern is consistent with the observations and can be explained by the sea breeze and mountain barrier effect. The sea wind tends to blow from the coast to the inland areas and is blocked by the mountains, so the major ozone precursors tend to accumulate in the northeastern part of the air basin and gradually lower, moving southwest to the coast.

Though this pattern has been consistent over the past four decades, the declining rate of ozone concentration over the basin is not evenly distributed. Since the inland area is affected more by the emissions precursors, ozone concentrations in that area were reduced much more dramatically than in the coastal area. Based on the observation data from those coastal sites, we also see that the ODVs of those sites remained almost stable, even with a significant reduction of emissions.

This pattern was also reflected by ozone-to-NOx emissions sensitivity. The coastal areas had a $dO_3/dENOx$ close to zero and did not change significantly over time. When we look at the $dO_3/dENOx$ of inland areas over different years, it is clear that the $dO_3/dENOx$ was mostly negative and continued to increase and became positive around 2000. This shows how the response of ozone to the NOx emissions changed, and indicates that the NOx emissions reductions were not beneficial to ozone control but have become more so, mostly for the inland areas. On the other hand, ozone-to-VOC emissions sensitivities decreased continually from 1985 onward. Spatially, $dO_3/dEVOC$ is higher in inland areas and lower along the coast, but the reduction rate of $dO_3/dENOx$ tends to be lower along the coast. This patterns indicates that the role of VOC in ozone control has been very important, but its relative importance has been decreasing. The inland area of the basin has seen more benefits from VOC reductions than the coastal area.

By comparing the empirical model and the CMAQ-HDDM model, we see that the general patterns for ozone concentration and sensitivities agree well with both the spatial distribution and temporal trend. The major difference is that the CMAQ-HDDM estimated more significant variations, both spatially and temporally. Spatially, the advantage of CMAQ-HDDM simulations is that they can capture ozone concentration and sensitivity variations caused by the spatial variation of local meteorology and the emissions. However, it may only reflect the pattern for a specific day, and there is a lack of overall information to reflect the general spatial distribution or temporal trend. On the other hand, the quadratic nature of the empirical function requires the empirical method to produce continuous spatial distributions, which means it is unable to capture hot or cold spots that are sensitive to local emissions, meteorologies, and geographic conditions. Therefore, using both methods together allows for a more comprehensive investigation of ozone-to-emissions response at both the macro and micro scales.

4.6 Summary

In this chapter, we combined the results from Chapter 2 (using the empirical method to investigate the ozone-to-emissions relationship) and Chapter 3 (using CMAQ-HDDM as another way to develop the ozone-emissions isopleth to investigate the ozone-to-emissions response) to make a comprehensive comparison between those two methods, and to answer the question we raised earlier: How well do chemical transport models, which are used to develop control strategies, capture ozone trends, and more importantly, sensitivities to emissions?

We used on the empirically developed ozone-emissions isopleth as references to evaluate the CMAQ-DDM derived isopleths. The first finding was that the HDDM-based method produced more spatial variations of the ozone-emissions response, which was driven by the spatial variations in both the emissions and meteorology, which are critical inputs to CMAQ but are not explicitly included in the empirical modeling. Qualitatively, the ozone-emissions responses produced similar-looking ozone isopleths, but further analyses revealed important differences. The sites that currently tend to experience the highest ozone levels are downwind of the central city area, and the ozone isopleths look similar, but the CMAQ-derived isopleths tend to have lower ozone levels, and large differences are found in the more extreme conditions (very high or very low emissions), where there are no data for developing the empirical model. Sites near the urban core, or along the coast, tend to have lower ozone, and the isopleths tend to be quite different, in part because the observed ODVs for those sites have varied less in response to emissions controls, and the driving factor of ozone variation has been more than just precursor emissions.

We found that the HDDM-based isopleth could better capture the detailed response under low NOx emissions, which is important for estimating ozone levels under future emission scenarios (much lower NOx and VOC emissions). In addition to the SRIDW method, the quadratic fitting method was also applied to develop the ozone-emission isopleth to help make the isopleth smoother and reduce the effect of extreme values from the simulation results due to daily variation. We observed that the HDDM quadratic-fitted isopleth was more similar to the empirically developed isopleth. This was expected, since both of those methods assume the ozone isopleth should follow a quadratic formation of VOC and NOx emissions, and used OLS to calculate the coefficient.

The empirically derived model has the lowest uncertainties along the historical emissions trajectory, so additional analyses were conducted to assess how closely the ozone-emissions sensitivities agreed between the two modeling approaches, as emissions changed between 1975 and 2018 (along the historical emissions trajectory), both with respect to ozone concentrations and ozone-to-emissions sensitivities. Similar to our findings based on the isopleth comparison, we saw that the observed ozone trends were captured well based on the CMAQ-derived isopleth for most of the sites (average $R^2 = 0.82$). Again, for the downwind high ozone locations, the ozone-to-NOx emissions relationships tended to have the correct sign over time, although there was not a 1:1 relationship. SN decreased in the 1980s for the first few years and started increasing continuously after 1990. The estimated increasing rates were similar from 1990 to 2010, based on both methods. CMAQ-estimated SV tended to be constant, with little variation before the year 2000, while the empirically estimated SV continued to decrease from the 1980s onward. For the coastal and urban core sites, there was a larger discrepancy between the observed and model-derived ozone-emissions sensitivities. While a number of reasons are identified for such differences, it appears that when applied to episodes chosen to capture high ozone levels in the downwind locations, CTMs may not capture how the higher ozone levels will respond in the locations further west, which includes many of the more highly populated regions.

In addition to the temporal emissions trajectory analysis, both the empirical and the CMAQ-HDDM methods were used to investigate the spatial distribution of the ozone concentration and ozone-to-emissions sensitivities. The results from both methods revealed similar patterns of spatial distribution. First, the ozone concentrations were higher over the northeastern part of the air basin and lower over the southwestern part of the air basin. Although this pattern has been consistent over the past four decades, the declining rate of ozone concentration over the basin was not evenly distributed. This pattern is also reflected by ozone-to-NOx emissions sensitivity. The coastal areas had a $dO_3/dENOx$ close to zero, which did not change significantly over time. When we looked at the $dO_3/dENOx$ of the inland area over different years, it was obvious that the $dO_3/dENOx$ was mostly negative but increased to positive. This shows that the response of ozone-to-NOx emissions has changed and indicates that NOx emissions reductions were not beneficial to ozone control, but have become increasingly beneficial mostly for the inland area.

On the other hand, ozone-to-VOC emissions sensitivities have been continuously decreasing since 1985. Spatially, $dO_3/dEVOC$ was higher in the inland area and lower along the coast, but the reduction rate of $dO_3/dENOx$ tended to be lower along the coast. These patterns indicate that the role of VOC in ozone control was very important, but its relative importance has been decreasing. BOC reductions are more beneficial in the inland areas of the basin.

The general patterns for ozone concentrations and sensitivities agree well with both spatial distribution and temporal trends. The major difference is that the CMAQ-HDDM model estimated more significant variations, both spatially and temporally.

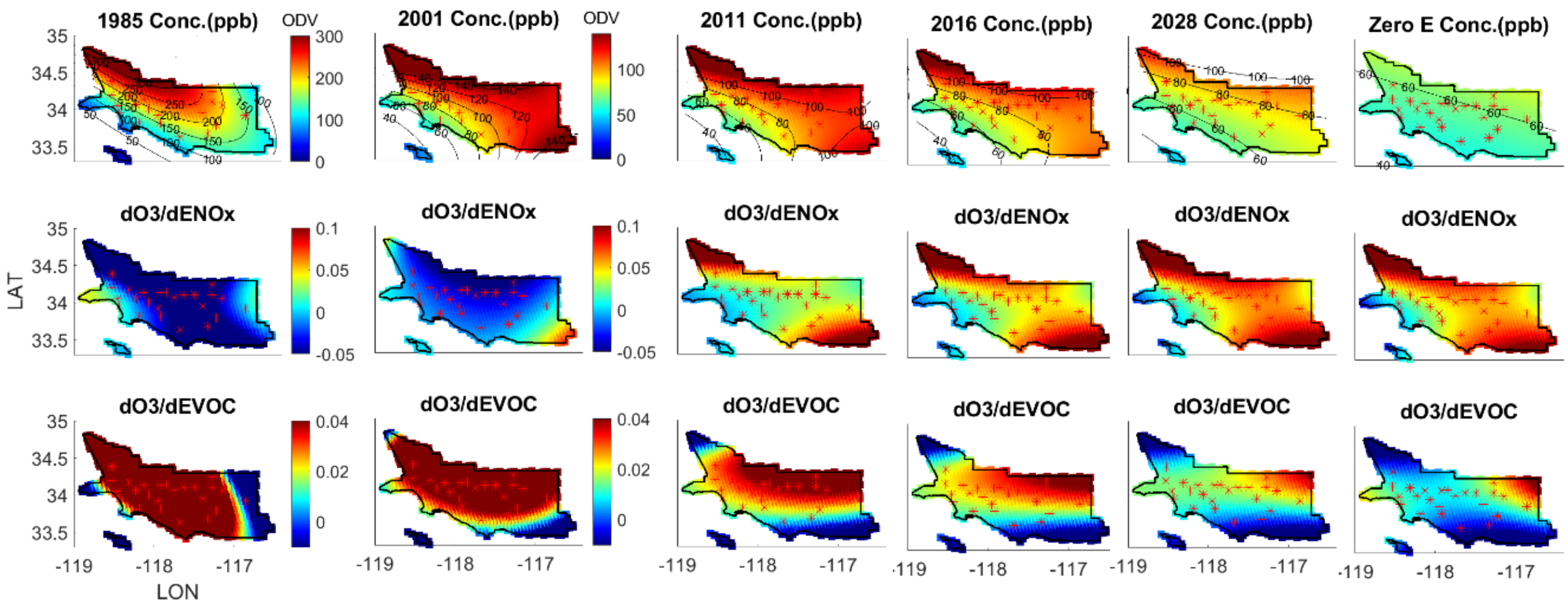

Figure 4.5 Spatial distribution of ozone concentrations and ozone-to-NOx and VOC emissions sensitivities over time (1985, 2001, 2011, 2016, 2028, and zeros emissions scenario) for the SoCAB based on the spatially integrated empirical model

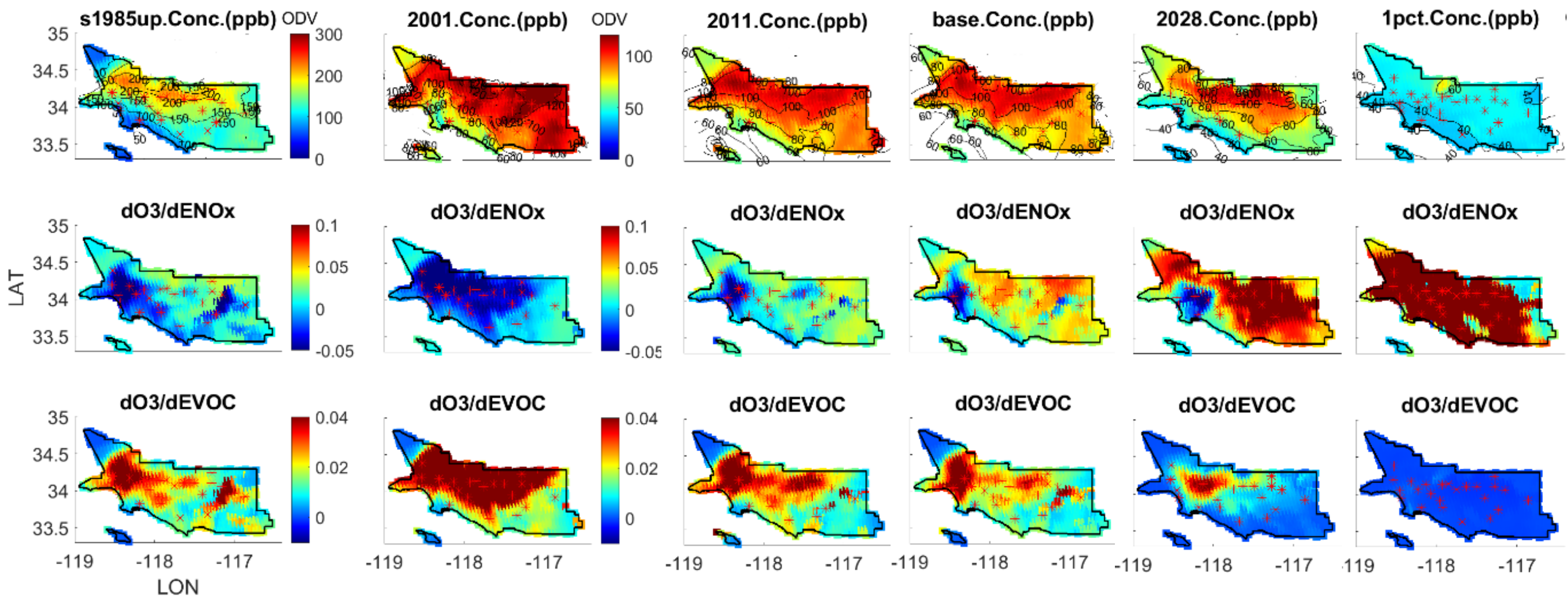

Figure 4.6 Spatial distribution of ozone concentrations and ozone-to-NOx and VOC emissions sensitivities over time (1985, 2001, 2011, 2016, 2028, and zeros emissions scenario) for SoCAB based on the CMAQ-HDDM simulations

Chapter 5: Uncertainty Analysis of Boundary Condition Impacts on the CMAQ-HDDM Modeling: Use of Alternative Boundary Conditions Derived from Hemispherical Modeling

5.1 Introduction

Chemical transport models (CTMs) simulations are sensitive to how boundary conditions (BCs) are set, particularly in regions near an upwind boundary. However, the boundary conditions are typically not observed, so setting BCs can introduce uncertainties. Boundary condition uncertainties can be particularly important when considering near-zero anthropogenic emissions of either VOC or NOx emissions, or both, leading to low simulated ozone. CMAQ and other regional CTMs can use default sets of BCs at the edges of the modeling domain (if nests are used, as is the case here, the BCs are applied to the "mother" domain). Global modeling using CTMs has also been used to provide BCs for finer resolution regional modeling (Emery et al., 2012; USEPA, 2020) and to provide estimates of the United States background ozone levels (Dolwick et al., 2015; Luo et al., 2020; Mueller and Mallard, 2011; Skipper et al., 2021).

The focus of this chapter is to describe the results from and analysis of extensive air quality modeling of the SoCAB using different sets of BCs for the 2016 emissions case and a near-zero anthropogenic emissions case to understand how the BCs would impact CTMs' estimation of ozone dynamics and the response to NOx and VOC emissions. While past research has focused on how setting BCs impacts ozone levels, we are particularly interested in how alternative BCs also impact the sensitivities of ozone-to-NOx and VOC emissions. In part, this is of specific interest because it can inform our prior analyses focusing on comparing simulated to observed ozone sensitivities. This also is important for regulatory analyses given how relative reduction factors (RRFs) are used in attainment demonstrations (Dunker et al., 2019; US EPA, 1999).

5.2 Methods

Four different simulations were conducted to assess how ozone, CO, NO_2, and VOC concentrations, as well as ozone-to-emission sensitivities, were impacted by alternate specifications of BCs. In addition to using BCs abstracted from a 12 km continental US (CONUS) domain, as is often done for regional modeling when using nested grids, we also obtained BCs for the SoCAB domain from a hemispheric CTM simulation from the US EPA (USEPA, 2020). This was done for 2016 base case emissions in the SoCAB, as well as for a case where emissions are set at 1% of the 2016 emissions to assess the role of BCs at very reduced levels.

5.2.1 Chemical Transport Modeling

Ozone, CO, NO_2, and VOC concentrations and ozone emissions sensitivities were calculated directly using the CMAQ-HDDM (Hakami et al., 2004). The model was applied to a two-month (June–July) 2016 period that experienced multiple high ozone episodes. The modeling was done using estimated emissions for 2016, along with a second set of simulations in which 1% of the 2016 NOx and VOC SoCAB emissions were used (Chapter 2).

In the base modeling, a nested grid modeling domain was used, with the outer domain covering the continental US (CONUS) using a 12 km horizontal resolution (Fig 3.1 and Appendix Figure B.1), and the inner domain having a 156 × 165 4 km x 4 km horizontal grid covering the SoCAB region (termed the LA4 domain as it covers Los Angeles and the surrounding area with a 4 km resolution grid). Default CMAQ BCs were used for this base case simulation.

As detailed in Chapter 3, emissions inputs for the 2016 base case modeling (2016 Base) were developed using the EPA's emissions modeling platforms ("www.epa.gov/air-emissions-modeling/2014-2016-version-7-air-emissions-modeling-platforms"). By utilizing these recent EPA emissions modeling platforms, the 2016 model-ready emissions were internally consistent with each other. BEIS was used to produce biogenic emissions off-line to help ensure consistency. This emission modeling platform uses SMOKE programs to generate hourly, gridded model species emissions fields that CMAQ requires as inputs.

The 2016 meteorological fields were generated using the Weather Research and Forecasting (WRF) model version 3.9.1.1, with inputs from NAM analysis and ADP observational datasets.

Further details of the model application and performance evaluation are found in Chapter 3 and Appendices B and C. Also, as described in Chapter 3, a reduced emissions case was conducted in which the emissions for both the 12 km CONUS domain and the LA4 domain were set at 1% of the 2016 emissions (2016, 1%). The same default BCs were used for the 12 km domain as for the base case (2016 BASE).

5.2.2 Alternative Hemispheric CMAQ Boundary Conditions

A second set of simulations was run using BCs abstracted from hemispheric-to-regional-scale CMAQ simulations (Mathur et al., 2018, 2017, 2016) conducted by the US EPA (2020). These BCs were generated from CMAQ simulations conducted as part of the most recent Policy Assessment for the Review of Ozone National Ambient Air Quality Standards (USEPA, 2020). The EPA modeling framework consisted of a series of nested runs for the year 2016, starting from a hemispheric-scale simulation with an ~108 km horizontal resolution, inside of which was nested a 36 km resolution simulation of North America, inside of which was nested a 12 km resolution simulation of the contiguous US. The system was applied in 2016, which is comparable to the modeling conducted as part of this study.

Two sets of BCs were provided. The first was a base emissions case in which all emissions were included in a set of nested simulations (H-CMAQ 2016). The second was a zero US anthropogenic (ZUSA) emissions case in which emissions were identical to the base case, except that anthropogenic emissions inside the US were not included (H-CMAQ ZUSA). The BCs for the LA4 grid were then generated from the 12 km CMAQ nest. The EPA simulations for both the 2016 emissions (H-CMAQ 2016) and H-CMAQ ZUSA cases were conducted across modeling scales (i.e., hemispheric to 36 km to 12 km). The BCs for the 4 km Los Angeles domain were extracted from the 12 km US simulations of the base and ZUSA cases and provided by EPA.

Other than the specific changes to the BCs described above, the meteorological fields and other CMAQ-HDDM configuration choices remained the same.

Table 5.1 Summary of the BCs and emissions inventories used for each simulation case. Separated by the simulation domain and resolution (CONUS 12 km and LA4 4 km).

Scenario	CONUS (12 km) Boundary Conditions	CONUS (12 km) Emissions	LA4 (4 km) Boundary Conditions	LA4 (4 km) Emissions

Static 2016	Default static BC	NEI 2016ff platform	Nested from default 12 km CONUS	NEI 2016ff platform
Static 1%	Default static BC	NEI 2016ff platform	Nested from default 12 km CONUS	1% of NEI 2016ff platform NOx and VOC emissions
H-CMAQ 2016	Nested from Hemispheric CMAQ	NEI 2016fe platform	Nested from H-CMAQ 2016 12 km CONUS	NEI 2016ff Platform
H-CMAQ ZUSA	Nested from hemispheric CMAQ	Zero US anthropogenic emissions (ZUSA)	Nested from H-CMAQ ZUSA 12 km CONUS	1% of the NEI 2016ff platform NOx and VOC emissions

5.3 Results and Discussion

Four sets of simulations were conducted based on different emissions levels and boundary conditions: 1) 2016 emissions with LA4 BC (Static, 2016); 2) 2016 emissions for the LA4 domain with boundary conditions from the hemispheric CMAQ system (H-CMAQ 2016); 3) 1% 2016 NOx and VOC emissions for the LA4 domain (Static 1%); and 4) 1% 2016 NOx and VOC emissions for the LA4 and ZUSA emissions hemispheric CMAQ simulation (H-CMAQ 1%). For each set of simulations, the same 13-day peak ozone period (June 2 to June 4 and July 20 to July 29) was used to evaluate the impact of alternative BCs.

We conducted quantitative comparisons for the 2016 base and 1% emissions cases of simulated MDA8 ozone, daily averaged CO, NO_2, and VOC concentrations, and ozone-to-emissions sensitivities between the results using two BCs for all sites over the 13-day period (Figure 5.1; Table 5.2). NO_2 concentrations using different BCs agreed well with R^2 ~ 1 and slope = 0.98, indicating that for the study period, the different BCs had very little effect on simulated NO_2 concentrations. For ozone, VOC, and CO, we observed that the results branched into two major groups: one was near the 1:1 line (Figure 5.1 blue dots; Table 5.2), while the other group showed that simulation using H-CMAQ BCs tended to estimate all three species lower than when using the static BCs (Figure 5.1 red dots; Table 5.2). Ozone-to-emissions sensitivities were relatively similar between BCs, though with some scatter, particularly for those results corresponding to the second group where the CO and VOC concentrations differed.

The results that do not agree well between the cases where the BCs were changed were almost all from two days, July 28 and July 29. Spatial plots over the July modeling period showed that the differences were driven by very elevated VOC and CO levels propagating into the domain from the northwest corner when using the static boundary condition 12 km simulations (both for the base 2016 and 1% emissions cases). These high levels then moved south and east, impacting the SoCAB. The two simulations using the hemispheric CMAQ system also showed elevated levels of CO and VOCs, but not nearly as high. These high levels were tracked down to the Soberanes Fire. The fire started in Monterrey County on July 22, continuing until October 12, and growing to 132,127 acres (Wikipedia). The Static 2016 and Static 1% emissions were both used the 2016ff NEI platform, while the hemispheric CMAQ simulations used the 2016fe NEI platform.

For July 28 and July 29, using the 2016 emissions, even with significant differences in the CO and VOC concentrations caused by the differences in the BCs, simulated ozone concentrations and sensitivities still fell mostly near the 1:1 line (Figures 4.1 & 4.2). The ozone spatial distributions were also similar for July 28 and July 29 between the two approaches for setting BCs. When looking at the comparisons for days other than July 28 and 29, all the species and sensitivities had R^2s and slopes close to 1 (Figures 5.1 & 5.2; Table 5.1). These findings suggest that for the SoCAB, ozone concentrations and ozone-to-emission sensitivities were mainly controlled by and sensitive to local emissions and meteorology rather than BCs. Even with considerable uncertainty involved in setting BCs, the CMAQ-HDDM ozone-to-emission sensitivities remain consistent.

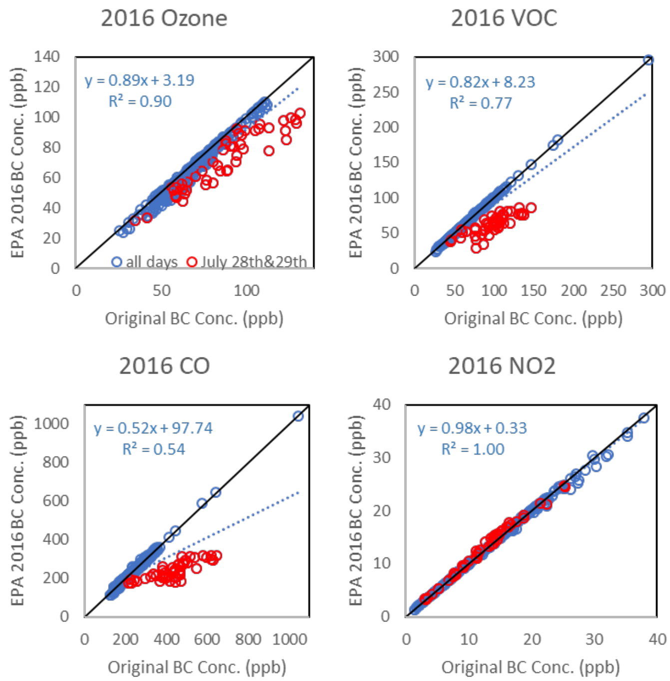

Figure 5.1 2016 emissions case: comparison of simulated daily averaged ozone, VOC, CO, and NO_2 concentrations between using EPA 2016 BC and using LA4 BC for all sites together over a 13-day study period. Red dots indicate the results for July 28 and 29. The regression equation and R^2 show the relationship based on all 13 days.

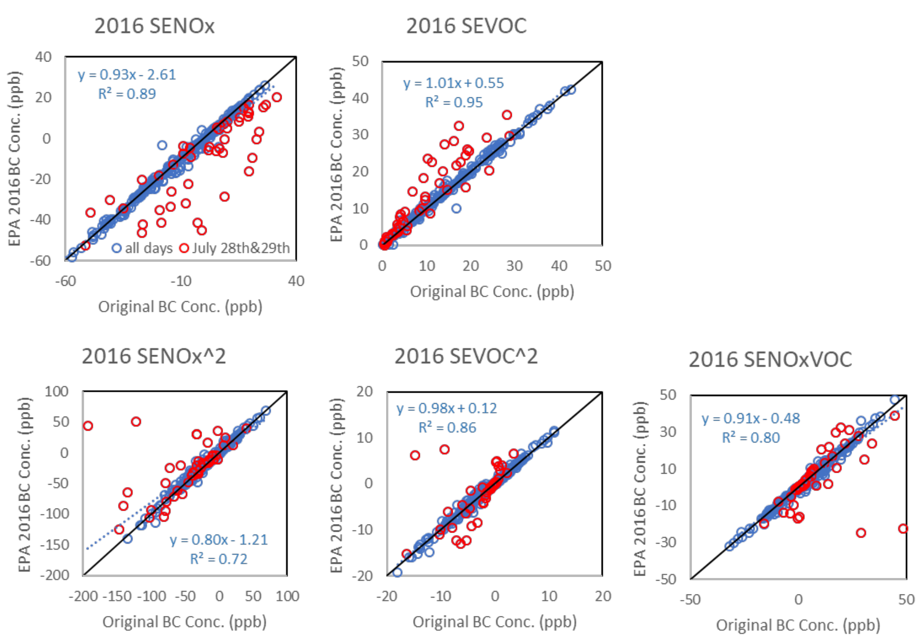

Figure 5.2 2016 emissions case: comparison of simulated daily averaged ozone-to-NOx and VOC emissions sensitivities between using EPA 2016 BC and using LA4 BC for all sites together over 13-days study period. SENOx and SEVOC are first-order ozone sensitivities to NOx and VOC emissions respectively. SENOX^2 and SEVOC^2 are second-order sensitivities of ozone-to-NOx and VOC emissions respectively. SENOxVOC is the second-order cross-sensitivity of ozone-to-NOx and VOC emissions. Red dots indicate the results for July 28 and 29. The regression equation and R^2 show the relationship based on all 13 days.

Table 5.2 Summary of comparison statistics of simulated species concentrations and ozone-to-emission sensitivities using hemispheric CMAQ 2016 and 12 km CMAQ BC. Statistic metrics include linear regression R^2, slope, and intercept. The comparison is separated by emissions levels (2016 emissions and 1% 2016 NOx and VOC emissions. Statistics were calculated based on different date groups, including all days, only July 28 & 29, and days other than July 28 & 29.

		2016			**1%**		
		all days	28th&29th	Others	all days	28th&29th	Others
Ozone	R^2	0.90	0.87	0.98	0.64	0.07	0.78
	Slope	0.89	0.73	1.03	0.95	0.47	1.01
	Intercept	3.19	7.50	-4.97	-9.06	6.63	-10.62
CO	R^2	0.54	0.65	0.99	0.43	0.56	0.98
	Slope	0.52	0.35	1.01	0.38	0.11	1.01
	Intercept	97.74	89.87	-5.35	46.54	79.82	-7.36
NO2	R^2	1.00	0.99	1.00	1.00	0.98	1.00
	Slope	0.98	0.99	0.98	1.03	1.06	1.03
	Intercept	0.33	0.56	0.26	-0.01	-0.03	-0.01
VOC	R^2	0.77	0.67	1.00	0.60	0.18	1.00
	Slope	0.82	0.49	1.01	0.58	0.20	1.01
	Intercept	8.23	14.81	-1.11	5.94	12.11	-0.08
SENOx	R^2	0.89	0.68	0.99	0.79	0.62	0.86
	Slope	0.93	0.84	0.99	1.01	0.88	1.05
	Intercept	-2.61	-10.82	-0.54	0.50	1.00	0.38
SEVOC	R^2	0.95	0.84	0.99	0.80	0.82	0.81
	Slope	1.01	1.20	1.00	1.17	1.62	1.17
	Intercept	0.55	1.33	0.17	0.00	0.00	0.00
SENOxEVOC	R^2	0.80	0.25	0.98	0.69	0.51	0.68
	Slope	0.91	0.55	1.01	1.25	1.85	1.25
	Intercept	-0.48	-0.06	-0.35	0.00	0.00	0.00
SENOx^2	R^2	0.72	0.24	0.98	0.75	0.50	0.81
	Slope	0.80	0.44	1.00	1.36	2.45	1.42
	Intercept	-1.21	-6.59	0.61	-0.07	-0.12	-0.04
SEVOC^2	R^2	0.86	0.33	0.99	0.76	0.26	0.78
	Slope	0.98	0.72	1.01	1.28	2.10	1.30
	Intercept	0.12	-0.19	0.12	0.00	0.00	0.00

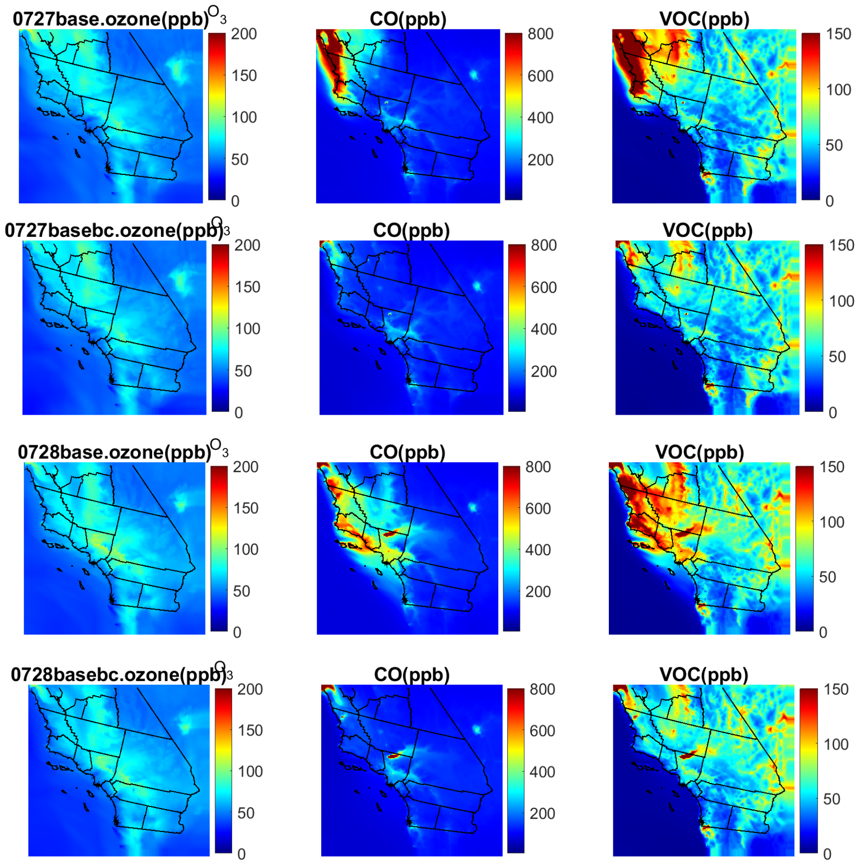

Figure 5.3 2016 emissions case: Spatial distribution of daily average ozone, CO, and VOC concentrations over the LA4 domain for July 27 and 28, based on both EPA 2016 BC and LA4 BC. First row: July 27 based on LA4 BC; Second row: July 27 based on EPA 2016 BC; Third row: July 28 based on 12 km CMAQ BC; Fourth row: July 28 based on EPA Hemispheric CMAQ 2016 BC.

We also conducted a quantitative comparison for the 1% 2016 NOx and VOC emissions cases using the two BCs (Static 1% and H-CMAQ 1%) for all sites together over the 13-day period (Figure 5.4; Table 5.1). Similar to the 2016 emissions case, NO_2 concentrations using the different BCs agreed well with R^2~1 and a slope = 1.03. For VOC and CO, we again observed two groups, with one group reflecting the results from July 28 and July 29, and having much lower simulated VOC and CO concentrations when using the hemispheric CMAQ with no US emissions. Since the emissions levels for the 1% cases were much lower, the differences were more evident (Figure 5.4 red dots). The results from days other than July 28 and 29 fell mostly along the 1:1 line (Figure 5.4, blue dots; Table 5.1). However, unlike cases using the 2016 emissions, the simulated ozone concentrations using the static BCs and those derived from the hemispheric CMAQ system were different (R^2 = 0.64, slope = 0.95, and intercept = 9.06). Of particular note is that the H-CMAQ 1% case has ozone levels biased about 11.5 ppb lower than the base method. This is not unexpected, given the higher ozone levels at the boundary of the 4 km domain when using the static boundary condition based on the default BCs for the 12 km mother domain, and given that the SoCAB domain is located near the western boundary. The winds are predominantly from the west, so this is typically an inflow boundary. For ozone-emissions sensitivities, the simulation results found that using different BCs agreed relatively well, while the correlation was poorer compared to the 2016 emissions case. The main difference was for second-order sensitivity to NOx emissions, where using the hemispheric CMAQ boundary led to more negative second-order sensitivities (offset by higher first-order sensitivities). For the 1% emissions cases, ozone sensitivities to NOx emissions sensitivity tended to be slightly higher, and the sensitivities to VOC emissions tended to be slightly lower when using BCs from hemispheric CMAQ.

For July 28 and 29, the simulated ozone concentrations and sensitivities deviated somewhat more from the 1:1 line than for other days (Figures 5.4 & 5.5), and the ozone spatial distributions were somewhat different. However, the simulated concentrations and sensitivities were mostly different for second-order sensitivity to NOx emissions.

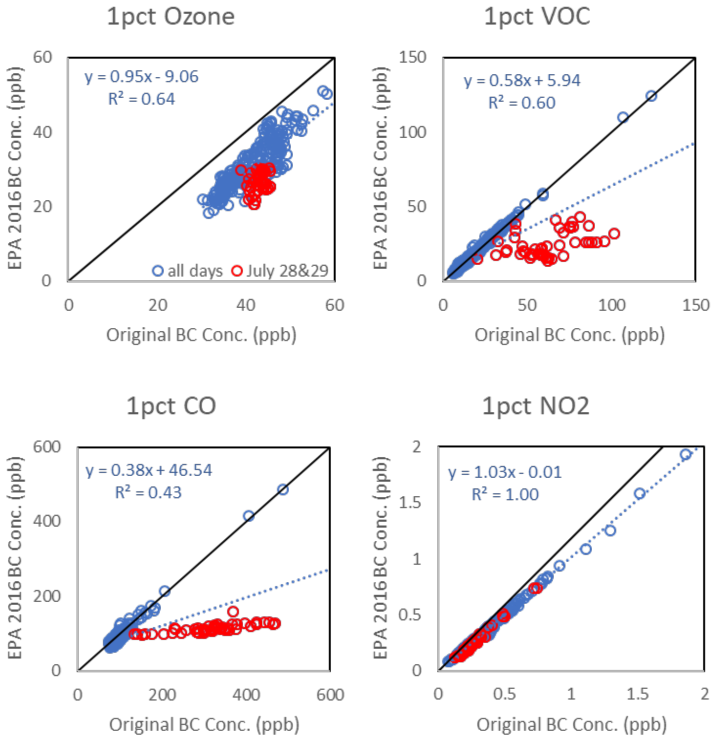

Figure 5.4 1% 2016 emissions case: comparison of simulated daily averaged ozone, VOC, CO, and NO_2 concentrations between using ZUSA BC and LA4 BC for all sites together over a 13-day study period. Red dots indicate the results for July 28 and 29. The regression equation and R^2 show the relationship based on all 13 days.

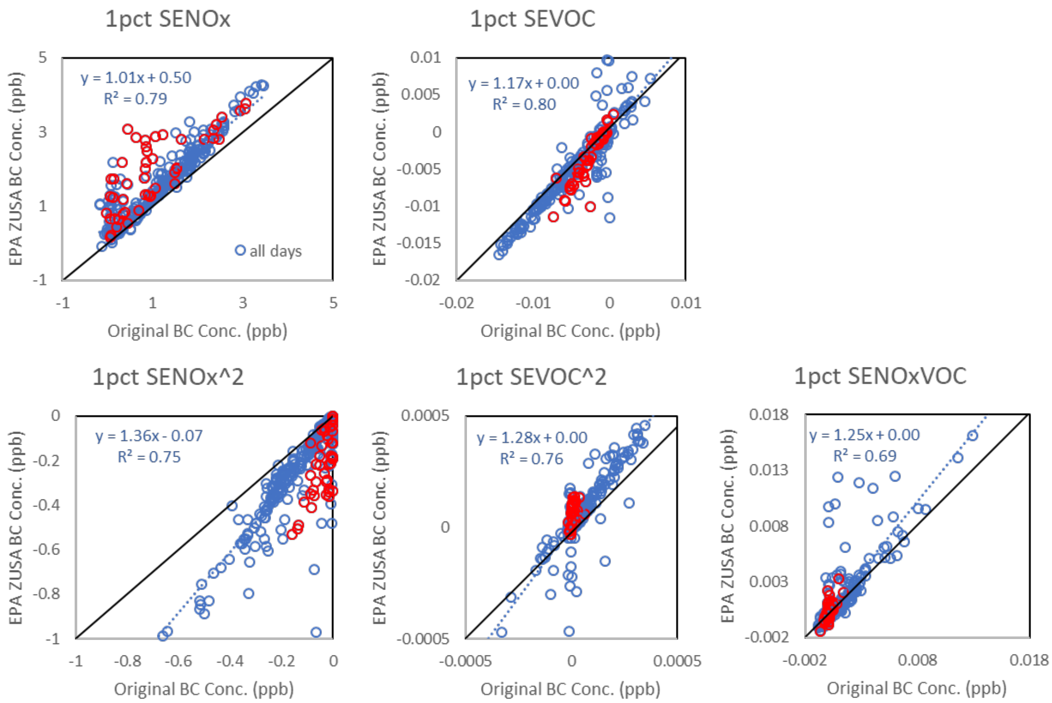

Figure 5.5 1% 2016 emissions case: comparison of simulated daily averaged ozone-to-NOx and VOC emissions sensitivities between using ZUSA BC and using LA4 BC for all sites together over a 13-day period. SENOx and SEVOC are ozone-to-NOx and VOC emissions' first-order sensitivities, respectively. SENOX^2 and SEVOC^2 are ozone-to-NOx and VOC emissions second-order sensitivities, respectively. SENOxVOC is ozone-to-NOx and VOC cross second-order sensitivity. Red dots indicate the results for July 28 and 29. The regression equation and R^2 show the relationship based on all 13 days.

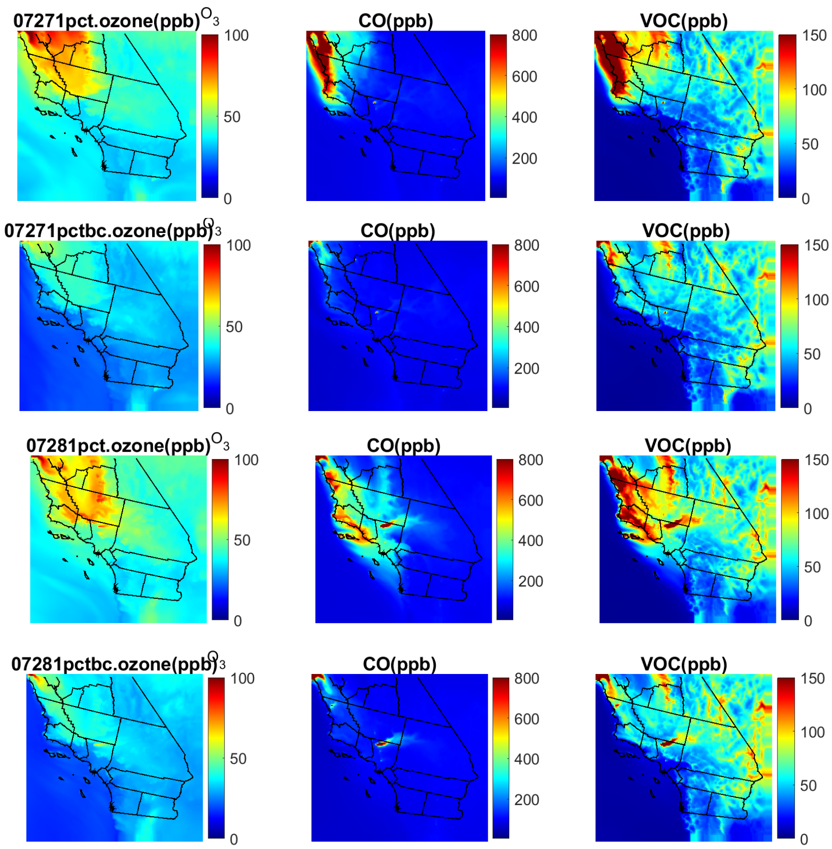

Figure 5.6 1% 2016 emissions case: Spatial distribution of daily average ozone, CO, and VOC concentrations over the LA4 domain for July 27 and 28, based on both ZUSA BC and LA4 BC. First row: July 27 based on LA4 BC; Second row: July 27 based on ZUSA BC; Third row: July 28 based on 12 km 1% CMAQ BCs; Fourth row: July 28 based on ZUSA Hemispheric CMAQ BC.

5.4 Summary

The focus of this chapter was to assess the impact of using an alternative set of BCs on air quality model results and model sensitivities. Application of CMAQ to the Southern California 4 km resolution domain was conducted using both the static BCs extracted from at 12 km CMAQ application at the continental scale and using boundary conditions from an application of hemispheric CMAQ for the same 2016 period. The meteorological fields, and other CMAQ-DDM configurations were kept the same. In addition to using the base case emissions, we also conducted a second set of simulations using anthropogenic emissions within the 4 km domain set at 1% of the original 2016 anthropogenic emissions, with BCs taken from a 12 km CMAQ simulation using similarly reduced anthropogenic emissions for comparison with BCs driven by a ZUSA hemispheric CMAQ emissions case. In summary, the four sets of simulations were: 1) 2016 emissions for both the 4 km LA domain and the 12 km US domain BCs; 2) 2016 emissions for both the 4 km LA domain and the 2016 hemispheric CMAQ BCs; 3) 1% of the 2016 NOx and VOC (and CO) emissions with boundary conditions taken from a 1% emissions applied to the 12 km resolution US domain; and 4) 1% 2016 NOx and VOC emissions with boundary conditions from the hemispheric, no US anthropogenic emissions simulation. For each set of simulations, the same 13-day peak ozone period (June 2 to June 4 and July 20 to July 29) was used.

The ozone results were similar when the 2016 base case emissions were used independent of the BCs, although larger differences were found for the last two days of the July simulation. When using 1% (NOx and VOC) emissions, the estimated ozone concentrations by using the hemispheric CMAQ, zero anthropogenic US emissions (ZUSA) BC, were about 11.5 ppb lower on average than when using the static boundary condition case. This was tied directly to having lower ozone fluxes to the LA4 domain. NO_2 concentrations using different BCs agreed well for both the 2016 case and the 1% case, which indicated that for the study period of the LA4 domain, different BCs had very little effect on simulated NO_2 concentrations.

For VOC and CO concentrations, the comparison branched into two major groups, with one group being along the 1:1 line with very little difference. The other group corresponded to July 28 and 29, when the VOC and CO concentrations, as simulated using the hemispheric CMAQ to provide BCs, were much lower. This was tracked down to the very different impact of the Soberanes Fire, located at the northwest boundary of the LA4 study domain. It was also tied to the emissions processing from different versions of the NEI emissions platforms used to construct the BCs.

For ozone-to-emission sensitivities, based on the simulation results, we found that using the different BCs agreed relatively well for the 2016 case, independent of whether the hemispheric or 12 km CMAQ results were used for providing boundary conditions. For the 1% LA4 emissions case, the sensitivities still agreed relatively well, though not as closely as when using the base case emissions. Ozone sensitivities to NOx emissions tended to be slightly higher, and sensitivities to VOC emissions tended to be slightly lower when using ZUSA BCs. This finding is expected because after shutting down all anthropogenic emissions, the BCs became more important.

These findings support the conclusion that the sensitivities of the SoCAB's ozone-to-emissions at current emissions levels are not very dependent on the BCs, which is an important and a positive result. Given the way attainment demonstration modeling is conducted, it is the accuracy of the sensitivity to emissions that is most important, as opposed to the close agreement between the simulated and observed ozone (though that agreement is also influential). On the other hand, different ozone BCs impact the absolute ozone concentrations, particularly for low (and zero) emissions cases.

Chapter 6: Summary and Conclusions

In this project, we developed, applied, and evaluated different methods to estimate ozone-emission relationships, with a focus on the South Coast Air Basin in California (SoCAB). The SoCAB has historically and currently experienced some of the highest, if not the highest, ozone levels in the United States. One objective of the work was to investigate the spatial pattern and variation of ozone isopleths by expanding the regression-based empirical method and applying that approach to multiple monitoring sites in different locations in the SoCAB. Another focus was to conduct extensive air quality modeling of the SoCAB for a number of historical and future years to understand how well the current chemical transport models (CTMs) captured ozone dynamics and the response to controls of NOx and VOC. Finally, ozone responses to emissions were directly compared between empirical and chemical transport model-derived sensitivities (including the use of isopleths).

In Chapter 2, we described the development and evaluation of the empirical methods to investigate ozone-emission relationships spatially using ozone design values observed at 24 monitoring sites within the SoCAB. Two different methods were developed and applied: 1) a multivariate regression model with ODV of each monitoring site as a response variable and annual averaged estimated NOx and VOC emissions as predictor variables using a quadratic relationship applied separately to data at each monitoring site, and 2) a multivariate regression model that included the spatial location (longitude and latitude) of the monitoring sites to build a single regression model for application across the SoCAB.

As found in prior studies (e.g., Milford et al., 1989), the ozone-emissions relationships varied across the SoCAB, with downwind peak ozone concentrations being generally higher than those found more in the city core or near the coast, and also more sensitive to emissions of NOx. Comparing the isopleths of locations in the city core (e.g., LA North Main) vs. more downwind (e.g., Azusa and Crestline), one sees that locations near the coast (upwind) have lower ODV levels, and ODVs are less sensitive to NOx emissions reductions than inland locations during high ozone periods. This is mainly caused by the meteorology and geographic features of the LA region and is related to the combined effects of surface sea breeze and mountain barriers. Sea breezes cause the transport of precursor pollutants from the coast to the inland, while mountain barriers lead to the accumulation of pollutants.

For both methods, the average resulting R^2 is higher than 0.9. This performance suggests that, at least near the observational values, the models capture how ozone responds to emissions changes. In order to further test the predictive ability of this model, we also conducted 10-fold cross validation leading to stable results with a high R^2 (> 0.9) and low RMSE. This analysis indicates that the decline of ODVs in the SoCAB over the past several decades is mainly (> 90%) caused by emissions reductions.

The spatially integrated model has some advantages over the collection of models developed for each site, particularly given that the estimated isopleths and performance are similar. Firstly, the spatial model can estimate the isopleth for locations without any monitoring sites. Another insightful application is to use the model to generate ODV spatial distribution at varying emission levels. We see that at current emissions levels, the ODVs are lower along the coast and increase when moving inland. Under zero anthropogenic emissions, the log model indicates that the ODVs are almost constant over the air basin, though slightly higher at the coast. The base (non-log) model shows a higher level at the coast, with a stronger negative gradient going inland. The reduced variable model has a constant zero-emissions level across the basin of 55.6 ppb.

In recent years, we have noticed that all sites have crossed the zero-NOx sensitivity lines, which means the further reduction of NOx emissions would be much more beneficial for ozone control.

Overall, these results are particularly important in providing information on the variation of sensitivities of ODV to emissions, both temporally and spatially. This provides insightful advice for policy making regarding future emission strategies at different locations.

We expanded the application of this empirical approach to further develop an exposure model to investigate the empirical model-based exposure isopleths for the SoCAB. We filtered the ozone concentration data by five metrics, so we could not only use ODV as the response variable, but also other ozone concentration metrics to train the model and build the exposure for different ozone metrics. Those metrics include: the maximum ozone value of each year, the annual mean of the eight-hour maximum ozone for each day, and the annual mean of the maximum ozone for the days for which the maximum ozone is higher than 40 ppb (the background ozone concentration), 60 ppb, and 70 ppb (equivalent to the current ozone standard), respectively.

From ozone exposure isopleths, we see that ozone exposure decreased from 1980 to 2019 as VOC and NOx emissions decreased. For ozone exposures under high ozone levels (ODV, peak, higher than 60 ppb, 70 ppb), emissions are transferred from above the zero-NOx-sensitivity line to below the zero-NOx-sensitivity line, which means that controlling NOx emissions led to slight increases in ozone exposure in previous years, with decreases in more recent years. Also, emissions in recent years are below the equal NOx-VOC sensitivity ridgeline, which suggests that controlling NOx is beneficial for decreasing high-level ozone exposure. For exposure higher than 40 ppb ozone, emissions for most of the previous years are above the zero-NOx-sensitivity line, while emissions are below the zero-NOx-sensitivity line and near the equal NOx-VOC sensitivity line in recent years, which indicates that controlling VOC was preferable in previous years, while either controlling VOC or NOx can decrease ozone exposure in more recent years. For exposure to mean ozone, emissions have been above the zero-NOx-sensitivity line in recent years, which indicates that decreasing VOC emissions diminishes exposure from the mean ozone.

The Chapter 3 details the application of an advanced chemical transport model (CMAQ-HDDM) to the SoCAB to investigate ozone-emissions relationships by simulating ozone concentrations and sensitivities to NOx and VOC emissions. Those results, including the sensitivities, were analyzed independently and also used to construct ozone-emission isopleths using a modified inverse distance-weighted method.

CMAQ-HDDM was applied to both past (1985, 2001, 2011, 2016) and future (2028) emission estimates at a 4 km resolution over the SoCAB using the CB6 mechanism. The model was applied covering the Continental US with a 12 km (horizontal) resolution, with a nested domain covering much of southern California with 156 × 165 horizontal grid cells resolved at 4 km spatial resolution. Simulations used meteorology from June 1, 2016 to July 31, 2016, as the base year, a period capturing multiple high ozone events. Emissions inventories for five years (1985, 2001, 2011, 2016, and 2028) were developed based on NEI inventories (as described in Chapter 3, back-casting to 1985 involved using CARB emissions estimates and scientific studies of emissions composition). For the most part, the five-year set of simulations found, qualitatively, the observed decreases in ozone, and that ozone will continue to decrease in the future. Simulated peak 2028 levels are about 18 ppb less than those in 2016.

CMAQ simulation results were evaluated by comparing simulated species concentrations with observed concentrations. For 2016 (the base year), a detailed evaluation was conducted using observations matched in time and space. For other years, model-observation comparisons were made using the rank ordering of both observed and simulated concentrations. Both the 2011 and 2016 comparisons show high consistency between simulated and observed MDA8 ozone concentrations, suggesting that the CMAQ simulations capture peak ozone values in terms of their relationship to estimated emissions. However, the 1985 and 2001 results both tended to be biased low (by about 20%) for capturing peak ozone levels. CO and NOx observations were also investigated, and it was found that the simulation tended to be biased high in NO_2-to-CO ratios over the entire year. We investigated multiple potential reasons that could lead to the low bias in the simulated ozone levels, and the final results suggest that the estimated VOC emissions should be about 40% higher, and the estimated NOx emissions should be about 20% lower than the inventories. This improves both the simulated ozone levels, and the NOx:CO relationship between the years.

Further analysis found that the emissions estimate bias varies with time, and a linear fit of emissions adjustments that led to the best fit with the observed ozone and ozone sensitivities suggests that the NOx emissions estimate was biased high by 19% in 1975, with the bias decreasing at 0.3% per year (i.e., suggesting that the estimated inventory is improving over time). For VOC, the analysis suggests that the 1975 emissions estimates were biased low by 43%, with the high bias reducing about 4.7% per year. There appears to be a residual bias, as suggested by others (Hassler et al., 2016; McDonald et al., 2018, 2012; Qin et al., 2021). This analysis is not conclusive that emissions biases are present, but is consistent with recent studies.

CMAQ's high-order decoupled direct method (HDDM) was used to calculate both first- and second-order sensitivities. We conducted a set of 15 CMAQ-HDDM simulations with different emissions levels, and 11 of the cases were used to develop ozone-NOx-VOC isopleth diagrams at locations across the basin, and another four of the cases were used to evaluate the simulated ozone-to-emissions sensitivities. Individual isopleths for each emissions scenario were generated using the first- and second-order sensitivities as terms in a quadratic Taylor series. A revised inverse distance-weighted method was developed for integrating the individual isopleths and for producing an isopleth combining the results from all 11 simulations. Another method was developed to construct ozone isopleths using the least squares fitting of the simulated ozone concentrations and sensitivities. Both methods lead to ozone-emissions isopleths that typically have a similar shape as the isopleths developed by other studies and those empirically derived, though they are quantitatively different. However, due to smoothing and developing reduced form ozone-emissions relationships, the isopleths do not exactly match the results from the underlying CMAQ simulations. A further issue in comparing the CMAQ-derived isopleths with the empirically derived isopleths is that the CMAQ simulations were developed based on the NEI, while the empirical isopleths were based on CARB-estimated emissions.

There are two very important caveats in the use of CMAQ (or empirically derived) isopleths. First, these regions are linked to MDA8 ozone using meteorologies that led to high ozone in the SoCAB (in this case, at Crestline, the monitor that has experienced a majority of the highest ODV in the SoCAB in recent years). At other times of the day, and on lower ozone days, ozone tends to be less positively sensitive, or even negatively sensitive, to NOx emissions, i.e., the conditions used to construct the isopleth were based on conditions that tend to favor NOx control effectiveness. This is appropriate, as the standard is based on high ozone conditions. A second point is that the choice of days is not driven by the highest ozone levels at each monitor separately, such that the conditions leading to seasonal peak ozone levels in Crestline are not the same as would be experienced in the urban Los Angeles core or along the coast.

Similar to the analysis used for the empirically based isopleths, the CMAQ-derived ozone isopleths were used to identify “NOx-saturated” conditions (where increased NOx emissions decrease peak ozone levels, i.e., SN = 0), and the region where, on a relative emissions reduction basis (i.e., per % of emissions), NOx emissions reductions lead to greater ozone decreases than the same percentage decrease in VOC emissions. The region between the two is where both NOx and VOC emissions reductions lead to ozone decreases, but VOC emissions reductions provide more benefit at reducing peak ozone at those sites on high ozone days. The CMAQ-derived isopleth for Crestline (the monitoring location with the highest modeled ozone for 2016) suggests that for much of the 1975–2018 period, peak ozone levels have been most sensitive to reducing VOCs, and, up until at least 2005, NOx controls would have led to ozone increases. Recent NOx emissions reductions, however, are pushing the SoCAB to a region where, on a percentage emissions basis, NOx emissions reductions will lead to greater ozone reductions than VOC emissions controls. Further, the Crestline ozone isopleth suggests that even with 100% reductions in anthropogenic emissions under some NOx emissions levels, ozone will remain elevated (e.g., the maximum ozone along the zero VOC emissions axis of the isopleth has a maximum of 78 ppb). This is due largely to biogenic emissions within the SoCAB, along with the transport of organics and CO into the SoCAB. However, analysis of ozone isopleths at urban cores and coastal sites (e.g., LA North Main) reveals very different responses to emissions.

The inland ozone concentration was located below the zero-SN line, which indicates that further reductions in NOx would be beneficial for ozone concentration mitigation. The coastal ozone concentration is located in the NOx-sensitive regime, well below the zero-SN line and the SN = SV line, which suggests that NOx reduction is effective in reducing ozone concentration. Despite the difference in first-order sensitivities, especially in SN, which differ in sign, the second-order sensitivities between the inland and coastal areas are similar.

We evaluated the DDM results themselves by various means, including comparing the DDM and brute force results and evaluating the uncertainty of the developed isopleth by using data withholding. The ozone concentrations calculated by the isopleths are all significantly correlated with the CMAQ-modeled concentrations, with R^2 values very close to 1.

In Chapter 4, we combined empirical and CTM modeling to comprehensively address a driving question motivating this project: “How well do chemical transport models, which are used to develop control strategies, capture observed ozone trends, and, importantly, sensitivities to emissions?” Both empirically and CTM-derived isopleths have weaknesses, as identified above, although the empirically derived relationships are derived from actual observations over multiple decades. Hence, we used the empirically developed ozone-emissions isopleths and sensitivities as a reference for evaluating CMAQ-HDDM-derived emissions sensitivities.

The HDDM-based sensitivities capture much more spatial variation in the ozone-emissions responses. This is expected, as the spatial variation of land use, emissions, and meteorological variables are key inputs to CTMs, while the empirically derived approaches have little or no explicit dependence on those inputs. For some sites (e.g., Crestline), we saw that the estimated ozone isopleths were qualitatively similar based on those two different methods. Detailed comparison of the ozone-emissions sensitivities according to historic (estimated) emission conditions does not follow a one-to-one relationship, but instead, though both CMAQ-based and empirically based methods have a similar trend in estimating the SN after 2010, we can see that CMAQ-estimated SN started growing much faster compared to empirically estimated SN.

A similar trend is found for other far-inland monitoring sites (e.g., Azusa), and these are the locations that typically experience the highest observed levels in the SoCAB. This indicates that the HDDM-derived response over the emissions space is consistent with the empirically derived response, which describes the overall characteristics of the ozone-emissions relationship based on long-term estimated emissions and ODV observations. For the more urban core and coastal sites with low ozone levels (e.g., LA North Main), the differences between methods are more substantial because other factors (such as meteorology) can play more important roles in ozone variations, apart from emissions. It is also shown that the HDDM-based isopleth can better capture the response of ozone-to-emissions under low NOx emissions, which is important for estimating projected ozone levels under future emissions scenarios (much lower NOx and VOC emissions).

In addition to the IDW method, the quadratic fitting method has also been applied to develop ozone-emission isopleths to help make the isopleths smoother and to reduce the effect of extreme values from the simulation results due to daily variation. We observed that the HDDM quadratic-fitted isopleth was more similar to the empirically developed isopleth. This was expected, since both of those methods assume that the ozone isopleth should follow a quadratic form relating ozone levels to VOC and NOx emissions.

To further evaluate the difference between HDDM-derived isopleth and the empirically derived isopleth, we compared the estimated historical trends (trajectory) of ozone concentrations and ozone-to-emissions sensitivities. We found that the observed ozone trends were captured well based on the HDDM-derived isopleth (R^2 = 0.87 and 0.98 for Azusa and Crestline), though the ozone levels tended to be higher when estimated by the HDDM isopleth, at about 10% for Azusa and less than 5% for Crestline. This finding strongly indicates that the CTM is able to effectively capture historical ozone concentration trends in different locations by applying robust integration methods (revised IDW here) to produce the isopleth. We observed a similar pattern in the comparison between the HDDM and empirically derived ozone-to-NOx emissions sensitivities.

In addition to the comparison of ozone levels and sensitivities along the "emissions trajectory," the empirical and CMAQ-HDDM methods were used to investigate the spatial distribution of the ozone concentration and ozone-to-emissions sensitivities. The results from both methods revealed similar patterns of the spatial distribution. First, the ozone concentrations are higher over the northeastern part of the air basin and lower over the southwestern part of the air basin. Though this pattern has been consistent over the past four decades, the declining rate of ozone concentration over the basin is not evenly distributed. This pattern is also reflected by ozone-to-NOx emissions sensitivity. The coastal areas have a dO3/dENOx close to zero, and this does not change significantly over time. In the early years, a very large portion of the SoCAB had a dO3/dENOx that was mostly negative. With time, the area with a negative NOx sensitivity has decreased, and now only the urban LA core area continues to have a negative NOx sensitivity. On the other hand, ozone-to-VOC emission sensitivities are almost always positive, although they have decreased over time. Spatially, the dO3/dEVOC is higher in inland areas and lower along the coast. This pattern indicates that the role of VOC in ozone control has been beneficial historically, though its relative importance is decreasing.

Comparing the two methods used to develop the HDDM-based ozone-emission isopleth finds there is no simple way to say which method is better than the other. Each has its own advantages in specific applications. Both methods are able to capture the ozone concentration trend along the historical emissions trend, but the HDDM-based isopleths tend to be biased high in recent years (while better capturing a leveling-off and even increases in the ODVs from and after 2012) and biased low in early years because of the biased-low estimation of 1985 ozone levels. The CMAQ-based method has a significant advantage in better capturing the spatial variations of sensitivities, which is especially important for urban sites that are sensitive to local emissions and meteorologies. However, for the coastal and urban core sites, there is a larger discrepancy between the observed and model-derived ozone-emission sensitivities. While a number of reasons have been identified for such differences, this suggests that CTMs, when applied to episodes chosen to capture high levels in the downwind locations, may not capture how the higher ozone levels will respond in the locations further west, which includes many of the more highly populated regions. The CMAQ-based method can better capture the rapid increase of SN when NOx emissions are much lower, while the empirical methods cannot, since there are no observation points with extremely low NOx emissions to train the model. While lacking the significant texture of sensitivities that the CMAQ-HDDM method has, the empirical method is still a good tool to use to capture the overall trend of ozone concentrations and sensitivities for inland sites like Crestline in a computationally effective way.

In Chapter 5, we conducted extensive air quality modeling of the SoCAB using different sets of BCs for the 2016 emissions case and the near-zero anthropogenic emissions case to understand how the BCs would impact the CTM's estimation of ozone dynamics and the response to NOx and VOC emissions. The BCs include regional and hemispheric boundary conditions, with emissions input, meteorology fields, and other CMAQ-DDM configurations staying the same. We found that NO_2 concentrations using different BCs agreed well for both the 2016 case and the 1% case. For ozone, VOC, and CO concentrations, however, the comparison branched into two major groups. The comparison of simulated concentrations using different BCs only slightly deviated from the 1:1 line for the 2016 case, but the estimated ozone concentrations using LA4 BC and ZUSA appeared to be more different. The estimated ozone concentrations when using ZUSA BC are about 11.5 ppb lower on average than when using LA4 BC. For ozone-to-emissions sensitivities, the simulation results from using different BCs agreed relatively well for the 2016 case, with some points scattered away from the 1:1 line. For the 1% case, the simulation results from using different BCs still agreed relatively well, while the correlation was poorer than for the 2016 emissions case. Ozone-to-NOx emissions sensitivity tends to be slightly higher, and ozone-to-VOC emissions sensitivity tends to be slightly lower when using ZUSA BC. For July 28 and 29, when larger differences were observed, the likely reason was that those two BCs made relatively different estimations of the emissions for the Soberanes Fire located at the northwest boundary of the study domain. This is likely caused by the emissions processing from different versions of NEI emissions platforms used to construct the BCs.

These findings suggest that for the SoCAB, the ozone concentrations and ozone-to-emission sensitivities are mainly controlled by and sensitive to local emissions and meteorologies rather than BCs. Even with considerable uncertainty involved in BCs (days like July 28 and 29), the CMAQ-HDDM can still simulate ozone concentrations to capture observations and estimate ozone-to-emissions sensitivities consistently. On the other hand, different BCs may play an important role in estimating background ozone concentrations. When estimating background ozone, CMAQ-HDDM can still estimate ozone-to-emission sensitivities consistently, while it is impacted more by BC uncertainties.

Overall, the major “take-home” messages are:

- Empirically developing ozone responses to emissions (and, likewise isopleths) is a potentially powerful method to understand how emissions controls have impacted peak ozone levels historically, and, within their limits, how they will respond to future emissions changes.
- Empirical modeling can be used to develop isopleths at individual locations or basin-wide.
- Use of an empirically-derived, spatial, ozone-emissions model finds that much of the reduction in exposure over the last four decades has come from VOC emissions reductions, and that future exposure reductions can be derived from both VOC and NOx emissions reductions.
- CMAQ modeling captured the reductions in ozone due to emissions decreases, but modeled levels were low for the two earliest years, and thus the simulated reductions were low.
- The CMAQ-derived isopleth were similar to those derived empirically for inland, higher ozone level, locations (though were biased low for high emissions levels), with a high correlation
- CMAQ-derived ozone sensitivities to NOx emissions were more highly correlated with those derived empirically than were VOC emissions sensitivities.

- CMAQ- and empirically derived isopleths both show that in earlier years (before about 2005) that VOC emissions reductions led to decreases in higher levels of ozone, off-setting potential increases due to NOx emissions reductions. In more recent years, ozone levels have become increasingly sensitive to reductions in NOx emissions, and that anthropogenic VOC emissions reductions will become less effective, though still beneficial, at reducing peak ozone levels downwind of the Los Angeles core area. Using CMAQ-HDDM, it is found that peak ozone levels in an increasingly small area of the core of Los Angeles will continue to be negatively sensitive to NOx emissions reductions.
- The approach to setting boundary conditions, i.e., using the default or using those derived from hemispherical modeling, had little impact on the sensitivities if the emissions were derived in a consistent fashion.

References

Baidar, S., Hardesty, R.M., Kim, S.W., Langford, A.O., Oetjen, H., Senff, C.J., Trainer, M., Volkamer, R., 2015. Weakening of the weekend ozone effect over California's South Coast Air Basin. Geophys. Res. Lett. 42, 9457–9464. https://doi.org/10.1002/2015GL066419

California Air Resources Board, 2018. iADAM Air Quality Data Statistics [WWW Document]. URL https://www.arb.ca.gov/adam/index.html

CEPAM: 2009 Almanac - Standard Emissions Tool [WWW Document], n.d. URL https://www.arb.ca.gov/app/emsinv/fcemssumcat2009.php (accessed 5.4.21).

CEPAM: 2016 SIP - Standard Emission Tool [WWW Document], n.d. URL https://www.arb.ca.gov/app/emsinv/fcemssumcat/fcemssumcat2016.php (accessed 5.4.21).

Chow, J.C., 2003. Introduction to Special Topic: Weekend and Weekday Differences in Ozone Levels. J. Air Waste Manage. Assoc. 53, 771–771. https://doi.org/10.1080/10473289.2003.10466224

Cohan, D.S., Hakami, A., Hu, Y., Russell, A.G., 2005. Nonlinear response of ozone to emissions: Source apportionment and sensitivity analysis. Environ. Sci. Technol. 39, 6739–6748. https://doi.org/10.1021/es048664m

Cox, P., Delao, A., Komorniczak, A., 2013. The California Almanac of Emissions and Air Quality - 2013 Edition.

Cox, P., Delao, A., Komorniczak, A., Weller, R., 2009. The California Almanac of Emissions and Air Quality - 2009 Edition.

Dolwick, P., Akhtar, F., Baker, K.R., Possiel, N., Simon, H., Tonnesen, G., 2015. Comparison of background ozone estimates over the western United States based on two separate model methodologies. Atmos. Environ. 109, 282–296. https://doi.org/10.1016/j.atmosenv.2015.01.005

Dunker, A.M., Koo, B., Yarwood, G., 2019. Standard and alternative procedures for projecting future ozone in the Houston area using relative reduction factors. Atmos. Environ. X 2, 100029. https://doi.org/10.1016/j.aeaoa.2019.100029

Dunker, A.M., Wilson, G., Bates, J.T., Yarwood, G., 2020. Chemical Sensitivity Analysis and Uncertainty Analysis of Ozone Production in the Comprehensive Air Quality Model with Extensions Applied to Eastern Texas. Environ. Sci. Technol. 54, 5391–5399. https://doi.org/10.1021/acs.est.9b07543

Emery, C., Jung, J., Downey, N., Johnson, J., Jimenez, M., Yarwood, G., Morris, R., 2012. Regional and global modeling estimates of policy relevant background ozone over the United States. Atmos. Environ. 47, 206–217. https://doi.org/10.1016/j.atmosenv.2011.11.012

Emery, C., Liu, Z., Russell, A.G., Odman, M.T., Yarwood, G., Kumar, N., 2017. Recommendations on statistics and benchmarks to assess photochemical model performance. J. Air Waste Manag. Assoc. 67, 582–598. https://doi.org/10.1080/10962247.2016.1265027

Emissions Modeling Platforms | Air Emissions Modeling | US EPA [WWW Document], n.d. URL https://www.epa.gov/air-emissions-modeling/emissions-modeling-platforms (accessed 5.4.21).

Fujita, E.M., Croes, B.E., Bennett, C.L., Lawson, D.R., Lurmann, F.W., Main, H.H., 1992. Comparison of emission inventory and ambient concentration ratios of co, nmog, and nox in california's south coast air basin. J. Air Waste Manag. Assoc. 42, 264–276. https://doi.org/10.1080/10473289.1992.10466989

Fujita, E.M., Stockwell, W.R., Campbell, D.E., Keislar, R.E., Lawson, D.R., 2003. Evolution of the Magnitude and Spatial Extent of the Weekend Ozone Effect in California's South Coast Air Basin. J. Air Waste Manage. Assoc. 53, 802–815. https://doi.org/10.1080/10473289.2003.10466225

Hakami, A., Odman, M.T., Russell, A.G., 2004. Nonlinearity in atmospheric response: A direct sensitivity analysis approach. J. Geophys. Res. Atmos. 109. https://doi.org/10.1029/2003JD004502

Hanna, S.R., 2007. Chapter 4.0 A review of uncertainty and sensitivity analyses of atmospheric transport and dispersion models. Dev. Environ. Sci. https://doi.org/10.1016/S1474-8177(07)06040-8

Hanna, S.R., Lu, Z., Frey, H.C., Wheeler, N., Vukovich, J., Arunachalam, S., Fernau, M., Hansen, D.A., 2001. Uncertainties in predicted ozone concentrations due to input uncertainties for the UAM-V photochemical grid model applied to the July 1995 OTAG domain. Atmos. Environ. 35, 891–903. https://doi.org/10.1016/S1352-2310(00)00367-8

Hanna, S.R., Russell, A.G., Wilkinson, J.G., Vukovich, J., Hansen, D.A., 2005. Monte Carlo estimation of uncertainties in BEIS3 emission outputs and their effects on uncertainties in chemical transport model predictions. J. Geophys. Res. Atmos. 110. https://doi.org/10.1029/2004JD004986

Harley, R.A., Hannlgan, M.P., Cass, G.R., 1992. Respeciation of Organic Gas Emissions and the Detection of Excess Unburned Gasoline in the Atmosphere. Environ. Sci. Technol. 26, 2395–2408.

https://doi.org/10.1021/es00036a010

Hassler, B., McDonald, B.C., Frost, G.J., Borbon, A., Carslaw, D.C., Civerolo, K., Granier, C., Monks, P.S., Monks, S., Parrish, D.D., Pollack, I.B., Rosenlof, K.H., Ryerson, T.B., Schneidemesser, E. von, Trainer, M., 2016. Analysis of long-term observations of NOx and CO in megacities and application to constraining emissions inventories. Geophys. Res. Lett. 43, 9920–9930. https://doi.org/10.1002/2016GL069894

Helwig, N.E., 2017. Multivariate Linear Regression [WWW Document]. URL http://users.stat.umn.edu/~helwig/notes/mvlr-Notes.pdf

Henneman, L.R.F., Liu, C., Mulholland, J.A., Russell, A.G., 2017a. Evaluating the effectiveness of air quality regulations: A review of accountability studies and frameworks. J. Air Waste Manage. Assoc. 67, 144–172. https://doi.org/10.1080/10962247.2016.1242518

Henneman, L.R.F., Shen, H., Liu, C., Hu, Y., Mulholland, J.A., Russell, A.G., 2017b. Responses in Ozone and Its Production Efficiency Attributable to Recent and Future Emissions Changes in the Eastern United States. Environ. Sci. Technol. 51, 13797–13805. https://doi.org/10.1021/acs.est.7b04109

Huang, M., Bowman, K.W., Carmichael, G.R., Lee, M., Chai, T., Spak, S.N., Henze, D.K., Darmenov, A.S., Silva, A.M. da, 2015. Improved western U.S. background ozone estimates via constraining nonlocal and local source contributions using Aura TES and OMI observations. J. Geophys. Res. Atmos. 120, 3572–3592. https://doi.org/10.1002/2014JD022993

Steven Manson, Jonathan Schroeder, David Van Riper, Tracy Kugler, and Steven Ruggles. IPUMS National Historical Geographic Information System: Version 15.0 [dataset]. Minneapolis, MN: IPUMS. 2020. http://doi.org/10.18128/D050.V15.0.

Jin, S., Demerjian, K., 1993. A photochemical box model for urban air quality study. Atmos. Environ. Part B. Urban Atmos. 27, 371–387. https://doi.org/10.1016/0957-1272(93)90015-X

Kanaya, Y., Pochanart, P., Liu, Y., Li, J., Tanimoto, H., Kato, S., Suthawaree, J., Inomata, S., Taketani, F., Okuzawa, K., Kawamura, K., Akimoto, H., Wang, Z.F., 2009. Rates and regimes of photochemical ozone production over Central East China in June 2006: A box model analysis using comprehensive measurements of ozone precursors. Atmos. Chem. Phys. 9, 7711–7723. https://doi.org/10.5194/acp-9-7711-2009

Kelly, N.A., Gunst, R.F., 1990. Response of ozone to changes in hydrocarbon and nitrogen oxide concentrations in outdoor smog chambers filled with Los Angeles air. Atmos. Environ. Part A, Gen. Top. 24, 2991–3005. https://doi.org/10.1016/0960-1686(90)90479-7

Kim, S.-W., McDonald, B.C., Baidar, S., Brown, S.S., Dube, B., Ferrare, R.A., Frost, G.J., Harley, R.A., Holloway, J.S., Lee, H.-J., McKeen, S.A., Neuman, J.A., Nowak, J.B., Oetjen, H., Ortega, I., Pollack, I.B., Roberts, J.M., Ryerson, T.B., Scarino, A.J., Senff, C.J., Thalman, R., Trainer, M., Volkamer, R., Wagner, N., Washenfelder, R.A., Waxman, E., Young, C.J., 2016. Modeling the weekly cycle of NOx and CO emissions and their impacts on O3 in the Los Angeles-South Coast Air Basin during the CalNex 2010 field campaign. J. Geophys. Res. Atmos. 121, 1340–1360. https://doi.org/10.1002/2015JD024292

Kinosian, J.R., 1982. Ozone-precursor relationships from EKMA diagrams. Environ. Sci. Technol. 16, 880–883. https://doi.org/10.1021/es00106a011

Lu, R., Turco, R.P., 1996a. Ozone distributions over the Los Angeles basin: Three-dimensional simulations with the smog model. Atmos. Environ. 30, 4155–4176. https://doi.org/10.1016/1352-2310(96)00153-7

Lu, R., Turco, R.P., 1996b. Ozone distributions over the los angeles basin: Three-dimensional simulations with the smog model. Atmos. Environ. 30, 4155–4176. https://doi.org/10.1016/1352-2310(96)00153-7

Luo, H., Astitha, M., Rao, S.T., Hogrefe, C., Mathur, R., 2020. Assessing the manageable portion of ground-level ozone in the contiguous United States. J. Air Waste Manag. Assoc. 70, 1136–1147. https://doi.org/10.1080/10962247.2020.1805375

Mathur, R., Kang, D., Napelenok, S., Xing, J., Hogrefe, C., 2018. A modeling study of the influence of hemispheric transport on trends in O3 distributions over North America, in: Springer Proceedings in Complexity. Springer, pp. 13–18. https://doi.org/10.1007/978-3-319-57645-9_2

Mathur, R., Xing, J., Gilliam, R., Sarwar, G., Hogrefe, C., Pleim, J., Pouliot, G., Roselle, S., Spero, T.L., Wong, D.C., Young, J., 2017. Extending the Community Multiscale Air Quality (CMAQ) modeling system to hemispheric scales: Overview of process considerations and initial applications. Atmos. Chem. Phys. 17, 12449–12474. https://doi.org/10.5194/acp-17-12449-2017

Mathur, R., Xing, J., Napelenok, S., Pleim, J., Hogrefe, C., Wong, D., Gan, C.M., Kang, D., 2016. Multiscale modeling of multi-decadal trends in ozone and precursor species across the northern Hemisphere and the United States, in: Springer Proceedings in Complexity. Springer, pp. 239–243. https://doi.org/10.1007/978-3-319-24478-5_39

McDonald, B.C., Dallmann, T.R., Martin, E.W., Harley, R.A., 2012. Long-term trends in nitrogen oxide emissions from motor vehicles at national, state, and air basin scales. J. Geophys. Res. Atmos. 117. https://doi.org/10.1029/2012JD018304

McDonald, B.C., de Gouw, J.A., Gilman, J.B., Jathar, S.H., Akherati, A., Cappa, C.D., Jimenez, J.L., Lee-Taylor, J., Hayes, P.L., McKeen, S.A., Cui, Y.Y., Kim, S.-W., Gentner, D.R., Isaacman-VanWertz, G., Goldstein, A.H., Harley, R.A., Frost, G.J., Roberts, J.M., Ryerson, T.B., Trainer, M., 2018. Volatile chemical products emerging as largest petrochemical source of urban organic emissions. Science (80-.). 359, 760–764. https://doi.org/10.1126/science.aaq0524

Menut, L., Vautard, R., Beekmann, M., Honoré, C., 2000. Sensitivity of photochemical pollution using the adjoint of a simplified chemistry-transport model. J. Geophys. Res. Atmos. 105, 15379–15402. https://doi.org/10.1029/1999JD900953

Milford, J.B., Russell, A.G., McRae, G.J., 1989. A new approach to photochemical pollution control: implications of spatial patterns in pollutant responses to reductions in nitrogen oxides and reactive organic gas emissions. Environ. Sci. Technol. 23, 1290–1301. https://doi.org/10.1021/es00068a017

Mueller, S.F., Mallard, J.W., 2011. Contributions of natural emissions to ozone and PM2.5 as simulated by the community multiscale air quality (CMAQ) model. Environ. Sci. Technol. 45, 4817–4823. https://doi.org/10.1021/es103645m

Parrish, D.D., 2006. Critical evaluation of US on-road vehicle emission inventories. Atmos. Environ. 40, 2288–2300. https://doi.org/10.1016/j.atmosenv.2005.11.033

Parrish, D.D., Young, L.M., Newman, M.H., Aikin, K.C., Ryerson, T.B., 2017. Ozone Design Values in Southern California's Air Basins: Temporal Evolution and U.S. Background Contribution. J. Geophys. Res. Atmos. 122, 11,166-11,182. https://doi.org/10.1002/2016JD026329

Pollack, I.B., Ryerson, T.B., Trainer, M., Neuman, J.A., Roberts, J.M., Parrish, D.D., 2013. Trends in ozone, its precursors, and related secondary oxidation products in Los Angeles, California: A synthesis of measurements from 1960 to 2010. J. Geophys. Res. Atmos. 118, 5893–5911. https://doi.org/10.1002/jgrd.50472

Pollack, I.B., Ryerson, T.B., Trainer, M., Parrish, D.D., Andrews, A.E., Atlas, E.L., Blake, D.R., Brown, S.S., Commane, R., Daube, B.C., de Gouw, J.A., Dubé, W.P., Flynn, J., Frost, G.J., Gilman, J.B., Grossberg, N., Holloway, J.S., Kofler, J., Kort, E.A., Kuster, W.C., Lang, P.M., Lefer, B., Lueb, R.A., Neuman, J.A., Nowak, J.B., Novelli, P.C., Peischl, J., Perring, A.E., Roberts, J.M., Santoni, G., Schwarz, J.P., Spackman, J.R., Wagner, N.L., Warneke, C., Washenfelder, R.A., Wofsy, S.C., Xiang, B., 2012. Airborne and ground-based observations of a weekend effect in ozone, precursors, and oxidation products in the California South Coast Air Basin. J. Geophys. Res. Atmos. 117, n/a-n/a. https://doi.org/10.1029/2011JD016772

Pusede, S.E., Cohen, R.C., 2012. On the observed response of ozone to NO_x and VOC reactivity reductions in San Joaquin Valley California 1995–present. Atmos. Chem. Phys. 12, 8323–8339. https://doi.org/10.5194/acp-12-8323-2012

Qian, Y., Henneman, L.R.F., Mulholland, J.A., Russell, A.G., 2019. Empirical Development of Ozone Isopleths: Applications to Los Angeles. Environ. Sci. Technol. Lett. 6, 294–299. https://doi.org/10.1021/acs.estlett.9b00160

Qin, M., Murphy, B.N., Isaacs, K.K., McDonald, B.C., Lu, Q., McKeen, S.A., Koval, L., Robinson, A.L., Efstathiou, C., Allen, C., Pye, H.O.T., 2021. Criteria pollutant impacts of volatile chemical products informed by near-field modelling. Nat. Sustain. 4, 129–137. https://doi.org/10.1038/s41893-020-00614-1

Qin, M., Yu, H., Hu, Y., Russell, A.G., Odman, M.T., Doty, K., Pour-Biazar, A., McNider, R.T., Knipping, E., 2019. Improving ozone simulations in the Great Lakes Region: The role of emissions, chemistry, and dry deposition. Atmos. Environ. 202, 167–179. https://doi.org/10.1016/j.atmosenv.2019.01.025

Reynolds, S.D., Blanchard, C.L., Ziman, S.D., 2004. Understanding the Effectiveness of Precursor Reductions in Lowering 8-Hr Ozone Concentrations—Part II. The Eastern United States. J. Air Waste Manage. Assoc. 54, 1452–1470. https://doi.org/10.1080/10473289.2004.10471003

Schwehr, B., Propper, R., 2009. Definitions of VOC and ROG [WWW Document]. URL https://www.arb.ca.gov/ei/speciate/voc_rog_dfn_1_09.pdf

Sierra, A., Vanoye, A.Y., Mendoza, A., 2013. Ozone sensitivity to its precursor emissions in northeastern Mexico for a summer air pollution episode. J. Air Waste Manage. Assoc. 63, 1221–1233.

https://doi.org/10.1080/10962247.2013.813875

Simon, H., Baker, Kirk (1) Simon, H.; Baker, K. R.; Phillips, S. Compilation and Interpretation of Photochemical Model Performance Statistics Published between 2006 and 2012. Atmos. Environ. 2012, 61, 124–139. https://doi.org/10.1016/j.atmosenv.2012.07.012.R, Phillips, S., 2012. Compilation and interpretation of photochemical model performance statistics published between 2006 and 2012. Atmos. Environ. 61, 124–139. https://doi.org/10.1016/j.atmosenv.2012.07.012

Skipper, T.N., Hu, Y., Odman, M.T., Henderson, B.H., Hogrefe, C., Mathur, R., Russell, A.G., 2021. Estimating US Background Ozone Using Data Fusion. Cite This Environ. Sci. Technol 55, 4512. https://doi.org/10.1021/acs.est.0c08625

Soberanes Fire - Wikipedia [WWW Document], n.d. URL https://en.wikipedia.org/wiki/Soberanes_Fire#References (accessed 5.20.21).

US Environmental Protection Agency, 1999. Guidance for Improving Weight of Evidence Through Identification of Additional Emission Reductions, Not Modeled.

US EPA, O., 2016. Air Quality Design Values [WWW Document]. US EPA.

USEPA, U.. E.P.A., 2020. Policy Assessment for the Review of the Ozone National Ambient Air Quality Standards, Epa-452/R-14-006.

Warneke, C., Gouw, J.A. de, Holloway, J.S., Peischl, J., Ryerson, T.B., Atlas, E., Blake, D., Trainer, M., Parrish, D.D., 2012. Multiyear trends in volatile organic compounds in Los Angeles, California: Five decades of decreasing emissions. J. Geophys. Res. Atmos. 117. https://doi.org/10.1029/2012JD017899

William, D.R., Burke, A., 2016. FINAL 2016 AIR QUALITY MANAGEMENT PLAN.

Yang, L., Yuan, Z., Luo, H., Wang, Y., Xu, Y., Duan, Y., Fu, Q., 2021. Identification of long-term evolution of ozone sensitivity to precursors based on two-dimensional mutual verification. Sci. Total Environ. 760, 143401. https://doi.org/10.1016/j.scitotenv.2020.143401

Yarwood, G., Grant, J., Koo, B., Dunker, A.M., 2008. Modeling weekday to weekend changes in emissions and ozone in the Los Angeles basin for 1997 and 2010. Atmos. Environ. 42, 3765–3779. https://doi.org/10.1016/j.atmosenv.2007.12.074

Yarwood, G., Whitten, G.Z., Jung, J., Heo, G., Allen, D.T., 2010. Final Report Development, Evaluation and

Testing of Version 6 of the Carbon Bond Chemical Mechanism (CB6).

Zhang, W., Trail, M.A., Hu, Y., Nenes, A., Russell, A.G., 2015. Use of high-order sensitivity analysis and reduced-form modeling to quantify uncertainty in particulate matter simulations in the presence of uncertain emissions rates: A case study in Houston. Atmos. Environ. 122, 103–113. https://doi.org/10.1016/j.atmosenv.2015.08.091